RMZ

MATERIALS and GEOENVIRONMENT

MATERIALI in GEOOKOLJE

RMZ – M&G, **Vol. 67**, No. 4
pp. 161–219 (2020)

Ljubljana, December 2020

RMZ – Materials and Geoenvironment
RMZ – Materiali in geookolje
ISSN 1408-7073

Old title/Star naslov
Mining and Metallurgy Quarterly/Rudarsko-metalurški zbornik
ISSN 0035-9645, 1952–1997

Published by/Izdajatelj
Faculty of Natural Sciences and Engineering, University of Ljubljana/
Naravoslovnotehniška fakulteta, Univerza v Ljubljani

Associated Publisher/Soizdajatelj
Institute for Mining, Geotechnology and Environment, Ljubljana/
Inštitut za rudarstvo, geotehnologijo in okolje
Velenje Coal Mine/Premogovnik Velenje
Slovenian Chamber of Engineers/Inženirska zbornica Slovenije

Editorial Office/Uredništvo
Technical editors/Tehnična urednika Blaž Janc and Jože Žarn
Secretary/Tajnica Nives Vukič

Editorial Address/Naslov uredništva
RMZ – Materials and Geoenvironment
Aškerčeva cesta 12, p. p. 312
1001 Ljubljana, Slovenija
Tel.: +386 (0)1 470 46 10
Fax.: +386 (0)1 470 45 60
E-mail: bostjan.markoli@ntf.uni-lj.si
joze.zarn@ntf.uni-lj.si

Published/Izhajanje
4 issues per year/4 številke letno

Partly funded by Ministry of Education, Science and Sport of Republic of Slovenia./Pri financiranju revije sodeluje Ministrstvo za izobraževanje, znanost in šport Republike Slovenije.

Articles published in Journal "RMZ M&G" are indexed in international secondary periodicals and databases:/Članki, objavljeni v periodični publikaciji „RMZ M&G", so indeksirani v mednarodnih sekundarnih virih:
CA SEARCH® – Chemical Abstracts®, METADEX®, GeoRef.

Annual subscription for individuals in Slovenia: 20 EUR, for institutions: 30 EUR. Annual subscription for the rest of the world: 30 EUR, for institutions: 50 EUR/Letna naročnina za posameznike v Sloveniji: 20 EUR, za inštitucije: 30 EUR. Letna naročnina za tujino: 30 EUR, inštitucije: 50 EUR

Transaction account/Tekoči račun
Nova Ljubljanska banka, d. d., Ljubljana: UJP 01100-6030708186

VAT identification number/Davčna številka
24405388

Online Journal/Elektronska revija
https://content.sciendo.com/view/journals/rmzmag/rmzmag-overview.xml?result=4&rskey=iClOT4#

Table of Contents

Kazalo

Original scientific papers
Izvirni znanstveni članki

Underwater noise in the Slovenian Sea **161**
Podvodni hrup v slovenskem morju
A. Popit

Monitoring after the conclusion of mining works **177**
Laboratorijske preiskave abrazivnosti kamnin in zemljin na področju geotehnologije in rudarstva
T. Hribar, T. Pečolar, G. Vižintin

Estimation of Depth to Bouguer Anomaly Sources Using Euler Deconvolution Techniques **185**
Ocena globine do virov Bouguerjeve anomalije z uporabo Eulerjevih dekonvolucijskih tehnik
G. O. Layade, H. Edunjobi, V. Makinde, B. Bada

Site characterization for engineering purposes using geophysical and geotechnical techniques **197**
Določevanje značilnosti območja za inženirske namene z uporabo geofizikalnih in geotehničnih metod
A. A. Alabi

Geochemical Fingerprinting pf Oil-Impacted Soil and Water Samples In Some Selected Areas in the Niger Delta **209**
Geokemični kazalniki z nafto nasičenih vzorcev zemljin in vode na nekaterih izbranih področjih delte reke Niger
A. V. Adeniyi, M. E. Nton, F. O. Adebanjo

Original Scientific Article

Received: March 08, 2021
Accepted: March 09, 2021
DOI: 10.2478/rmzmag-2020-0018

Underwater noise in the Slovenian Sea

Podvodni hrup v slovenskem morju

Andreja Popit*
Institute for Water of the Republic of Slovenia, Ljubljana, Slovenia
*andreja.popit@izvrs.si

Abstract

Continuous underwater noise has been monitored in the Slovenian sea near the lighthouse foundation at Debeli Rtič since February 2015, according to the EU Marine Strategy Framework Directive (MSFD). Anthropogenic noise sources (e.g. seawater densities, dredging activities and cleaning of the seafloor) and meteorological noise sources (e.g. wind speed and precipitation) were analysed in relation to the measured underwater noise levels using several graphical and statistical methods. The results of this study showed that average equivalent continuous underwater noise levels were, by 11 dB ($L_{eq,63\ Hz}$) and 5 dB ($L_{eq,125\ Hz}$), higher in the intervals when dredging activities took place than in the intervals when these activities were absent. Variation in underwater noise levels was partly related to the variation of the ship densities, which could be explained by the relatively small acoustic propagation in the shallow seawater. Precipitation level did not indicate any significant association with the variations in continuous underwater noise levels, though some larger deviations in the wind speed were found to be associated with the larger fluctuations in continuous underwater noise levels.

Keywords: underwater noise, shallow sea, measuring equipment, natural and anthropogenic sound sources

Povzetek

V slovenskem morju izvajamo kontinuirne meritve podvodnega hrupa ob svetilniku pri Debelem rtiču od februarja 2015. Meritve potekajo v skladu z Okvirno direktivo o morski strategiji. Za analizo antropogenih virov hrupa (gostota ladij, poglabljanje in čiščenje morskega dna) in meteoroloških virov hrupa (hitrost vetra in padavine) v povezavi z izmerjenimi ravnmi podvodnega hrupa smo uporabili grafične in statistične metode. Rezultati te študije so pokazali, da so bile povprečne ekvivalentne ravni kontinuirnega podvodnega hrupa za 11 dB (Leq, 63 Hz) in 5 dB (Leq,125 Hz) višje v času, ko so potekale dejavnosti poglabljanja, kot v času, ko so teh dejavnosti ni bilo. Nihanja ravni podvodnega hrupa so bila v manjši meri povezana z nihanji gostote ladij, kar lahko razložimo z relativno majhno akustično propagacijo v plitvem morju. Padavine niso bile veliko povezane z nihanji ravni podvodnega hrupa, medtem ko so bila nekatera večja nihanja hitrosti vetra povezana z večjimi nihanji ravni kontinuirnega podvodnega hrupa.

Ključne besede: podvodni hrup, plitvo morje, merilna oprema, naravni in antropogeni viri zvoka

Introduction

The background or ambient noise in the seas and oceans is composed of natural (i.e. meteorological (wind speed, surface waves, precipitation), geological (tectonic processes) and biological) and anthropogenic (i.e. marine traffic) noise sources. It varies with the location and frequency of underwater sound. In regions with high shipping densities, the frequency band between 10 Hz and 200 Hz is primarily associated with shipping activity, constituting the largest anthropogenic contribution to the underwater ambient sound [1–11].

Most of the noise power radiated into the water by surface ships comes from propeller cavitation [1, 4, 12]. Propeller noise is generated through several cavitation noise mechanisms:

tip vortex cavitation, different types of blade cavitation, hub vortex cavitation, pressure pulses due to wake inhomogeneity at the propeller plane, pressure pulses generated by the rotating propeller blades and singing due to resonance between blade natural frequencies and trailing edge vortices. Some vessels emit strong structural noise radiation arising from their hydraulic systems, gears, compressors or other noisy machinery [4].

An increase in the low-frequency ocean ambient noise levels was observed between 1963 and 2001 on the continental slope of Point Sur, California [7, 8, 13], between 1964 and 2004, westwards of the San Nicolas Island, California [14] and between 1978 and 1986 in the Northeast Pacific Ocean [15]. This was related to the shipping vessel traffic. The number of commercial vessels in the world's oceans approximately doubled and the gross tonnage quadrupled between 1965 and 2003, with a corresponding increase in horsepower of the vessels. Increases in commercial shipping are believed to account for the observed increase in the low-frequency ambient noise [14].

More recently, between 2006 and 2016, observations made in the Northeast Pacific, Equatorial Pacific and in the South Atlantic Ocean show a slightly decreasing trend in low-frequency ambient noise levels [16, 17]. This trend may be attributed to the fact that world vessel size and gross tonnage have increased considerably over the recent years, while the number of vessels has decreased [18–21].

Wind-generated sea-surface agitation governs much of the ambient noise in the frequency band between 200 Hz and 100,000 Hz. Wind-generated noise is largely the consequence of bubbles created in the process of wave-breaking. At lower frequencies (<500 Hz), the oscillation of bubble clouds themselves are considered to be the source of the sound [22, 23] while, at higher frequencies (>500 Hz), the excitation of resonant oscillations by individual bubbles generates the sound [7, 24, 25].

At very high frequencies, ~100,000 Hz, thermal noise generated by the random motion of water molecules begins to dominate. The thermal noise spectral density at 100,000 Hz is 20–25 dB re 1 μPa^2/Hz [7].

Rain can produce a peak in the ambient sound pressure spectral density (around 60 dB re 1 μPa^2/Hz) in the vicinity of 15 kHz, corresponding to rain rates ranging from 2 mm/h to 5 mm/h, measured at different wind speeds [7, 26].

Underwater ambient noise is generated not only by the combination of environmental sea state and anthropogenic contributions (e.g. shipping), but also by significant amounts of biological noise from fish, invertebrates and whales. Biological noise may generate major background noise in some areas. Marine mammals, such as whales and dolphins, rely on sound to communicate with each other, locate their prey and find their way over long distances. All these activities, critical to their survival, are being interfered with by the increasing levels of noise from ships [1, 4, 27–33]. The European Commission's Marine Strategy Framework Directive (MSFD) 2008/56/EC [34] and International Maritime Organization(IMO) guidelines for the reduction of underwater noise from commercial shipping [35] have addressed underwater noise pollution from shipping, as well as the promotion of the use of the appropriate mitigation measures.

The EC MSFD 2008/56/EC [34] guidelines require the Member States to prepare a Marine Management Plan. These requirements were incorporated in Slovenian law by passing the Water Act [36] and by the Decree on the detailed content of the Marine management plan [37]. According to this legislation, Slovenia started to monitor continuous underwater noise near the lighthouse foundation at Debeli Rtič since February 2015.

The aim of our study was to analyse continuous underwater noise measurements from 2015 until 2018. The measured ambient low-frequency noise levels were most probably due to anthropogenic activities such as marine traffic, dredging activities and cleaning of the seafloor, as well as to meteorological factors such as precipitation and wind. These levels were analysed through the proposed methodology and results of this study were discussed in this article.

Materials and methods

Underwater noise measuring station and measured quantities

A permanent underwater noise measurement station was established on the concrete foundation of a masonry lighthouse 300 m off the coast at Debeli Rtič, Slovenia in February 2015 (Figure 1a). The coordinates of the lighthouse are Lat.: 45°35′ 28.2″ N, Lon.: 13°41′ 59.1″ E. The associated measuring equipment was composed of a spherical omnidirectional hydrophone (Type 8105, Bruel & Kjaer) installed at a depth of 4 m (Figure 1b) (sea depth at that location was 5 m). The hydrophone is connected to a sound analyser of Type 2250 Bruel & Kjaer, which includes a sound level meter and an octave-based frequency analyser, operating in the frequency band of 6.3–20 kHz. The hydrophone with a cable was installed through a metal pipe 1 m away from the lighthouse foundation to a depth of approx. 1 m above the seabed, as shown in Figure 1b [38]. A sound analyser was closed inside the lighthouse in a waterproof casing, according to the standard National Electrical Manufacturers Association (NEMA) IP65 protocols, and maintaining resistance to water jets was ensured. The measuring system was connected to the batteries that were charged by a solar panel [38, 39].

The mathematical definition of the measured equivalent continuous sound level (Eq. 1) (also called time-average sound level), L_{eq}, is 20 times the logarithm to base 10 of the ratio of the root mean square sound pressure (p_{rms}) during a time interval to the reference sound pressure (p_0, which is 1 µPa) [40]:

$$L_{eq}(t) = 10\log_{10}\left(\frac{p_{rms}}{p_0}\right)^2 = 20\log_{10}\left(\frac{p_{rms}}{p_0}\right) \quad (1)$$

Root mean square of the sound pressure level (p_{rms}) (Eq. 2) in Pascals (Pa) [41] can be represented as:

$$p_{rms} = \left(\frac{1}{(t_2 - t_1)} \int_1^2 p(t)^2 \, dt\right)^{\frac{1}{2}} \quad (2)$$

where, P_{rms} or the mean square sound pressure is the time integral of squared sound pressure over a specified time interval divided by the duration of the time interval; and t_1 and t_2 are the start and stop times of the time interval over which the mean is evaluated.

The RMS sound pressure is calculated by first squaring the values of sound pressure, averaging over the specified time interval and then taking the square root.

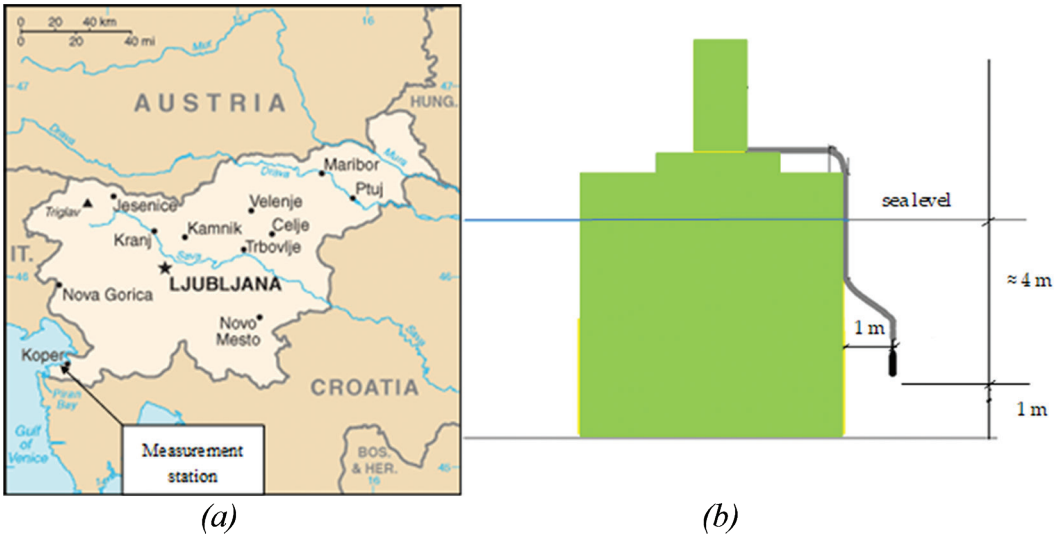

Figure 1: *Location of the permanent underwater noise measurement station near Debeli Rtič in the Slovenian Sea (A) and a sketch of the lighthouse at Debeli Rtič on which the measuring equipment is installed showing the hydrophone at a depth of 4 m (sea depth at the location is 5 m) (B) [38].*

Frequency analysis software enables derivations of the equivalent continuous sound levels in 1/3-octave band with centre frequencies between 6.3 Hz and 20 kHz, in the resolution of 10 s. Daily arithmetic mean values were calculated and recorded on a hard disc of 1 Terabyte (TB). The memory capacity of the disc enables recordings for 75 days.

Measured data were transferred, displayed and analysed using BZ-5503 Measurement Partner Suite [40] software. This software can be used for data archival, data preview and data export, for post-process and export to other formats, online data display and remote access and operation, as well as for maintenance of the sound level meter software.

With BZ-5503 Measurement Partner Suite, daily equivalent continuous sound levels (L_{eq} values) in the 1/3-octave band with centre frequencies between 6.3 Hz and 20 kHz were analysed.

Methodology used for processing continuously measured data

The first step in data processing was, in our case, done by the sound analyser of Type 2250 (Bruel & Kjaer), which calculates equivalent continuous sound levels in 1/3-octave bands. Then we proceeded with the second step in data processing, to calculate the annual average of the continuous sound level.

For monitoring and assessing anthropogenic continuous low-frequency sound in water (D11C2) we used annual average of the squared sound pressure in 1/3-octave bands, one centred at 63 Hz and the other at 125 Hz, both expressed as a level in decibels in units of dB re 1 µPa, according to the requirements of the Commission Decision EU/2017/848 [42]. The unit of measurement used for the criteria D11C2 is the annual average of the continuous sound level per unit area; proportion (percentage) of extent in square kilometres of the assessment area.

For this purpose we used the arithmetic mean (*AM*) in time *T* [43] (Eq. 3), which shows compatibility with L_{eq} metric:

$$AM(T) = \frac{1}{N(T)} \sum_{n=1}^{N(T)} p_n(T) \qquad (3)$$

where $N(T)$ is the number of snapshots of duration *T* in 1 year (Eq. 4) (assuming that the data are continuous, and contain no gaps for an entire year):

$$N(T) = \frac{1\ \text{year}}{T} \qquad (4)$$

where $p_n(T)$ is the mean square sound pressure at the n-th snapshot of duration *T*.

The arithmetic mean is expressed as sound pressure level (*SPL*) (Eq. 5) in dB re µPa [43]:

$$L_{AM}(T) = 10\log_{10} \frac{AM(T)}{p_{ref}^2} \qquad (5)$$

where $p_{ref} = 1$ µPa.

Annual averages of the continuous sound level and standard deviation (STDEV) for 1/3-octave bands with centre frequencies of 63 Hz and 125 Hz were calculated using daily averages, which were calculated using the sound analyser.

The results of the underwater noise measurements from the measuring station at Debeli Rtič were analysed and reviewed using the BZ-5503 Measurement Partner Suite Software [39]. The equivalent unweighted continuous noise levels within 1/3-octave frequency bands with centre frequencies of 63 Hz $L_{eq,63\ \text{Hz}}$ and 125 Hz $L_{eq,125\ \text{Hz}}$ (in dB), according to the MSFD 2008/56/EC [34], were exported into an excel spreadsheet for further analyses. The underwater noise data were available at half-hour intervals for the following periods: from 13 February 2015 to 5 May 2015; 26 September 2015 to 31 December 2015; 18 August 2016 to 1 November 2016; 6 July 2017 to 27 August 2017; and 18 August 2018 to 31 December 2018.

Average hourly values of equivalent continuous underwater noise levels in 1/3-octave bands with centre frequencies of 63 Hz and 125 Hz for each measuring period were prepared and presented on diagrams.

Asymmetry (*A*) (Eq. 6) was used to test the normality of the distribution of underwater noise levels. Asymmetry was

used to indicate the direction of data asymmetry [44]:

$$A = \tag{6}$$

where m_2 and m_3 are the second and third moments around the average.

The j-th moment is calculated by the Eq. (7), represented below [44]:

$$m_j = \frac{\sum_{i=1}^{n} (x_i - \bar{x})^j}{n} \tag{7}$$

When A is 0, the data set is symmetric to its mean and the data are distributed symmetrically or normally (Gaussian distribution). At $A < 0$ the data are asymmetric to the left and at $A > 0$ the data are asymmetric to the right. If $A < -1$ or $A > 1$ the distribution is very asymmetric.

If A is between −1 and −0.5 or between 0.5 and 1, the distribution is moderately asymmetric. If A falls between −0.5 and 0 or between 0 and 0.5, the distribution is approximately symmetric.

The statistics were calculated in Excel (Microsoft).

Methodology for the analysis of anthropogenic sources (ship densities, dredging and cleaning activities) of the underwater noise in the canals of the Port of Koper

Marine traffic in the sea is monitored with the Automatic Information System (AIS). Obtained AIS data concerning locations of the ships were analysed in the North Adriatic Sea for 2015, 2016, 2017 and 2018 to prepare hourly data on the ship densities in four different areas around the underwater noise measuring station at the lighthouse at Debeli Rtič, Slovenia. These four areas were namely within a radii of 2 nautical miles (NM) and 5 NM from the measuring station, in the Gulf of Trieste and the Gulf of Venice. Data on ship densities were prepared for each period during which underwater noise levels were recorded.

Average hourly ship densities in all four areas around the measuring station, for each period in which underwater noise levels were recorded, were presented graphically in combination with the average hourly continuous underwater noise levels in 1/3-octave bands with centre frequencies of 63 Hz and 125 Hz. Asymmetry (A) was used to test the normality of the distribution of ship densities.

Dredging activities were carried from 7 September 2015 to 26 October 2015 from 7:00–21:00 h, while cleaning activities of the seafloor in the canals of the Port of Koper were carried out from 18 August 2016 to 31 August 2016, and from 22 September 2016 to 29 September 2016 from 8:00–16:00 h (Table 1). Dredging was carried out in the sea with a dredger and a trailed harrow for levelling the seabed, while the cleaning work was carried out from the mainland with the help of the Link-Belt LS-108B excavator crane.

On the diagram concerning ship density in the four areas around the measuring station in combination with the average hourly continuous underwater noise levels in 1/3-octave bands with centre frequencies of 63 Hz and 125 Hz, were drawn red arrows indicating dredging and cleaning activities.

Average equivalent continuous underwater noise levels during dredging and cleaning activities were analysed. Separately, average equivalent continuous levels of underwater noise were analysed at the time when there were no anthropogenic activities (Table 1). These analyses were performed to check whether the average values (AVE) of equivalent continuous underwater noise levels, in 1/3-octave bands with centre frequencies of 63 Hz and 125 Hz at the time of dredging and cleaning activities, were higher than at the time when these activities were not being executed.

Methodology for the analysis of meteorological sources of the underwater noise

In this section, wind speed and precipitation were analysed as meteorological sources of underwater noise. Half-hourly data on wind speeds (m/s) from the Piran buoy (Lon.: 13.5454°, Lat.: 45.5481°, altitude: 0 m) and half-hourly data on precipitation (mm) from the meteorological station in the Port of Koper (Lon.: 13.7448°, Lat.: 45.5645°, Altitude: 2 m), in the periods in which underwater noise

Table 1: *Periods with and without the anthropogenic activity*

Type of anthropogenic activity	Periods with the anthropogenic activity	Periods without any anthropogenic activity
Dredging	26.09.2015–26.10.2015 (7:00–21:00 h)	26.09.2015–26.10.2015 (22:00–6:00 h)
Cleaning of the seafloor	18.08.2016–31.08.2016 & 22.09.2016–29.09.2016 (8:00–16:00 h)	18.08.2016–31.08.2016 & 22.09.2016–29.09.2016 (17:00–7:00 h)

levels were recorded, were obtained from the Environmental Agency of the Republic of Slovenia (ARSO).

Average hourly wind speeds and precipitation levels in the individual periods were calculated and presented graphically in combination with average hourly continuous underwater noise levels in 1/3-octave bands with central frequencies of 63 Hz and 125 Hz. Furthermore, asymmetry (A) was used to test the normality of the distribution of the average hourly wind speeds and average hourly precipitation data.

Results

The average continuous underwater noise levels in the 1/3-octave bands with centre frequencies of 63 Hz ($L_{eq,63\ Hz}$) and 125 Hz ($L_{eq,63\ Hz}$) in dB re 1 µPa, average ship densities in the four areas around the measuring station ($\rho_{L,2\ NM}$, $\rho_{L,5\ NM}$, $\rho_{L,\ Trieste.}$ and $\rho_{L,\ Venice}$), average wind speeds (v_v) in m/s and average precipitation (h_p) in mm in each measurement period are presented in Table 2.

The average $L_{eq,63\ Hz}$ and $L_{eq,125\ Hz}$ levels measured in the Slovenian Sea during the period 2015–2018 (Table 2) were 82.8–101.1 dB re 1 µPa and 83.9–98.1 dB re 1 µPa, respectively. The ship densities were 2–252. The average wind speed was 1.8–4.6 m/s and the average precipitation was 0.02–0.07 mm.

The $L_{eq,125\ Hz}$ data were distributed close to the normal (Gaussian) distribution in all measuring periods (they were slightly asymmetric to the right or left), as the value of A was close to 0 (Table 3). The $L_{eq,63\ Hz}$ data were distributed moderately asymmetrically to the right (A = 0.5–1.1), except for the period from 18 August 2016 to 1 November 2016, when they were distributed approximately symmetrically (A = −0.4) (Table 3).

The $\rho_{L,2\ NM}$ data were distributed moderately asymmetrically to the right in all measuring periods and the $\rho_{L,5\ NM}$ data and $\rho_{L,\ Trieste}$ were distributed very asymmetrically to the left in the first two periods, very asymmetrically to the right in the third and fifth periods and approximately symmetrical in the fourth period. The $\rho_{L,\ Venice}$ data were moderately asymmetrically distributed to the left in the first two periods, and moderately asymmetrically to the right to approximately symmetrically in the other periods (Table 3).

The v_v data were distributed very asymmetrically to the right in all measuring periods, except in the period from 18 August 2016 to 1 November 2016, in which they were distributed moderately asymmetrically to the right. The h_p data were distributed very asymmetrically to the right in all measuring periods (Table 3).

The relationship of the measured ambient low-frequency noise levels with the anthropogenic activities (ship densities, dredging and cleaning activities) is shown in the diagrams (Figures 2–6) of the average hourly ship densities in the four areas around the underwater noise measuring station ($\rho_{L,2\ NM}$, $\rho_{L,5\ NM}$, $\rho_{L,\ Trieste.}$ and $\rho_{L,\ Venice}$) in combination with the average hourly continuous underwater noise levels in 1/3-octave bands with centre frequencies of 63 Hz and 125 Hz. Blue curve presents $L_{eq,63\ Hz}$, black curve presents $L_{eq,125\ Hz,}$ violet curve presents ship density 2 NM from the measuring station, yellow curve presents ship density 5 NM from the measuring station, green curve presents ship density in the Gulf of Trieste and

Table 2: *The results of AVE and STDEV calculations of $L_{eq,63\,Hz}$, $L_{eq,125\,Hz}$, $\rho_{L,2\,NM}$, $\rho_{L,5\,NM}$, $\rho_{L,\,Trieste}$, $\rho_{L,\,Venice,}$ dredging, cleaning activity, v_v and h_p in different measuring periods*

Average of AVE and STDEV	From 13.02.2015 to 05.05.2015	From 26.09.2015 to 31.12.2015	From 18.08.2016 to 01.11.2016	From 06.07.2017 to 27.08.2017	From 18.08.2018 to 31.12.2018
AVE & STDEV of $L_{eq,63\,Hz}$	83.0 ± 15.1	82.8 ± 10.8	101.1 ± 6.9	86.7 ± 7.7	88.6 ± 5.7
AVE & STDEV of $L_{eq,125\,Hz}$	89.0 ± 13.1	83.9 ± 2.5	97.5 ± 6.8	85.2 ± 3.3	98.1 ± 3.9
AVE & STDEV of $\rho_{L,2\,NM}$	2 ± 2	3 ± 2	5 ± 3	5 ± 3	5 ± 3
AVE & STDEV of $\rho_{L,5\,NM}$	24 ± 9	37 ± 7	45 ± 6	52 ± 6	52 ± 8
AVE & STDEV of $\rho_{L,\,Trieste}$	35 ± 13	50 ± 10	58 ± 8	71 ± 9	70 ± 11
AVE & STDEV of $\rho_{L,\,Venice}$	117 ± 52	186 ± 51	252 ± 53	246 ± 48	247 ± 56
AVE & STDEV of v_v	4.6 ± 3.3	4.5 ± 3.8	4.6 ± 2.7	1.8 ± 1.2	2.0 ± 1.6
AVE & STDEV of h_p	0.02 ± 0.13	0.04 ± 0.35	0.07 ± 0.61	0.02 ± 0.31	0.05 ± 0.32

AVE, average value; NM, nautical miles; STDEV, standard deviation.

Table 3: *The results of asymmetry (A) calculations of $L_{eq,63\,Hz}$, $L_{eq,125\,Hz}$, $\rho_{L,2\,NM}$, $\rho_{L,5\,NM}$, $\rho_{L,\,Trieste}$, $\rho_{L,\,Venice,}$ dredging, cleaning activity, v_v and h_p in different measuring periods*

Asymmetry	From 13.02.2015 to 05.05.2015	From 26.09.2015 to 31.12.2015	From 18.08.2016 to 01.11.2016	From 06.07.2017 to 07.08.2017	From 18.08.2018 to 31.12.2018
A of $L_{eq,63\,Hz}$	1.0	0.5	−0.4	1.1	0.6
A of $L_{eq,125\,Hz}$	0.2	0.1	0.0	0.1	−0.1
A of $\rho_{L,2\,NM}$	0.8	0.7	0.6	0.6	1.0
A of $\rho_{L,5\,NM}$	−1.7	−3.0	1.1	0.4	2.0
A of $\rho_{L,\,Trieste}$	−1.6	−2.8	1.1	0.2	1.4
A of $\rho_{L,\,Venice}$	−0.7	−0.6	0.6	0.8	0.5
A of v_v	1.1	1.2	0.8	1.1	2.4
A of h_p	20.5	16.2	14.8	22.4	10.9

NM, nautical miles.

brown curve presents ship density in the Gulf of Venice (Figures 2–6).

Many gaps in the ship densities in 2015 (evident in Figures 2 and 3) and one major gap (evident in October 2018 in Figure 6) were due to the reason that AIS System did not operate during these periods.

The red arrow on the diagram of average hourly ship densities (Figure 3) indicates dredging activities, which took place from 26 September 2015 to 26 October 2015. The red arrows on the diagram of average hourly ship densities (Figure 4) show cleaning activities at the seafloor in the canals of the Port of

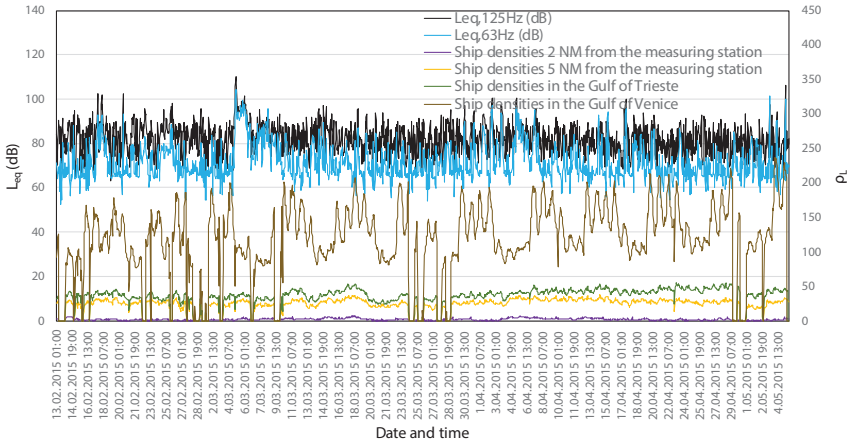

Figure 2: *Diagram of the average hourly ship densities in the areas of 2 NM and 5 NM from the measuring station in the Gulf of Trieste and the Gulf of Venice in combination with the average hourly continuous underwater noise levels in 1/3-octave bands with centre frequencies of 63 Hz and 125 Hz (Leq) in the period from 12 February 2015 to 5 May 2015. NM, nautical miles.*

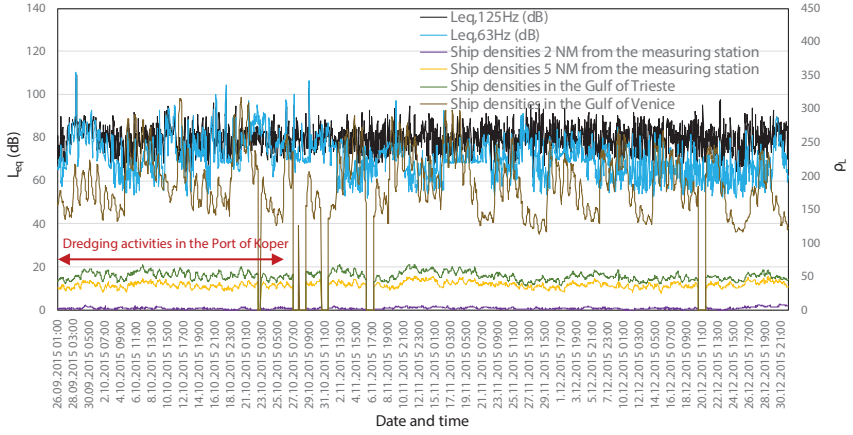

Figure 3: *Diagram of the average hourly ship densities in the areas of 2 NM and 5 NM from the measuring station in the Gulf of Trieste and the Gulf of Venice in combination with the average hourly continuous underwater noise levels in 1/3-octave bands with centre frequencies of 63 Hz and 125 Hz (L_{eq}) during the period from 26 September 2015 to 31 December 2015. The red arrow indicates the period from 26 September 2015 to 26 October 2015, when dredging activities were done in the Port of Koper. NM, nautical miles.*

Koper during the following periods: 18–31 August 2016 and 22–29 September 2016.

The results presented on these diagrams (Figures 2–6) are interpreted and discussed in the subsection Discussion.

The average equivalent continuous underwater noise levels in 1/3-octave bands with centre frequencies of 63 Hz and 125 Hz were higher in the intervals by ≈ 11 dB ($L_{eq,63\ Hz}$) and 5 dB ($L_{eq,125\ Hz}$) when dredging activities took place than in the intervals when these activities were absent (Table 4). In addition, the average equivalent continuous underwater noise levels, were for 7 dB ($L_{eq,63\ Hz}$) and 7 dB ($L_{eq,125\ Hz}$), lower in the intervals, when cleaning activities took place than in the intervals when these activities were absent (Table 4).

The relationship of the measured ambient low-frequency noise levels with the meteorological factors is depicted in the diagrams (Figures 7–11) of the average hourly wind speeds and average hourly precipitation in each measuring period, in combination with the average hourly continuous underwater noise levels in 1/3-octave bands with centre frequencies of 63 Hz and 125 Hz. Blue curve presents $L_{eq,63\ Hz}$, black curve

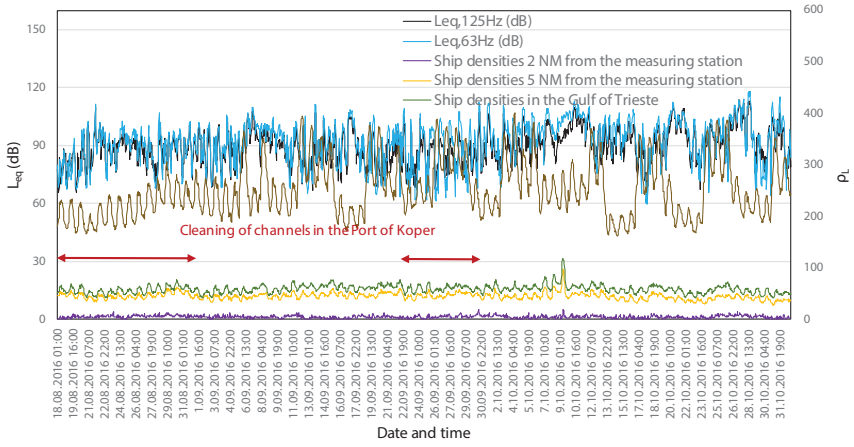

Figure 4. *Diagram of the average hourly ship densities in the areas of 2 NM and 5 NM from the measuring station in the Gulf of Trieste and the Gulf of Venice in combination with the average hourly continuous underwater noise levels in 1/3-octave bands with centre frequencies of 63 Hz and 125 Hz (L_{eq}) during the period from 18 August 2016 to 1 November 2016. The red arrows indicate the periods 18–31 August 2016 and 22–29 September 2016, during which cleaning of the channels in the Port of Koper was performed. NM, nautical miles.*

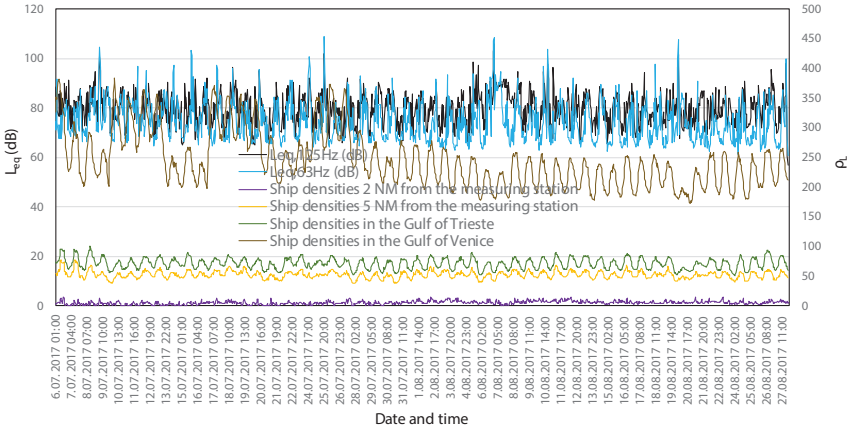

Figure 5. *Diagram of the average hourly ship densities in the areas of 2 NM and 5 NM from the measuring station in the Gulf of Trieste and the Gulf of Venice in combination with the average hourly continuous underwater noise levels in 1/3-octave bands with centre frequencies of 63 Hz and 125 Hz (L_{eq}) during the period from 6 July 2017 to 27 August 2017. NM, nautical miles.*

presents $L_{eq,125\ Hz,}$ brown curve presents wind speed and green columns on the x-axis present precipitation. The results presented in these diagrams (Figures 7–11) are discussed in the subsection Discussion.

Discussion

In this section, the relationship between the pressures in the Slovenian Sea that arise from anthropogenic activities (ship densities, dredging activities and cleaning of the seafloor) and the equivalent continuous levels of underwater noise in 1/3-octave bands with centre frequencies of 63 Hz ($L_{eq,63\ Hz}$) and 125 Hz ($L_{eq,125\ Hz}$) (dB) is discussed. Furthermore, the relationship between the continuous underwater noise levels and the meteorological parameters (wind speed (m/s) and precipitation (mm)) is also commented upon.

The average continuous underwater noise levels ($L_{eq,63\ Hz}$ and $L_{eq,125\ Hz}$) measured in the Slovenian Sea (Table 2) were similar to those reported in the literature, which were found to be associated with the shipping noise [1–21]. Large variations of the $L_{eq,63\ Hz}$ levels were highly related to variations of the $L_{eq,125\ Hz}$

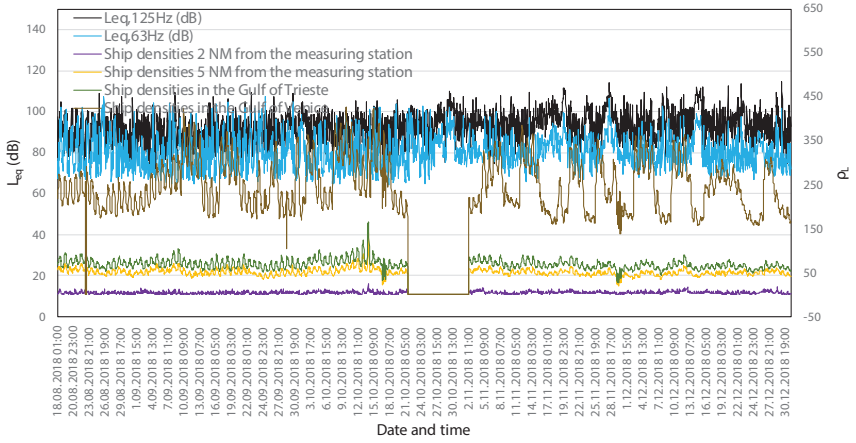

Figure 6: *Diagram of the average hourly ship densities in the areas of 2 NM and 5 NM from the measuring station in the Gulf of Trieste and the Gulf of Venice in combination with the average hourly continuous underwater noise levels in 1/3-octave bands with centre frequencies of 63 Hz and 125 Hz (L_{eq}) in the period from 18 August 2018 to 31 December 2018. NM, nautical miles.*

Table 4: *The results of AVE and STDEV calculations of $L_{eq,63\ Hz}$ and $L_{eq,125\ Hz}$ in the periods with and without the anthropogenic activity*

Type of the anthropogenic activity	*AVE* & *STDEV* of $L_{eq,63\ Hz}$ during the period of anthropogenic activity	*AVE* & *STDEV* of $L_{eq,63\ Hz}$ during the period without anthropogenic activity
Dredging	26.9.2015–26.10.2015 (7:00–21:00 h) $L_{eq,63\ Hz}$ = 89.4 ± 16.9 dB re 1 µPa $L_{eq,125\ Hz}$ = 88.6 ± 10.1 dB re 1 µPa	26.9.2015–26.10.2015 (22:00–6:00 hr) $L_{eq,63\ Hz}$ = 79.5 ± 13.5 dB re 1 µPa $L_{eq,125\ Hz}$ = 83.3 ± 7.2 dB re 1 µPa 27.10.2015–31.12.2015 (00:00–24:00 hr) $L_{eq,63\ Hz}$ = 78.5 ± 12.9 dB re 1 µPa $L_{eq,125\ Hz}$ = 83.5 ± 7.0 dB re 1 µPa
Cleaning of the seafloor	18.8.2016–31.8.2016 (8:00–16:00) 22.9.2016–29.9.2016 (8:00–16:00) $L_{eq,63\ Hz}$ = 94.3 ± 12.3 dB re 1 µPa $L_{eq,125\ Hz}$ = 90.6 ± 8.6 dB re 1 µPa	18.8.2016–31.8.2016 (17:00–7:00) 22.9.2016–29.9.2016 (17:00–7:00) 30.9.2016–1.11.2016 (00:00–24:00 hr) $L_{eq,63\ Hz}$ = 101.4 ± 14.7 dB re 1 µPa $L_{eq,125\ Hz}$ = 97.7 ± 12.5 dB re 1 µPa

AVE, average value; STDEV, standard deviation.

levels (Figures 2–6). Average hourly continuous underwater noise levels ($L_{eq,63\ Hz}$ and $L_{eq,125\ Hz}$) presented in Figures 2–6 show that the levels of $L_{eq,63\ Hz}$ were, for most of the measured days, lower than $L_{eq,125\ Hz}$, which is in accordance with the data presented in Table 2. This can be explained by the fact that the propagation of underwater noise in the shallow seawater at 63 Hz is lower than that at 125 Hz.

The results of this study showed that average equivalent continuous underwater noise levels were higher in the intervals by 11 dB (Leq,63 Hz) and 5 dB (Leq,125 Hz) when dredging activities took place, than in the intervals when these activities were absent. Furthermore, the average equivalent continuous underwater noise levels were found to be lower in the intervals when cleaning activities took place, than when such activities were absent (Table 4). This finding indicated that cleaning activities were not related to the underwater noise levels. This might be explained by the fact that cleaning of the seafloor was performed with an excavator from the mainland.

The lowest average ship densities were measured within the areas of the radii of

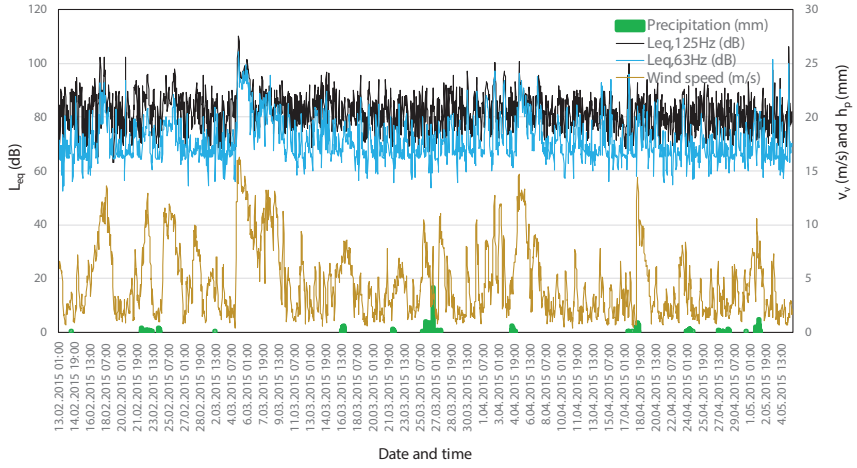

Figure 7: *Diagram of the average hourly wind speeds (v_v) and average hourly precipitation (h_p) in combination with the average hourly continuous underwater noise levels in 1/3-octave bands with centre frequencies of 63 Hz and 125 Hz (L_{eq}) during the period from 12 February 2015 to 5 May 2015.*

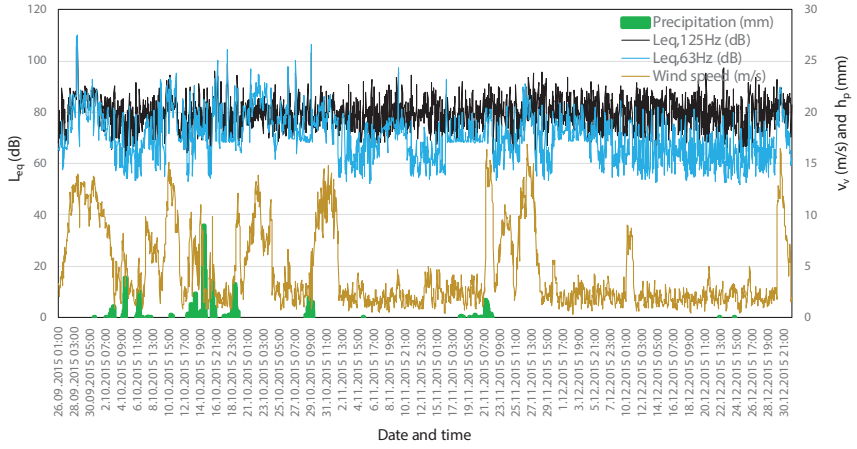

Figure 8: *Diagram of the average hourly wind speeds (v_v) and average hourly precipitation (h_p) in combination with the average hourly continuous underwater noise levels in 1/3-octave bands with centre frequencies of 63 Hz and 125 Hz (L_{eq}) in the period from 26 September 2015 to 31 December 2015.*

2 NM and 5 NM from the measuring station, while higher ship densities were observed in the Gulf of Trieste; the maximum ship densities were observed in the Gulf of Venice, as expected (Table 2). The most likely reason underlying the fact that variation in underwater noise levels was partly related to the variation of the ship densities (Figures 2–6), could be the relatively small acoustic propagation in the shallow sea [45, 46]. Acoustic propagation in shallow water environments was reported to be complex because of interference due to seafloor and sea surface sound reflections and sound transmission losses [47, 48]. Shallow water channels do not allow propagation of low-frequency signals due to the wave-guide effect; this implies that there would be a lower cut-off frequency below which sound waves would not propagate, since the sound propagates into the sea bed [49, 50]. This phenomenon leads to the less significant contribution of shipping to underwater noise.

Figures 7–11 demonstrate that precipitation is not greatly associated with the fluctuations in continuous underwater noise levels, while some larger deviations in the wind speed are associated with the larger fluctuations in continuous underwater noise levels. This could be explained by the fact that wind blowing over the sea generates waves that,

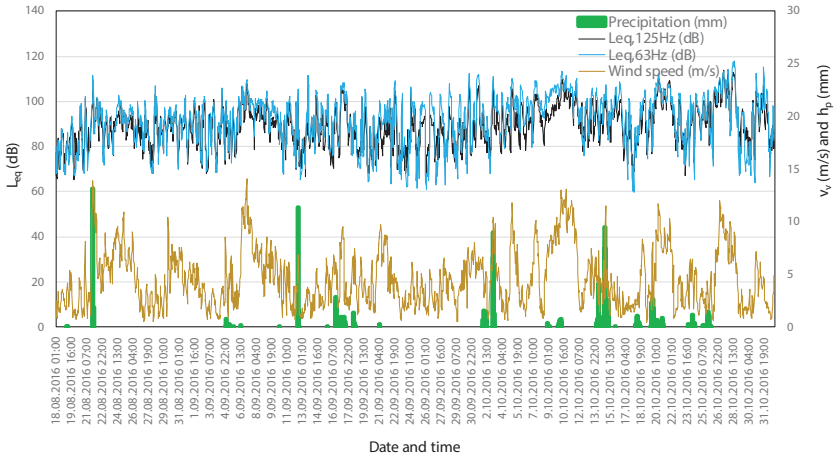

Figure 9: *Diagram of the average hourly wind speeds (v_v) and average hourly precipitation (h_p) in combination with the average hourly continuous underwater noise levels in 1/3-octave bands with centre frequencies of 63 Hz and 125 Hz (L_{eq}) in the period from 18 August 2016 to 1 November 2016.*

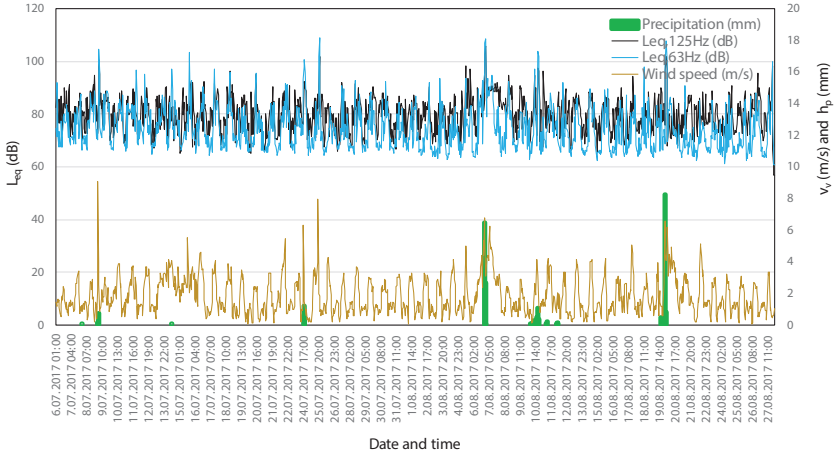

Figure 10: *Diagram of the average hourly wind speeds (v_v) and average hourly precipitation (h_p) in combination with the average hourly continuous underwater noise levels in 1/3-octave bands with centre frequencies of 63 Hz and 125 Hz (L_{eq}) in the period from 6 July 2017 to 27 August 2017.*

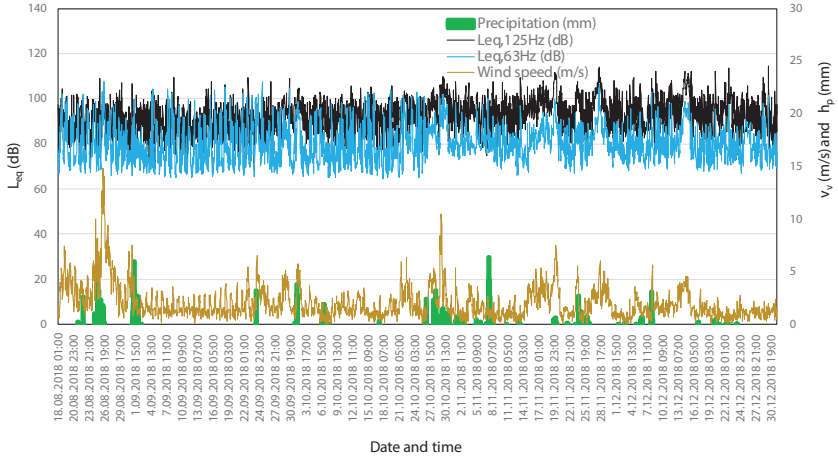

Figure 11: *Diagram of the average hourly wind speeds (v_v) and average hourly precipitation (h_p) in combination with the average hourly continuous underwater noise levels in 1/3-octave bands with centre frequencies of 63 Hz and 125 Hz (L_{eq}) in the period from 18 August 2018 to 31 December 2018.*

when they are large enough, break and produce underwater sound. This phenomenon is well described in several previous studies [7, 9, 22–25].

Conclusion

The results of our study have indicated that the underwater noise levels in the Slovenian Sea are related to dredging activity in the Port of Koper and are partly related to variations of the ship densities. Some larger deviations in the wind speed were found to be associated with the larger fluctuations in continuous underwater noise levels, while precipitation was not related to the underwater noise. Use of larger data sets is suggested to ensure that it becomes possible to further study and evaluate underwater noise levels in relation to man-made or natural sound sources.

Acknowledgements

The current study was funded by the Ministry for the Environment and Spatial Planning, Slovenia. The AIS data from the year 2015 were obtained by the BALMAS project partnership. The AIS data from 2016 to 2018 were obtained by the Slovenian Maritime Administration in the frame of the Ministry for Infrastructure.

References

[1] Southall, B.L., Scholik-Schlomer, A.R., Hatch, L., Bergmann, T., Jasny, M., Metcalf, K., Weilgart, L., Wright A.J. (2017): Underwater noise from large commercial ships—International Collaboration for Noise Reduction. In: *Encyclopedia of Maritime and Offshore Engineering*, John Wiley & Sons, DOI:10.1002/9781118476406.emoe056.

[2] Garrett, J.K., Blondel, P., Godley, B.J., Pikesley, S.K., Witt, M.J., Johanning, L. (2016): Long term underwater sound measurements in the shipping noise indicator bands 63 Hz and 125 Hz from the port of Falmouth Bay, UK. *Marine Pollution Bulletin*, 110(1), pp. 438–448, DOI:10.1016/j.marpolbul.2016.06.021.

[3] Merchant, N.D., Blondel, P., Dakin, D.T., Dorocicz, J. (2012): Averaging underwater noise levels for environmental assessment of shipping. *The Journal of the Acoustical Society of America*, 132(4), pp. 343–349, DOI:10.1121/1.4754429.

[4] Abrahamsen, K., Norway, H. (2012): The ship as an underwater noise source. In: *Proceedings of the 11th European Conference on Underwater Acoustics*. Edinburgh, Scotland, 02–06 July 2012, DOI:10.1121/1.4772953.

[5] McKenna, M.F., Ross, D., Wiggins, S.M., Hildebrand, J.A. (2012): Underwater radiated noise from modern commercial ships. *The Journal of Acoustical Society of America*, 131(1), pp. 92–103, DOI:10.1121/1.3664100.

[6] Bardyshev, V.I. (2008): Underwater surf noise near sea coasts of different types. *Acoustical Physics*, 54(6), pp. 939–948, DOI:10.1134/S1063771008060109.

[7] Dahl, P.H., Miller, J.H., Cato, F.H., Andrew, R.K. (2007): Underwater ambient noise. *Acoustics Today*, 3(1), pp. 23–33.

[8] Wenz, G.M. (1962): Acoustic ambient noise in the ocean: Spectra and sources. *The Journal of the Acoustical Society of America*, 34(12), pp. 1936–1956, DOI:10.1121/1.1909155.

[9] National Research Council. (2003): Committee on potential impacts of ambient noise in the ocean on marine mammals. *Ocean Noise and Marine Mammals*. National Academies Press: Washington.

[10] Estabrook, B.J., Ponirakis, D.W., Clark, C.W., Rice, A.N. (2016): Widespread spatial and temporal extent of anthropogenic noise across the Northeastern Gulf of Mexico shelf ecosystem. *Endangered Species Research*, 30, pp. 267–282, DOI:10.3354/esr00743.

[11] Wenz, G.M. (1971): Review of underwater acoustic research: noise. *The Journal of the Acoustical Society of America*, 51(3B), pp. 1010–1024, DOI:10.1121/1.1912921.

[12] Wales, S.C., Heitmeyer, R.M. (2002): An ensemble source spectra model for merchant ship-radiated noise. *The Journal of the Acoustical Society of America*, 111(3), pp. 1211–1231, DOI:10.1121/1.1427355.

[13] Andrew, R.K., Howe, B.M., Mercer, J.A., Dzieciuch, M.A. (2002): Ocean ambient sound: Comparing the 1960s with the 1990s for a receiver off the California coast. *Acoustics Research Letters*, 3(2), pp. 65–70, DOI:10.1121/1.1461915.

[14] McDonald, M.A., Hildebrand, J.A., Wiggins, S.M. (2006): Increases in deep ocean ambient noise in the Northeast Pacific west of San Nicolas Island, California. *The Journal of the Acoustical*

Society of America, 120(2), pp. 711–718, DOI:10.1121/1.2216565.

[15] Ross Chapman, N., Price, A. (2011): Low-frequency deep ocean ambient noise trend in the Northeast Pacific Ocean. *The Journal of the Acoustical Society of America*, 129(5), pp. 161–165, DOI:10.1121/1.3567084.

[16] Andrew, R.K., Howe, B.M., Mercer, J.A. (2011): Long-time trends in ship traffic noise for four sites off the North American West Coast. *The Journal of the Acoustical Society of America*, 129(2), pp. 642–651, DOI:10.1121/1.3518770.

[17] Miksis-Olds, J.L., Nichols S.M. (2016): Is low-frequency ocean sound increasing globally. *The Journal of the Acoustical Society of America*, 139(1), pp. 501–511, DOI:10.1121/1.4938237.

[18] United Nations (2020): Review of Maritime Transport 2019. United Nations Conference on Trade and Development, *United Nations Publication*, pp. 132.

[19] United Nations (2019): Handbook of Statistics 2019 – Maritime transport, United Nations Conference on Trade and Development, *United Nations Publication*.

[20] Berns, S.G., Dragt, J., Van Bergen, T. (2015): Global Trends to 2030 – Impact on Port Industry. Deloitte: China.

[21] EUROSTAT – European statistics [online]. Renewed (2/22/2021) [cited 2/25/2021]. Available on: http://ec.europa.eu/eurostat/data/database.

[22] Prosperetti, A. (1988): Bubble-related ambient noise in the ocean. *The Journal of the Acoustical Society of America*, 84(3), pp. 1024–1054, DOI:10.1121/1.396740.

[23] Carey, W.M., Browning, D.G. (1988): Low-frequency ocean ambient noise: Measurements and theory. In: *Sea Surface Sound*. Kerman, B.R. (ed.). Kluwer Academic: Dordrecht, pp. 361–376.

[24] Banner, M.L., Cato, D.H. (1993): Physical mechanisms of noise generation by breaking waves – a laboratory study. In: *Natural Physical Sources of Underwater Sound – Sea Surface Sound (2nd Edition)*, Kerman, B.R. (ed.). Kluwer Academic: Dordrecht, pp. 429–436.

[25] Medwin, H., Beaky, M.M. (1989): Bubble sources of the Knudsen sea noise spectra. *The Journal of the Acoustical Society of America*, 89, pp. 1124–1130, DOI:10.1121/1.398104.

[26] Ma, B.B., Nystuen, J.A., Lien, R.C. (2005): Prediction of underwater sound levels from rain and wind. *The Journal of the Acoustical Society of America*, 177(6), pp. 3555–3565, DOI:10.1121/1.1910283.

[27] Marley, S.A., Salgado Kent, C.P., Erbe, C., Parnum, I.M. (2017): Effects of vessel traffic and underwater noise on the movement, behavior, and vocalizations of bottlenose dolphins in an urbanized estuary. *Scientific Reports*, 7(1), pp. 13437, DOI:10.1038/s41598-017-13252-z.

[28] Knudsen, V.O., Alford, R.S., Emling, J.W. (1962): Underwater ambient noise. *Journal of Marine Research*, 7(3), pp. 410–429.

[29] Fish, M.P. (1964): Biological sources of sustained ambient sea noise. In: *Marine Bio-Acoustics*, Tavolga, W.N. (ed.). Pergamon: Oxford.

[30] Cato, D.H. (1978): Marine biological choruses observed in tropical waters near Australia. *The Journal of the Acoustical Society of America*, 64(3), pp. 736–743, DOI:10.1121/1.382038.

[31] Au, W.W., Mobley, J., Burgess, W.C., Lammers, M.O., Nachtigall. P.E. (2000): Seasonal and diurnal trends of chorusing humpback whales wintering in waters off Western Maui. *Marine Mammal Science*, 16(3), pp. 530–544, DOI:10.1111/j.1748-7692.2000.tb00949.x.

[32] Erbe, C. (2002): Underwater noise of whale-watching boats and potential effects on killer whales (*Orcinus orca*), based on an acoustic impact model. *Marine Mammal Science*, 18(2), pp. 394–418, DOI:10.1111/j.1748-7692.2002.tb01045.x.

[33] Hallers-Tjabbes, C.C. (2007): Underwater noise from maritime sources and impact on marine life. *WMU Journal of Maritime Affairs*, 6(2), pp. 225–233, DOI:10.1007/BF03195117.

[34] Directive of the European Parliament and of the Council (2008/56): Establishing a framework for community action in the field of marine environmental policy (Marine Strategy Framework Directive), *Official Journal of the European Union*, 25. 6. 2008, L164, pp. 19–40.

[35] IMO, MEPC.1/Circ.833 (2014): Guidelines for the reduction of underwater noise from commercial shipping to address adverse impacts on marine life. International Maritime Organization (IMO), London, pp. 6.

[36] Water Act (2015): *Official Gazette of the Republic of Slovenia*, No. 67/2002, 57/2008, 57/2012, 100/2013, 40/2014 and 56/2015, pp. 117.

[37] Decree on the detailed content of the Marine management plan (2013): *Official Gazette of the Republic of Slovenia,* No. 92/2010 and 20/2013, pp. 13.

[38] Deželak, F., Čurović, L., Jenko, J. (2015): Strokovne podlage za vzpostavitev sistema nadzora nad podvodnim hrupom v skladu z Direktivo o morski strategiji (2008/56/ES), Rezultati četrtletnih

kontinuiranih meritev podvodnega hrupa na merilni postaji, Inštitut za vode Republike Slovenije, Ljubljana, pp. 22.

[39] Popit, A., Zupančič, G. (2018): Brief review of the Slovenian approach to data pre-processing, data processing and presentation of noise indicator data. *Quietmed Project Internal Report*.

[40] Bruel & Kjaer (2016): Hand-held analyzer types 2250, 2250-L and 2270. *Instruction Manual*, pp. 140.

[41] Robinson, S.P., Lepper, P.A., Hazelwood, R.A. (2014): Good practice guide no. 133 – Underwater noise measurement. *National Physical Laboratory*. pp. 95.

[42] Commission Decision laying down criteria and methodological standards on good environmental status of marine waters and specifications and standardized methods for monitoring and assessment, and repealing Decision 2010/477/EU (EC/2017/848): *Official Journal of the European Union*, 18. 5. 2017, L125, pp. 43–74.

[43] Dekeling, R., Tasker, M., Van der Graaf, S., Ainslie, M., Andersson, M., André, M., Borsani F., Brensing, K., Castellote, M., Cronin, D., Dalen, J., Folegot, T., Leaper, R., Pajala, J., Redman, P., Robinson, S., Sigray, P., Sutton, G., Thomsen, F., Werner, S., Wittekind, D., Young, J.V. (2014): Monitoring guidance for underwater noise in European Seas, Part I: Executive Summary, *JRC Scientific and Policy Report*, EUR 26557 EN, Publications Office of the European Union, Luxembourg, pp. 16.

[44] Pirc, S. (1997): Statistika v geologiji: Učni pripomoček. Univerza v Ljubljani, Naravoslovnotehniška fakulteta, Oddelek za geologijo, Ljubljana, pp. 59.

[45] Merchant, N.D., Brookes, K.L., Faulkner, R.C., Bicknell, A.W.J., Godley, B.J., Witt, M.J. (2016): Underwater noise levels in UK waters. *Scientific Reports*, 6, 36942, DOI:10.1038/srep36942.

[46] Kozaczka, E., Grelowska, G. (2018): Propagation of ship-generated noise in shallow sea. *Polish Maritime Research*, 25, pp. 37–46, DOI:10.2478/pomr-2018-0052.

[47] Meyer, V., Audoly, C. (2017): A comparison between experiments and simulation for shallow water short range acoustic propagation. In: *ICSV 24th, International Congress on Sound and Vibration*, London, United Kingdom.

[48] Duncan, A.J., Gavrilov, A.N., McCauley, R.D, Parnum, I.M. (2013): Characteristics of sound propagation in shallow water over an elastic seabed with a thin cap-rock layer, *The Journal of the Acoustical Society of America*, 134(1), pp. 207–215, DOI:10.1121/1.4809723.

[49] Urick, R.J. (1983): Principles of underwater sound. 3rd edn. McGraw-Hill: New York.

[50] Robinson, S.P., Lepper, P.A. (2013): Scoping study: Review of current knowledge of underwater noise emissions from wave and tidal stream energy devices. *Technical Report*, September 2013, The Crown Estate: London, pp. 71.

Original scientific paper

Received: Mar 24, 2021
Accepted: Mar 24, 2021
DOI: 10.2478/rmzmag-2020-0020

Monitoring after the conclusion of mining works

Monitoring po opustitvi rudarskih del

Tomaž Hribar[1,*], Tomaž Pečolar[1], Goran Vižintin[2]

[1] Institute for Mining, Geotechnology and Environment, Slovenčeva 93, 1000 Ljubljana, Slovenija
[2] University of Ljubljana, Faculty of Natural Sciences and Engineering, Aškerčeva 12, 1000 Ljubljana, Slovenija
*tomaz.hribar@irgo.si

Abstract

After mining works are completed and the mine is permanently closed, the holder of the mining rights must carry out monitoring in accordance with the applicable legislation and for the purpose of controlling the extraction area. This includes monitoring of the changes that have occurred during the process of mining, both on the surface and below it. This article presents an example of a monitoring program after the mining works are completed. The extraction of raw mineral material in an underground mine results in various impacts on the surface and underground space. The areas or segments of monitoring are divided into two parts in this article: The underground part includes monitoring of the geomechanical, climatic, and hydrogeological changes, while monitoring on the surface requires special attention to be paid to the stability conditions of the surface above old mine works and hydrogeological conditions in the area above the extraction or impact area. A practical example of the monitoring program that needs to be made when a mine closes is given in the article. The program covers areas, presents the ways and methods of measurement, as well as reporting of the measurements. The analysis procedure of already existing measurements, which need to be analyzed and included in the preparation of the monitoring program, is also presented.

Key words: monitoring, stability, extraction area, measurement method

Povzetek

Po opustitvi rudarskih del in trajnem zaprtju rudnika mora nosilec rudarske pravice skladno z veljavno zakonodajo in z namenom nadzorovanja pridobivalnega prostora izvajati monitoring. Monitoring obsega spremljavo sprememb, ki so nastale ob izvajanju rudarskih del, tako na površini kot pod njo.

V članku so predstavljena izhodišča za izdelavo programa monitoringa po opustitvi rudarskih del. Pridobivanje mineralne surovine v podzemnem rudniku ima za posledico različne vplive na površino in podzemni prostor. Področja oziroma segmenti monitoringa so v nalogi razdeljeni v dva dela. Jamski del spremljave obsega spremljavo geomehanskih, klimatskih in hidrogeoloških sprememb. Podobno je potrebno predvideti spremljavo dogajanj na površini, kjer je posebna pozornost posvečena stabilnostnim razmeram površine nad jamskimi deli in hidrogeološkim razmeram v območju pridobivalnega prostora oziroma vplivnem območju.

Podan je praktičen prikaz programa monitoringa, ki ga je potrebno izdelati ob zaprtju rudnika. V programu so zajeta področja, predstavljeni načini in metode meritev, kakor tudi poročanje o le teh. Prav tako je predstavljen postopek analize že obstoječih meritev, ki jih je potrebno analizirati in vključiti v izdelavo programa monitoringa.

Ključne besede: monitoring, stabilnost, pridobivalni prostor, metoda meritev

Introduction

In the field of mining, during its operation and gradual closure, it is necessary to prepare technical mining documentation in the form of projects and programs to monitor the effects of mining on the underground and surface areas for different periods [1]. With regard to the type of mining and the method of closing the mine, further impact monitoring is required. For this, it is necessary to develop a program on which further monitoring and measurements will be based [1].

Due to montangeological conditions, it is not yet possible to leave underground areas completely unattended during the mine closure phase. Based on previous experience, it is indicated by both geomechanical and hydrological developments in the areas of operation of individual mines that the impact trend does not slow down with the closure of the mine, and hence further monitoring is needed. The effects of mining are manifested on the surface in the form of deformations, hydrological phenomena, and stability effects on structures or terrain configuration [1, 2].

Generally, mines already have an established system for monitoring their impacts at the extraction area, in the form of a concession deed and a contract. This system needs to be analyzed, updated, and give detailed further procedures for monitoring. In this way, we can determine which areas are suitable for further use in other fields and which areas need continued protection.

A network of observations must be established in the wider area of the mine throughout the mining process as well as during its gradual closure. This covers the areas both below and above the surface of the entire extraction area, but they are divided by individual excavation fields or caves. Impact measurements are carried out on individual segments, such as visual observations, deformation measurements, and hydrological and geomechanical conditions [1–3].

The measurement results of individual areas and segments need to be combined, comprehensively analyzed, and the basis for further categorization of the impact area given. Measurements and observations of both the underground and surface areas, which contain data on the movements, inflows, flows, and levels of groundwater and surface water, as well as changes in the geomechanical characteristics of the area, must be collected and analyzed. The results of the analyses must be presented in the monitoring program in such a way that it is possible to categorize the impacts, which are divided into individual categories.

Based on the measurement results analysis, it is necessary to determine the critical or limit

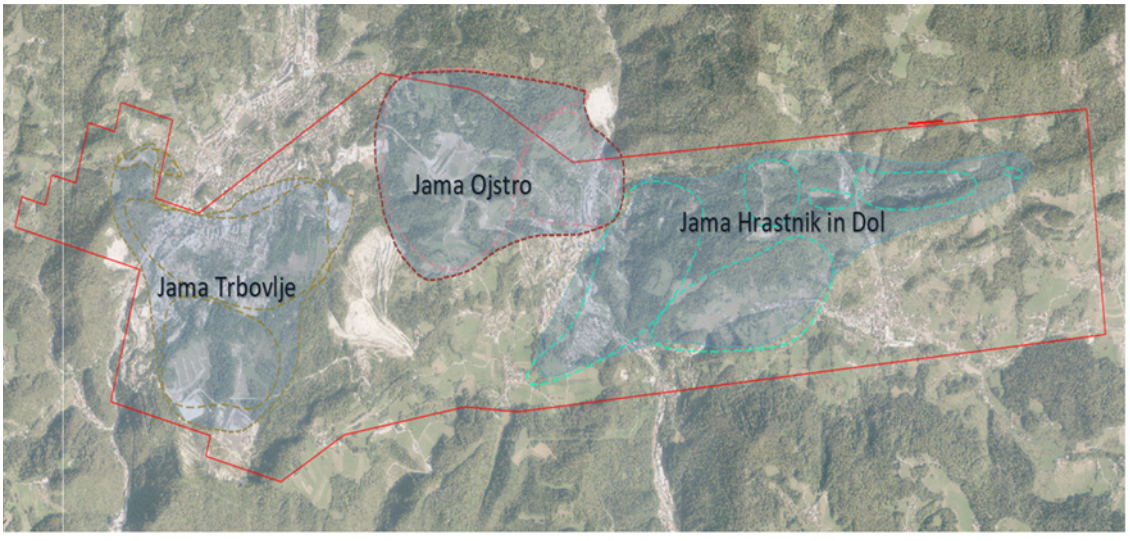

Figure 1: *Depiction of the RTH extraction area and areas of underground work [1].*

values of the individual observation parameters for movements, flows or water levels, and the geomechanical characteristics of the materials for each category [2].
A practical example of preparing a monitoring program for the RTH coal mine is shown in the article.
The monitoring program includes monitoring the impacts of mining both in the underground and on the surface area of the RTH extraction area. The underground part comprises four caves, while the surface area covers the entire extraction area through two municipalities. The area we address in this article is both an erosion and an impact area.
The preparation of the monitoring program considers all applicable legislation, rules, standards, and existing technical documentation, as well as geological and geotechnical data obtained from previous measurements in this area.

Monitoring system

The monitoring activities prescribed by the program must be carried out on the underground part and on the surface by individual segments and later defined into categories based on the analysis of the results. The segments are as follows [1–3]:
Visual inspections on the underground and surface areas;
— Underground climate control;
— Geotechnical measurements of underground structures and of the surface area;
— Hydrological measurements in the mine and on the surface;
— Surface movement measurements.

The measurement methods and equipment are defined in the monitoring program for individual observations and segments of measurements. Consequently, and with regard to the nature of the observed area, the specificity of an individual measurement and observation, and the accuracy and frequency of an individual measurement are determined.
The monitoring program defines the interpretation of the results of individual areas and segments. Furthermore, it defines how the measurement results are placed in the impact categorization.
Visual inspections must be carried out in the open sections of individual caves and on the entire surface of the extraction area, as prescribed in the monitoring program. Attention should be paid to the permanent structures in the cave, such as transport routes and paths intended for drainage. Surveys of the surface area are carried out with patrols, which can be a problem, as some areas are more difficult to access. During patrols of the underground parts, climate measurements are performed by recording possible gases, the temperature, and wind direction and strength.
Geotechnical measurements in the underground and surface areas are carried out in accordance with the program and include the following [1]:
— Deformation measurements of underground areas (extensometers, dynamometers, and measuring anchors);
— Surface stability measurements (inclinometers);
— Hydrogeological measurements in the mine (measurements of flows, inflows, and outflows of water);
— Hydrogeological measurements on the surface (piezometers, flows and water levels, physical and chemical properties of water);
— Surface movement measurements (classical terrestrial methods, GNSS, UAVs).

Figure 2 shows the surface deformations due to underground works, which must be monitored in accordance with the monitoring program by using inclination measurements and geodetic methods.
When surveying surface movements, classical geodetic and GNSS equipment are used, by which the measurement methods and procedures are known. In recent times, there has been potential in using unmanned aerial vehicles, which make visual and measurement observations much easier. However, they cannot be used for creating images of the entire RTH extraction space, as a large part of the area is inhabited, and at the same time there would be too much data captured, which would be difficult to process. This method is suitable for hard-to-reach areas, where an individual sur-

Table 1: *The scope of unmanned aerial vehicle uses in mining [4].*

Surface mines	Underground mines	Closed mines
- Mine operation	- Geotechnical characterization	- Land subsidence monitoring
- 3D mapping	- Rock size distribution	- Recultivation
- Bank stability	- Monitoring and measurement of gases	- Surface mapping
- Mine safety	- Mine rescuing	- Detecting gas pockets
- Structure monitoring		- Acid leakage monitoring
- Facility management		

Figure 2: *Surface deformations.*

face could be inspected visually and measured in a relatively short time.

Alternative observation method

Observations of surface changes both underground and on the surface can be carried out with relatively simple newer methods of monitoring and observations using unmanned aerial vehicles. Recently, this method has become a more established one and for which we can determine relative as well as absolute changes with the help of surface model analyses. The problem that arises when using aerial recordings is in the large amount of data, accuracy, and relatively demanding equipment. Furthermore, these methods may be limited due to legislation that restricts the use of unmanned aerial vehicles in urban areas.

Recordings of the state of the area in different periods can be captured with advanced aerial photography technology using unmanned aerial vehicles, which capture point clouds and photo-document the state of the surface. The results of aerial photography are presented in various visualization forms such as point clouds, 3D area models (digital surface model) and DOF (digital ortho photo). We combine all this in AutoCAD Civil 3D, where we get a high-quality base for calculating masses. Table 1 gives the areas where unmanned aerial vehicles are used in mining and Figure 3 shows examples of some unmanned aerial vehicles.

Due to its content and method of processing, observations with the help of unmanned aerial vehicles interfere with the field of GIS (Geographic Information System) or computer-aided spatial information systems, which provide a modern management, organizational, and business basis for capturing, storing, searching, processing, analyzing, displaying, and disseminating spatial data. The emphasis is on various analyses of spatial data [5].

Aerial photography with unmanned aerial vehicles means a noncontact photogrammetric capture of spatial data. The results of the overflight are aerial photographs of the area taken with a digital camera attached to the vehicle. Due to image matching, individual photos must overlap by at least 65%. Using image matching and photogrammetric methods, we can orient the bunch of images along both the horizontal and height axes. Thus, we obtain volume data in a relative coordinate system, which is oriented into the national coordinate system with the help of classical or GNSS technologies [4].

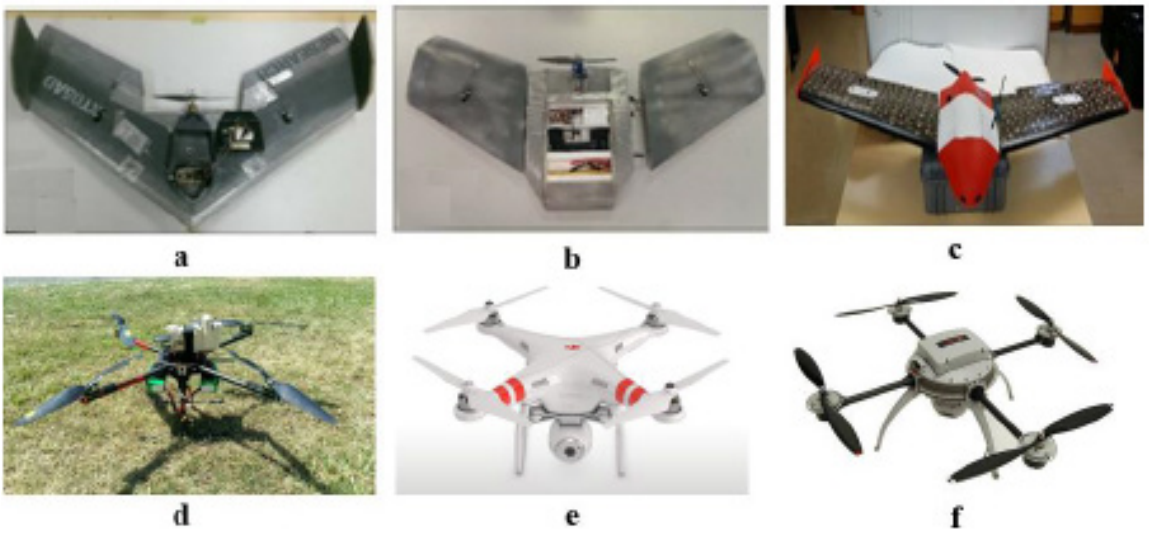

Figure 3: *Unmanned aerial vehicles suitable for surface use: (A) Teklite, (B) GoSurv, (C) Swamp Fox, (D) Quadcopter, (E) Phantom 2 Vision+, and (F) Aeryon Scout [4].*

Field data, measured with an unmanned aerial vehicle within different periods, is imported into AutoCAD CIVIL 3D as a cloud of points. Surface modeling is performed using the geostatic surface adjustment method.

The basic idea is in the detailed recognition of some characteristics of the general course of the surface, which is to be determined from the data. These findings are used to estimate and determine values on missing or undefined parts of the surface. In the kriging method, the most important criterion is the smoothness of the surface, which we try to ensure by using statistical methods. Kriging is not a method that can be used automatically and without understanding the given area, as it requires the user to be present and actively participate in certain decisions [6].

As a result of modeling individual captured images, surface models of different periods (DMRs) are obtained [7]. We attach these images on the same points on the edges, which enables us to compare the volumes between different time measurements. AutoCAD CIVIL 3D allows us to compare different surface models as a composite grid of points in the base model (existing state) and comparative models (derived state) [8]. The volume of the mathematical formation of the surface difference is defined by the exact height differences of any point of the model. Both the capturing method and the DMR modeling method must be defined in advance by the monitoring program and are conditioned by the terrain configuration itself [9].

Monitoring area categorization

The monitoring area categorization parameters are based on the results and interpretation of the impact measurements of individual segments and areas [10]. The combined data of individual segments and areas are comprehensively analyzed, and the impact area categorization basis is provided [11].

The impact categories are as follow:

— Category I: The observation parameters are above the permitted values and cause instability of the terrain, so that further intensive monitoring and ongoing remediation of the area is required.
— Category II: The observation parameters are within the limit values and still affect the lability of the terrain, so further monitoring and, if necessary, remediation of the area is required.
— Category III: The observation parameters are below the limit values and no further observations are required.

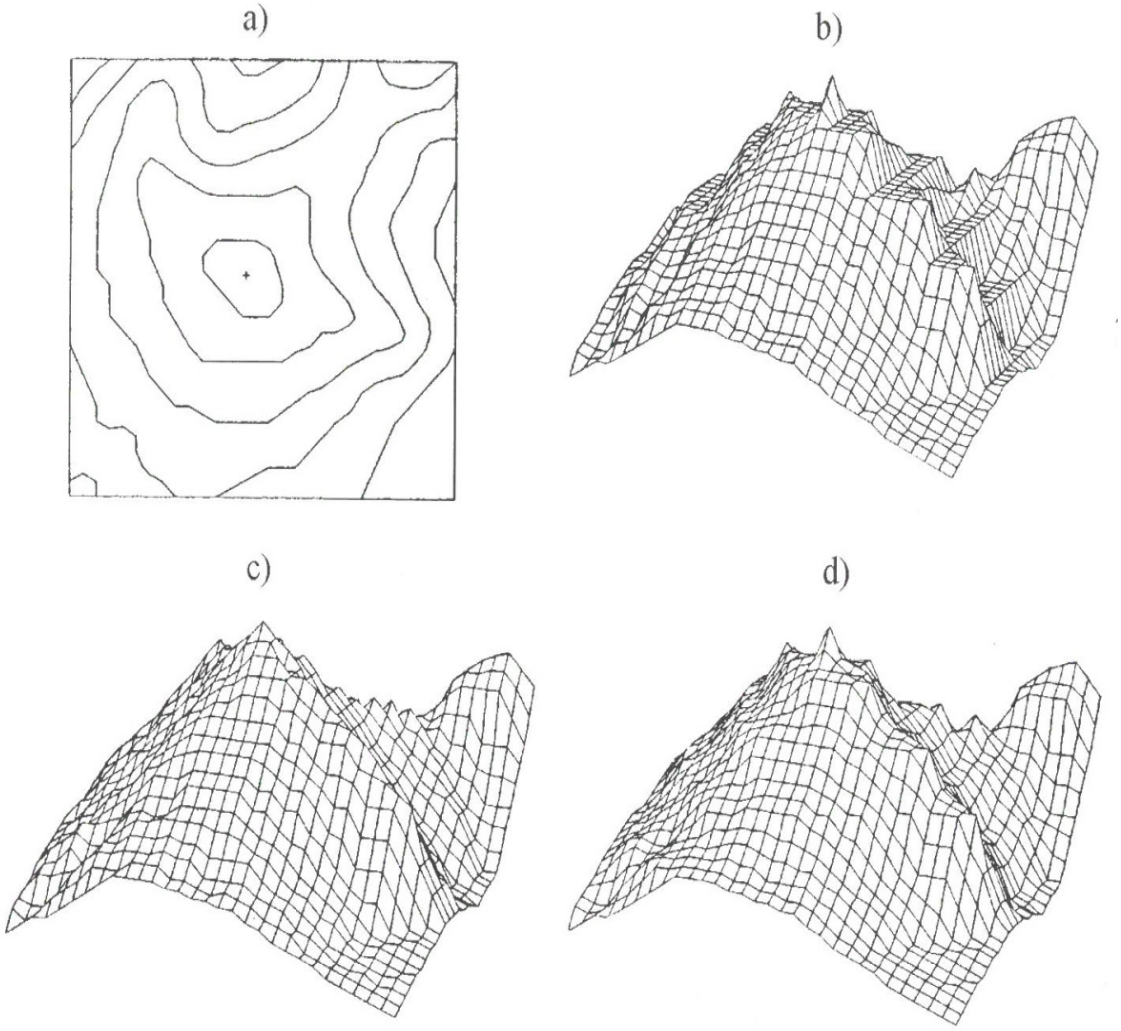

Figure 4. *DMR display made with different interpolation algorithms.* **(A)** *Isohypse of a hypothetical area.* **(B)** *DMR constructed by vertical scanning algorithms.* **(C)** *DMR constructed by maximum slope algorithms.* **(D)** *DMR produced by the weighted average algorithm [5].*

— Category IV: The observation parameters show that the area is suitable for further use for other purposes as well.

A summary of the limits of the individual categories for movements and inclinations is given in Table 2.

The interpretation of measurements must be carried out based on the periodic measurement reports of individual segments, performed by a professionally trained team, which also leads and coordinates the measurements [12].

The purpose of the measurements is to follow the time development of deformations on the surface, in the surface layers in critical areas, as well as in the entire extraction area. It is necessary to unambiguously determine the stability situation in populated areas, both within the security pillars and beyond.

The basic criterion for determining additional measurements is the time development of the measured parameters of all measurements. Since the measurements are carried out on different geological surfaces, it is impossible to give a general criterion of the permitted movement of the terrain in length units where it is necessary to act with mining or construction works.

Table 2: *Impact categorization [1].*

	Category [Limit]			
Segment	**I**	**II**	**III**	**IV**
Movement measurements	Above 50 mm, also new measurement sites	Up to 50 mm and deformation trend	Up to 20 mm and deformation trend	Below 20 mm
Inclinometer measurements	Above 50 mm, also new measurement sites	Up to 50 mm and deformation trend	Up to 20 mm and deformation trend	Below 10 mm

Figure 5: *Remediated area above the mining area.*

Conclusion

To monitor the impacts of mining in the wider area of the mine, it is necessary to prepare technical mining documentation in the form of a monitoring program during its operation and during the implementation of its gradual closure.

A network of observations must be established in the wider area of the mine throughout the mining process and the gradual closure of the mine. This covers the area both below the surface and on the surface of the entire extraction area, by individual excavation fields or caves. Impact measurements are carried out by individual segments, such as visual observations, deformation measurements, and hydrological and geomechanical conditions.

Based on the analysis of the measurement results, critical or limit values of individual observation parameters for movements, flows or water levels, and geomechanical characteristics of materials are determined for each category and are as follows:

Category I: The observation parameters are above the permitted values and cause instability of the terrain, so that further intensive monitoring and ongoing remediation of the area is required.

Category II: The observation parameters are within the limit values and still affect the lability of the terrain, so further monitoring and, if necessary, remediation of the area is required.

Category III: The observation parameters are below the limit values and no further observations are required.

Category IV: The observation parameters show that the area is suitable for further use for other purposes as well.

The article shows a practical example of preparing a monitoring program for the RTH coal mine. The monitoring program analyzes the performed works and defines the areas where the works are still being carried out or have already been carried out, and then adjusts the monitoring activities accordingly.

Measurement methods and equipment must be defined in the monitoring program for individual observations or measurement segments. Consequently, and with regard to the nature of the observed area, the specificity of individual measurement methods and observations, and the accuracy and frequency of individual measurements are determined.

The monitoring program also defines the interpretation of the results of individual areas and segments and predicts the way in which the measurement results must be placed in the impact categorization.

References

[1] Hribar, T. (2018): *Program monitoringa na območju Pridobivalnega prostora RTH za obdobje 2018 do 2023*. IRGO: Ljubljana, 106 p.

[2] RP (1996): *Meritev posedkov in premikov ter določitev ukrepov v primeru anomalij, št. 21/409/02-96/LF*. IRGO: Ljubljana.

[3] Poročilo o izvedbi študije (2001): *Dvigovanje podtalnice po prenehanju črpanja vode v AB polju jame Trbovlje, št. GV7210 641 IS/210 610*. IRGO: Ljubljana.

[4] Shahmoradi, J., Talebi, E., Raghanchi, P., Hassanalian, M. (2020): A Comprehensive review of applications of drone technology in the mining industry. *Drones*, 4(3), pp. 2–25, DOI:10.3390/drones4030034.

[5] Kvamme, K., Oštir-Sedej, K., Stančič, Z., Šumrada, R. (1997): *Geografski informacijski sistemi*. Znanstvenoraziskovalni center SAZU, 476 p.

[6] Zimmerman, D.A., De Marsily, G., Gotway, C.A., Marietta, M.G., Axness, C.L., Beauheim, R.L., Bras, R.L., Carrera, J., Dagan, G., Davies, P.B., Gallegos, D.P., Galli, A., Gómez-Hernández, J., Grindrod, P., Gutjahr, A.L., Kitanidis, P.K., Lavenue, A.M., McLaughlin, D., Neuman, S.P., Ramarao, B.S., Ravenne, C., Rubin, Y. (1998): A comparison of seven geostatistically based inverse approaches to estimate transmissivities for modeling advective transport by groundwater flow. *Water Resources Research*, 34(6), pp. 1373–1413.

[7] Balenović, I., Marjanović, H., Vuletic, D. (2015): Quality assessment of high density digital surface model over different land cover classes. *Periodicum Biologorum*, 117(4), pp. 459–470.

[8] Hargitai, H., Willner, K., Buchroithner, M. (2019): Methods in planetary topographic mapping: A review. In: *Planetary Cartography and GIS*, Horgitai, H. (ed.). Springer International Publishing, pp. 147–174.

[9] James, M.R., Robson, S. (2012): Straightforward reconstruction of 3D surfaces and topography with a camera: Accuracy and geoscience application. *Journal of Geophysical Research: Earth Surface*, 117(F3), pp. 1–17.

[10] Pardo, J.M., Lozano, A., Herrera, G., Mulas, J., Rodríguez, Á. (2013): Instrumental monitoring of the subsidence due to groundwater withdrawal in the city of Murcia (Spain). *Environmental Earth Sciences*, 70(5), pp. 1957–1963.

[11] Tomás, R., Cano, M., García-Barba, J., Vicente, F., Herrera, G., Lopez-Sanchez, J.M., Mallorquí, J.J. (2013): Monitoring an earthfill dam using differential SAR interferometry: La Pedrera dam, Alicante, Spain. *Engineering Geology*, 157, pp. 21–32.

[12] Herrera, G., Álvarez-Fernández, M.I., Tomás, R., González-Nicieza, C., López-Sánchez, J.M., Álvarez-Vigil, A.E. (2012): Forensic analysis of buildings affected by mining subsidence based on Differential Interferometry (Part III). *Engineering Failure Analysis*, 24, pp. 67–76.

Original scientific article

Received: Jan 18, 2021
Accepted: Jan 25, 2021
DOI: 10.2478/rmzmag-2020-0016

Estimation of Depth to Bouguer Anomaly Sources Using Euler Deconvolution Techniques

Ocena globine do virov Bouguerjeve anomalije z uporabo Eulerjevih dekonvolucijskih tehnik

Gideon Oluyinka Layade[1,*], Hazeez Edunjobi[1], Victor Makinde[1], Babatunde Bada[2]
[1]Department of Physics, Federal University of Agriculture, Abeokuta
[2]Department of Environmental Management & Toxicology, Federal University of Agriculture, Abeokuta
*Layadeoluyinka018@gmail.com

Abstract

The geophysical measurement of variations in gravitational field of the Earth for a particular location is carried out through a gravity survey method. These variations termed anomalies can help investigate the subsurface of interest. An investigation was carried out using the airborne satellite-based (EGM08) gravity dataset to reveal the geological information inherent in a location. Qualitative analysis of the gravity dataset by filtering techniques of two-dimensional fast Fourier transform (FFT2D) shows that the area is made up of basement and sedimentary Formations. Further enhancements on the residual anomaly after separation show the sedimentary intrusion into the study area and zones of possible rock minerals of high and low density contrasts. Quantitative interpretations of the study area by 3-D Euler deconvolution depth estimation technique described the depth and locations of gravity bodies that yielded the gravity field. The result of the depth to basement approach was found to be in the depth range of 930 m to 2,686 m (for Structural Index, SI = 0). The research location is a probable area for economic mineral deposits and hydrocarbon exploration.

Key words: gravitational field, intrusion, enhancements, anomalous sources, density contrasts

Povzetek

Izvedene so bile geofizikalne meritve sprememb zemeljskega gravitacijskega polja na določenih lokacijah. Spremembe gravitacijskega polja, imenovane anomalije, so lahko v pomoč pri raziskovanju določenega podzemnega območja. V raziskavi so bili za obravnavano območje uporabljeni podatki gravitacijskega zemeljskega modela (EGM08). Kvalitativna analiza gravitacijskih podatkov s filtracijskimi tehnikami dvo-dimenzionalne hitre Fourierjeve transformacije (FFT2D) prikazuje, da območje sestavljajo kamnine podlage in sedimentne formacije. Nadaljnje analize prikazujejo sedimentne intruzije v obravnavano območje in območja potencialnih kamninskih mineralov z visokim in nizkim kontrastom gostote. Kvantitativna interpretacija obravnavanega območja s tehniko 3D Eulerjeve dekonvolucije razkriva globino in lokacijo gravitacijskih teles, ki vplivajo na spremembo gravitacijskega polja. Rezultat analize je globina do kamninske podlage, ki se nahaja v območju od 930 m do 2,686 m (za strukturni indeks SI = 0). Raziskovana lokacija je potencialno območje za ekonomično pridobivanje mineralnih surovin in raziskovanje ogljikovodikov.

Ključne besede: gravitacijsko polje, intruzija, izboljšave, viri anomalij, kontrast gostote

Introduction

The inherent physical properties of sub-surface media such as sediments, rocks, voids, water, contacts among others are examined through geophysical survey [1]. Among these geophysical surveys is the gravity method which is primarily concerned with measuring gravitational field as part of potential field measurement [2–3]. It tries to determine the nature of the subsurface by relating the measured gravitational fields to density contrasts. Gravity survey can be carried out on the ground and can also be airborne but the airborne survey helps to cover areas that cannot be easily accessible, e.g. on waters [4]. Previous works in the locality have used magnetic method and rock petrography to investigate the study area. A number of techniques can be employed to yield the near surface spread of parameters describing the variations which include the 3-D analytic signal technique [5], Werner deconvolution, [6], 3-D Euler deconvolution, [7] and Multiple Source Werner deconvolution [8].

Qualitatively, the gravity data is interpreted in order to describe and explain some important features which the results of the survey exposed with respect to possible geological formations and structures yielding the anomalies [9]. While the quantitative interpretations involve numerical estimation of the depths and dimensions of anomalous sources. The research is thus, to estimate depths to gravity sources in the area of Abeokuta and environ using Bouguer gravity data. Hence, the application of 3-D Euler deconvolution technique for computing the burial depths of anomalies.

In 1867, Sir Isaac Newton proposed two laws upon which the gravity method is based: the law of universal gravitation that describes the force of attraction between two separate bodies of known masses [10–11] and the law of motion, which relates the applied force to the rate of change of momentum of a body.

Mathematically:

$$F = \frac{GMm}{R^2} \quad (1)$$

Where:

F = force of attraction between two separate bodies

G = constant of gravitation ($G = 6.67 \times 10^{-11}$ Nm^2/kg^2)

M = mass of the earth

m = mass of the second body

R = separating distance

Also, the second law of motion can be expressed as:

$$F = \frac{dp}{dt} \quad (2)$$

Thus:

$$F = \frac{d(mv)}{dt} = mg \quad (3)$$

Where:

F = the applied force of attraction

dp = momentum change

dt = time difference

Equations (1) and (3) give:

$$g = G\frac{M}{R^2} \quad (4)$$

Equation (4) is the gravitational field of the Earth on any mass.

Description and Geologic Setting of the study area.

The location of the study area is represented by Figure 1 within latitude ($7^o.00^l$–$7^o.30$) N and longitude ($3^o.00^l$–$3^o.30$) E spanning 3,025 km^2 area. Basement complex (Abeokuta formation) and sedimentary (Ewekoro formation) respectively are the predominant geological nature of the area [12]. While the older granites which are magmatic in nature are of Precambarian age to early Palaeozoic [13]. Gneiss-migmatite complex comprising of gneisses, calcsilicate, quartzite, amphibolites and biotite-hornblende schist is the most

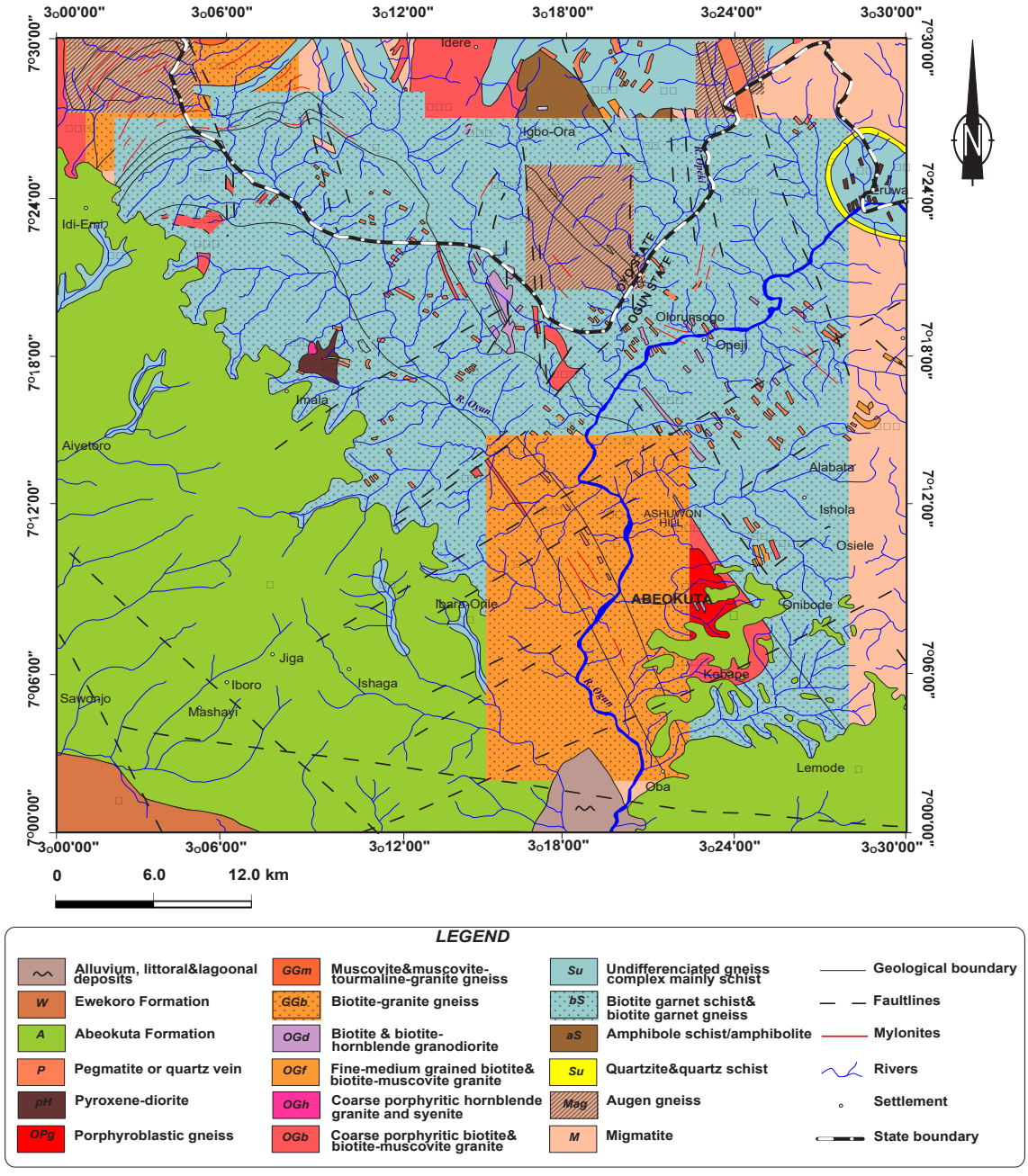

Figure 1: *Geological Map of the Study Area.*

widely spread rock formation in the area according to Rahaman [14].

Methodology

The acquired gravity dataset of the study area through Bureau Gravimetrique Internationale (BGI) was processed to produce the Bouguer anomaly map (Figure 2) after being reprojected from the Universal Transverse Mercator of Zone 32 Northing (UTM 32N) to that of UTM 31N. A two-dimensional fast Fourier transform (FFT2D) filter named Magmap, which is an extension of Oasis Montaj (version 8.4) was applied on the Bouguer anomaly map to produce the Radially Average Power Spectrum (RAPS), presented as Figure 4. The spectrum

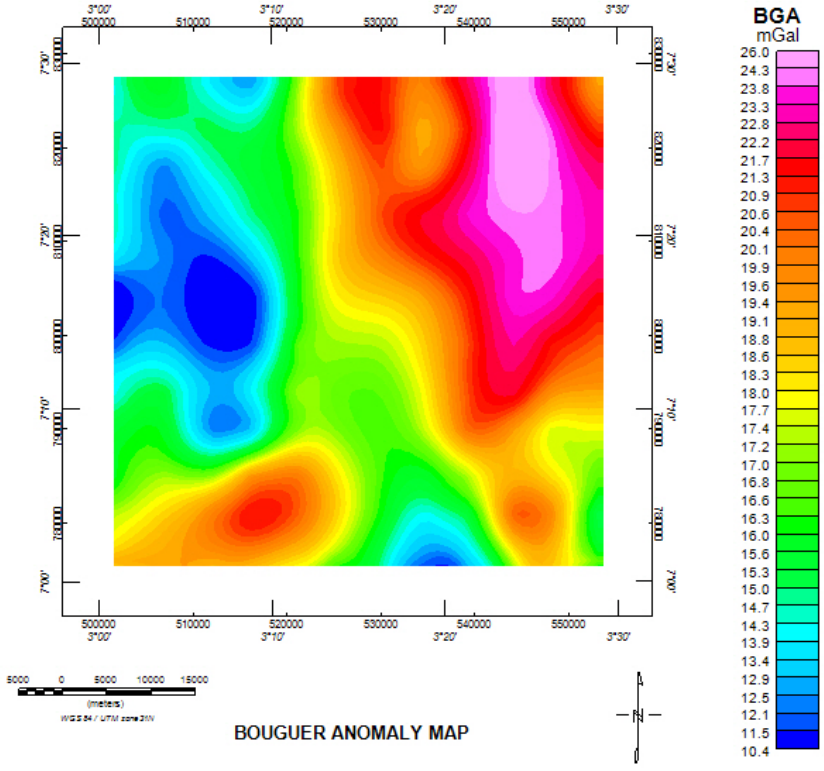

Figure 2: *Bouguer Gravity Field of Abeokuta.*

aided the visualisation of the three demarcation of deep, intermediate and shallow anomalous gravity sources. Each of the segment is a representative of the gravity responses at given depths. Depth is proportional to the slope of the line segment [15–16]. This research requires a Regional-Residual separation technique to enhance shallower signals. A High-pass filter was employed to obtain the residual anomaly map (Figure 5). Subsequently, residual anomaly map was produced from the Bouguer gravity field [1, 17] by setting the cut-off wavenumber at 0.02 cycles/km to process the intermediate and shallow sources as the residual anomaly. The resulting residual anomaly was thereafter processed to produce the derivative of the field along the X-direction (Figure 6) and the Analytic signal map, the Analytic signal map (Figure 7) was observed to be a bit noisy and hence, upward continued at 1 km in order to sharpen the edges of anomalous sources and geological boundaries. These were also achieved through a two-dimensional fast Fourier transform (FFT2D), to accentuate structures linked with near surface causes [18].

The standard 3D Euler-deconvolution method is based on homogeneity equations that relate the gradients' components of the potential field to the source location. The structural index (SI), η having values ranging from 0–2 for gravity sources [19]. These sources are described by different theoretical geometries with corresponding SI as follows; Sphere - (η =2), Vertical line end (pipe) - (η =1), Horizontal line (cylinder) - (η =1), Thin bed fault - (η =1), and Thin sheet edge - (η =0) respectively [20]. The 3D Standard Euler equation for potential field according to [20–21] is defined as:

$$x\frac{\partial T}{\partial x} + y\frac{\partial T}{\partial y} + z\frac{\partial T}{\partial z} + \eta T = x_0\frac{\partial T}{\partial x} + y_0\frac{\partial T}{\partial y} + z_0\frac{\partial T}{\partial z} + \eta b \quad (5)$$

The coordinates of the measuring point are x, y, and z; b is a base level; the coordinates of the source location are x_0, y_0, and z_0; while T is the total potential field respectively.

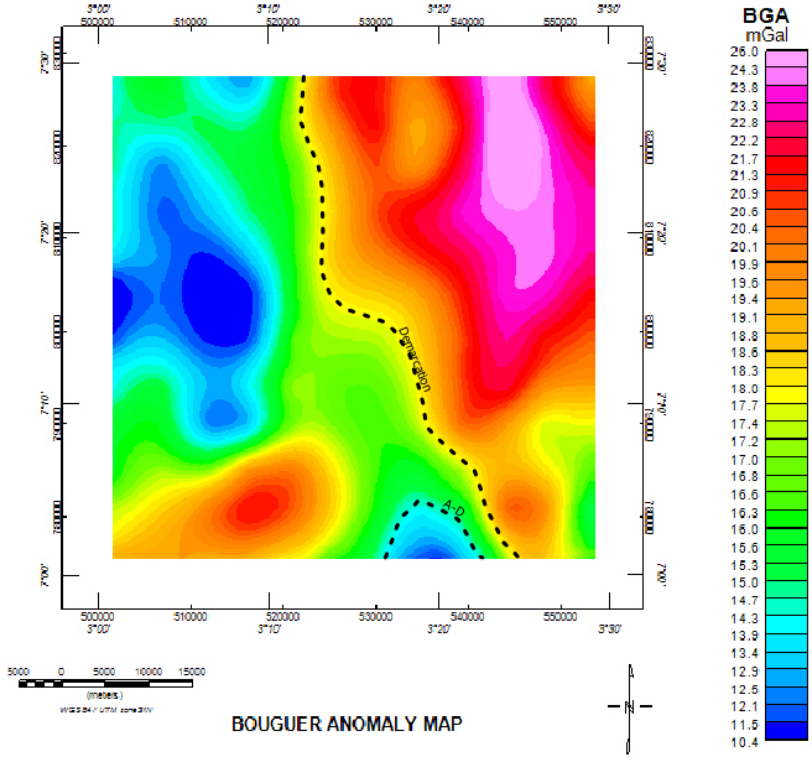

Figure 3: *Bouguer Anomaly Map showing some geological features.*

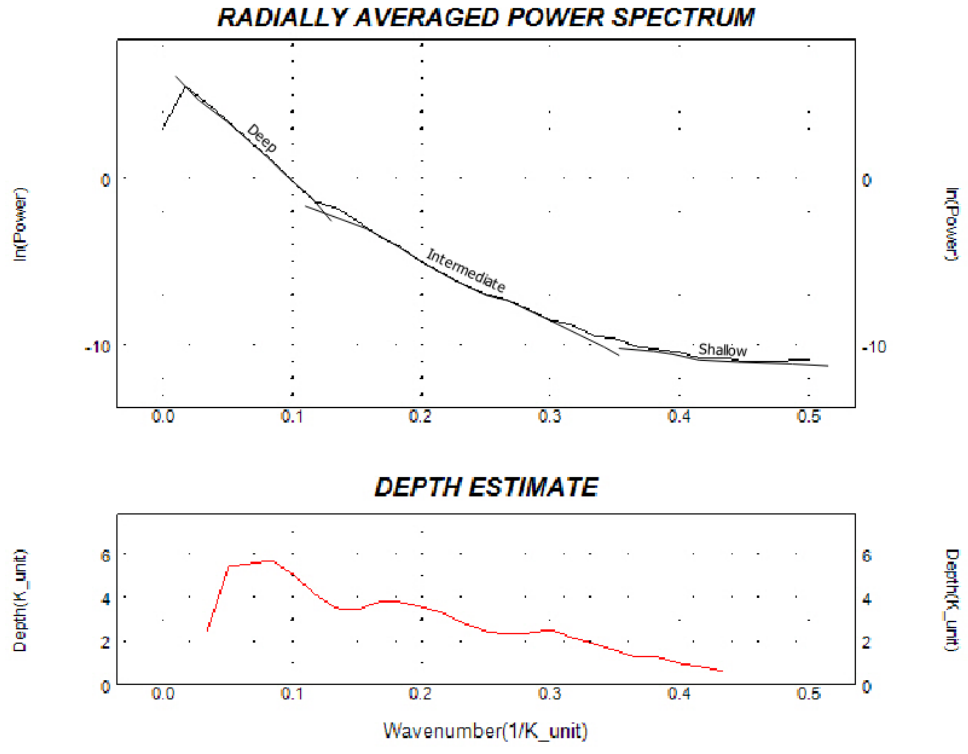

Figure 4: *Radially Averaged Power Spectrum of the Gravity Field.*

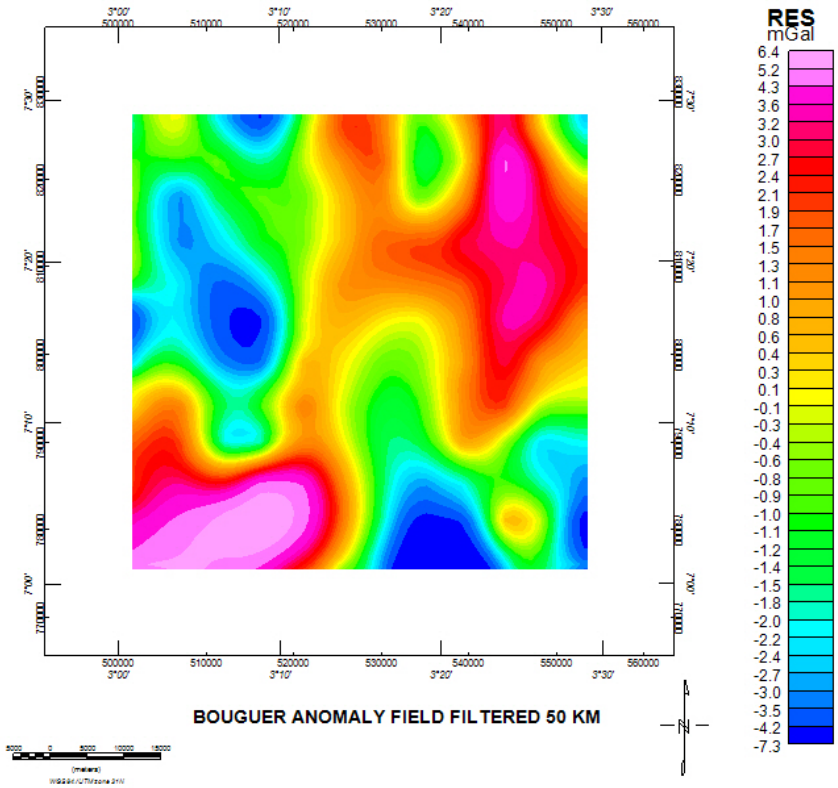

Figure 5: *Residual Anomaly Field (Bouguer Gravity Field High-Pass filtered at 50 km).*

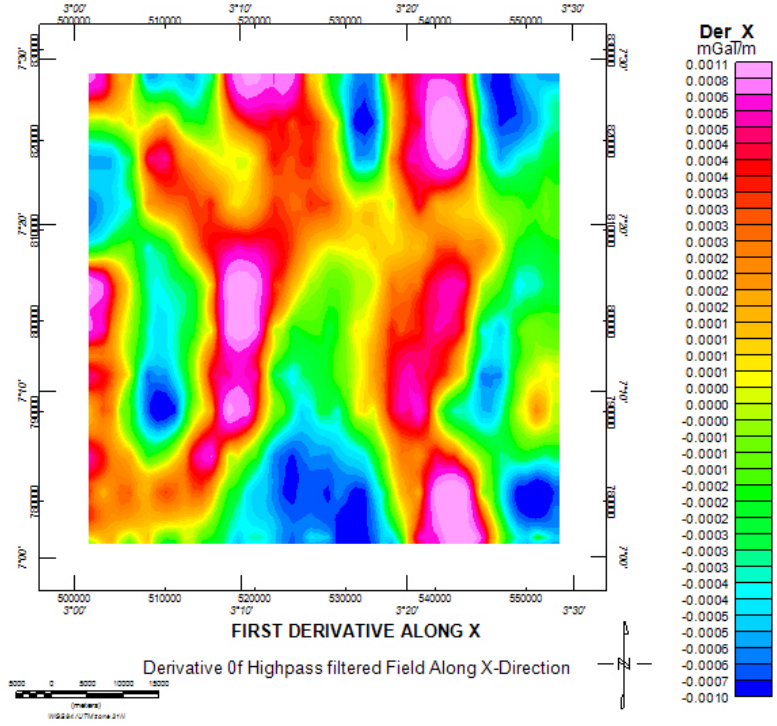

Figure 6: *First Horizontal Derivative along X-Direction.*

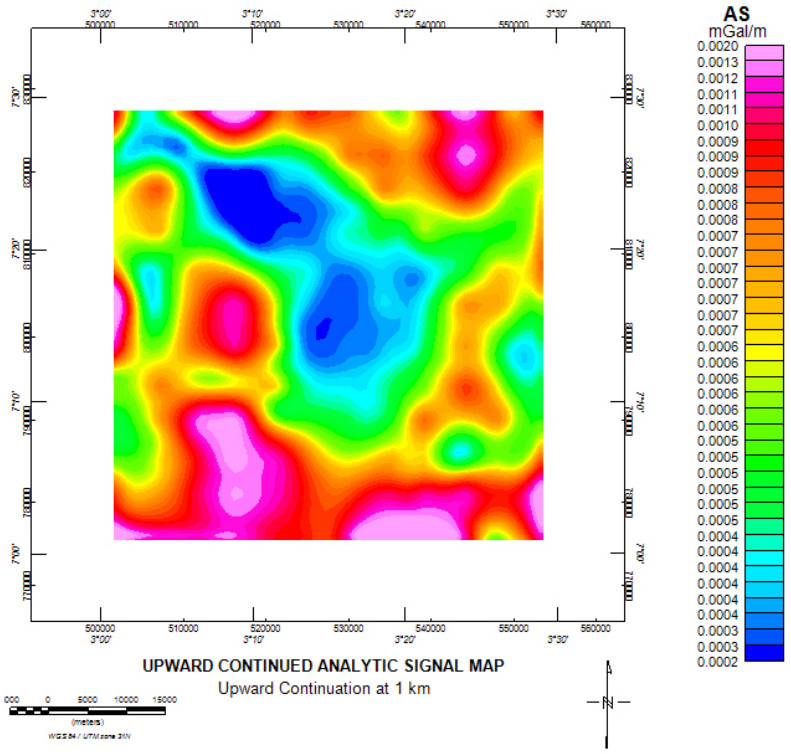

Figure 7: *Upward Continued Analytic Signal Map.*

In computing the standard Euler deconvolution solutions, the recommendations from the findings of [20] were adopted by using the different structural indices of 0, 1 and 2 were tried in solving the solutions but only SI equals 1 gave a geologically meaningful solution, which reveals that the area is possibly characterized by structures like faults, contacts and thin sheet edge (dike), [22]. A square window size of 3000 by 3000 m containing number of grid cells in the gridded dataset was used in order to accommodate the depth of sources, as investigated by previous researches in the study area.

Results and Discussions

Qualitative Treatment

The digitized data set of the area produced the Bouguer gravity map in Figure 2 and the radially average power spectrum in Figure 3. The anomaly was filtered to describe features associated with intermediate and shorter wavelengths. While Figure 5 shows the residual map for the separated Bouguer anomaly grid. Subsequently, the derivative maps of the field were generated from the high-pass filtered gravity filed, one of which is the derivative along X – direction presented as Figure 6 and the Analytic signal map that Figure 7 represents.

In Figure 2, a gravity value ranging from 10.40 mGal to 26.40 mGal is observed on the Bouguer anomaly field. The anomaly map reveals high gravimetric values, towards northeastern zone of the area, which conforms to the lithological differences in the subsurface. On the other hand, within the southern, southwestern and northwestern regions, the variations in the lithology of the intra-basement of the area recorded low gravimetric values. Furthermore, the dominance of high gravity values around the Northeastern portion is a representative of possible undifferentiated gneiss complex which is mainly schist around '**Eruwa'** (when compared with the Geological map of the study area). The portion marked **'A-D'** on Figure 3 are alluvial and lagoonal deposits at the Oba area and the **'demarcated'** marked region which is the transition zone that divides the

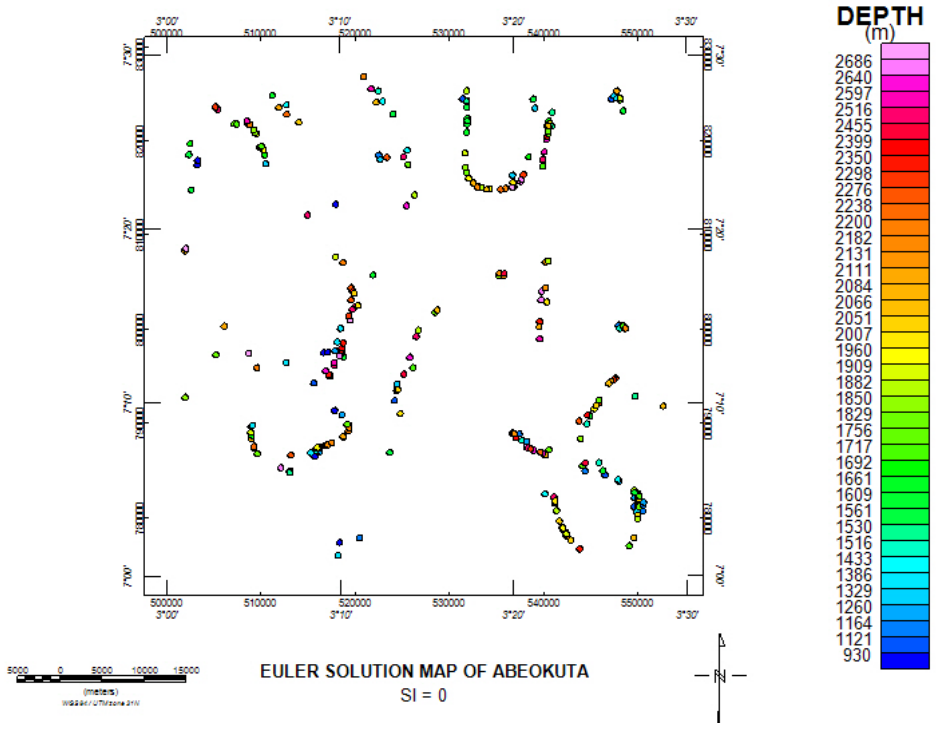

Figure 8: *Euler Solution Map of Abeokuta, for the Structural Index SI = 0.*

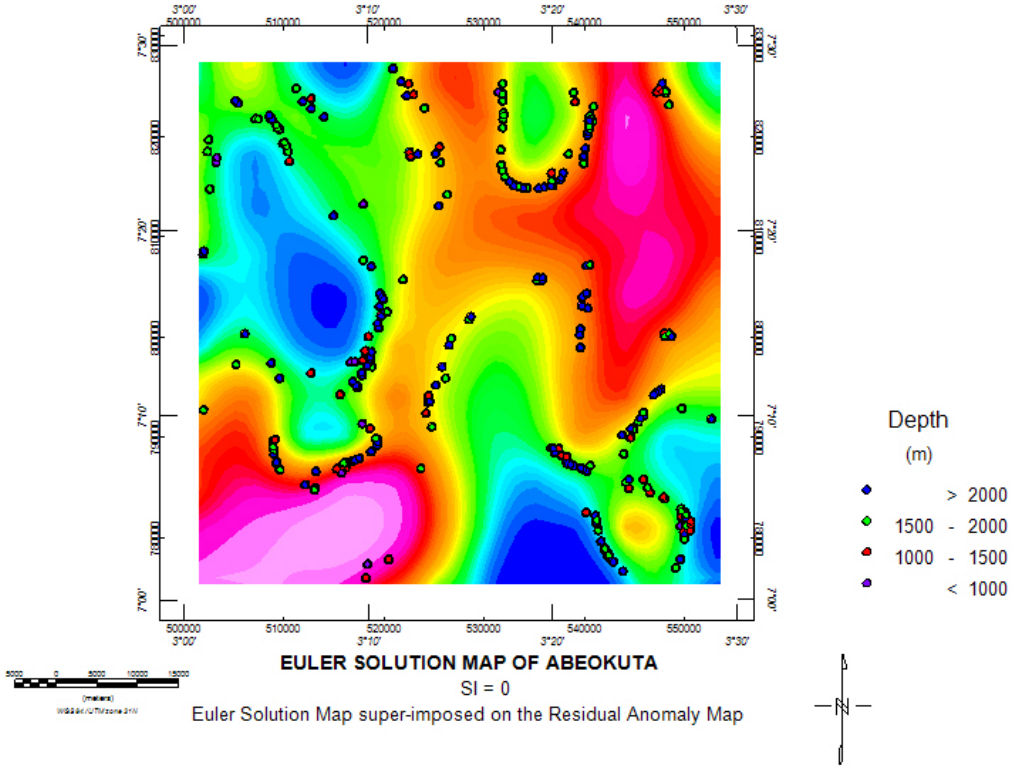

Figure 9: *Euler Solution Map superimpose on the Residual Anomaly Map.*

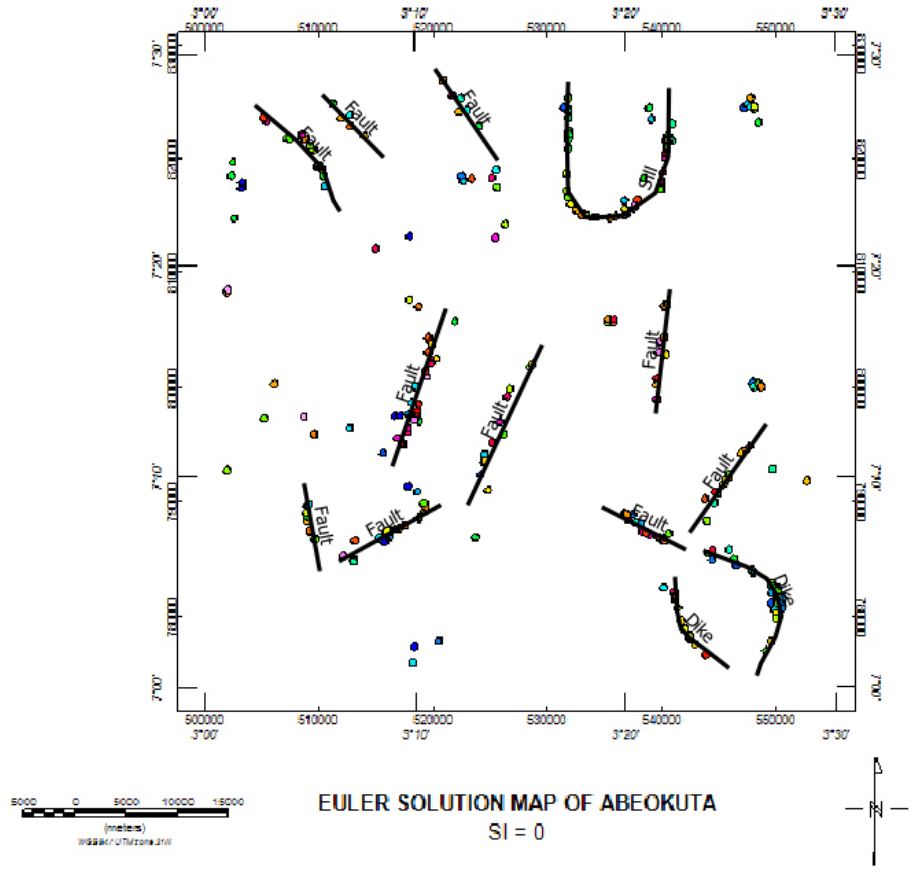

Figure 10: *Lineament Map of the Study Area, inferred on the Euler Solution Map.*

study location into two distinctive geological Formations of Basement and Sedimentary Formations.

The residual anomaly map in Figure 5 (Gravity field filtered at 50 km) has intermediate and short wavelengths with values ranging from -7.3 mGal to 6.4 mGal. In the southern and northern zones, gravity values are high but varies in Northwestern and Southeastern regions. In parts of the study area, there are sedimentary intrusions into the northern zones with low gravity values, other low-density areas suggest possible sedimentation (like Araromi and Abeokuta Formations).

High pass–filtered residual anomaly grid gave rise to the derivative grids contained in Figures 6 and 7 to enhance the visualization and localization of the anomalous sources. The anomalies of the first horizontal derivative along the X-direction are aligned along N-S trend laterally, the anomalies or structures that trend in the same direction are from the same tectonic event, as posited by [23], while the regional effects of the total field have been attenuated. The range of anomaly for the Analytic Signal in Figure 7 is 0.002 mGal to 0.02 mGal with high gravity responses spatially distributed all over the area.

Depth Estimation and Structural Evaluation

The Figure 8 shows the Euler map with SI equals 0 having maximum range of 2,350 m to 2,686 m and average of 2,518 m (deep sources); and a minimum range of 930 m to 1,260 m with an average minimum depth of 1,095 m (shallow sources).

The depth to basement of gravity anomalous sources evaluated in this research is a true representation of the sedimentary thickness, the works of [24] and [25] in and around the study area are all in agreement with the results of this research. The depth range obtained

can slightly hold prospect for hydrocarbon accumulation as posited by [26] that the minimum sedimentary thickness required for hydrocarbon exploration is 2,300 m.
Figure 10 represents the lineament map of inferred structures on the Euler depth solution map. The elongation of continuous plotted solutions confirms the presence of geological structures like faults, dike and/or sill in the area of investigation.

Conclusion

The qualitative interpretation of the area by the filtering techniques reveal the distinct features of basement and sedimentary Formations of the area. Alluvial deposits zone, sedimentary intrusions into the area and regions of possible high and low-density rock minerals have been mapped.
Conclusively, the depths to basement of gravity sources in the area show prospects for hydrocarbon exploration and holds high potential for economic minerals exploration.

References

[1] Reynolds, M.J. (1997): *Introduction to applied and environmental geophysics*. John Wiley and Sons: New York, USA, 796 p.

[2] Mickus, K., Hinojosa, J. (2002): The complete gravity gradient tensor derived from vertical gravity data: A Fourier Transform technique. *Journal of Applied Geophysics*, 46, 159–174.

[3] Nicolas, O.M. (2009): The Gravity Method. *Exploration for Geothermal Resources,* pp. 1–9.

[4] Telford, W.M., Geldart, L.P., Sheriff, R.E. (1990): *Applied geophysics* (2nd edition), Cambridge University Press: Cambridge, 770 p.

[5] Roest, W.R., Verhoef, J., Pilkington, M. (1992): Magnetic interpretation using 3-D analytic signal. *Geophysics,* 57, 116–125.

[6] Hartman, R.R., Tesky, D.J., Friedberg, J.L. (1971): A system for rapid digital aeromagnetic interpretation. *Geophysics*, 36, pp. 891–918.

[7] Reid, A.B., Allsop, J.M., Granser, H., Millett, A.J., Somerton, I.W. (1990): Magnetic interpretation in three dimensions using Euler deconvolution. *Geophysics,* 55, pp. 80–99.

[8] Hansen, R.O., Simmonds, M. (1993): Multiple-source Werner deconvolution. *Geophysics*, 58, pp. 1792–1800.

[9] Revees, C. (2005): *Aeromagnetic Surveys; Principles, Practice and Interpretation*. GEOSOFT, 155 p.

[10] Telford, W.M., Geldart, L.P., Sheriff, R.E., Keys, D.A. (1976): *Applied Geophysics.* Cambridge University Press, 860p.

[11] Rivas, J. (2009): *Gravity and Magnetic Methods*. *Short course on Surface Exploration for Geothermal Resources*. United Nations University, LaGeo: Elsavador, pp. 1–13.

[12] Obaje, N.G. (2009): Geology and mineral resources of Nigeria*. Lecture Note in Earth Science Series,* 120.

[13] Jones, H.A., Hockey, R.O. (1964): The Geology of Parts of Southwestern Nigeria. *Bulletin of Geological Survey of Nigeria*, 31, pp. 101–102.

[14] Rahaman, M.A. (1976): *Review of the basement geology of south western Nigeria in Geology of Nigeria*. Elizabethan publishing company: Lagos, pp. 41–58.

[15] Naidu, P.S. (1968): Spectrum of Potential Field due to randomly distributed sources. *Geophysics*, 33, pp. 337–345.

[16] Spector, A., Grant, F.E. (1970): Statistical models for interpreting aeromagnetic data. *Geophysics*, 35, pp. 293–302.

[17] *Layade, G.O., Adebo, B.A., Olurin, O.T., Ganiyu, O.M. (2015):* Separation of Regional-Residual Anomaly Using Least Square Polynomial Fitting Method. *Journal of the Nigerian Association of Mathematical Physics,* 30, pp. 69–180.

[18] Hesham, S.Z., Hesham, T.O. (2016): Application of High-Pass Filtering Techniques on Gravity and Magnetic Data of the Eastern Qattara Depression Area, Western Desert, Egypt. *National Research Institute of Astronomy and Geophysics,* 5, pp. 106–123.

[19] Thompson, D.T. (1982): A new technique for making computer-assisted depth estimates from magnetic data*. Geophysics,* 47(1), pp*.* 31–37.

[20] Reid, A.B., Allsop, J.M., Thurston, J.B. (2014): The structural index in gravity and magnetic Interpretation: Errors, uses and abuses. *Geophysics,* 79(4), pp. 61–66.

[21] Adegoke, J.A., Layade, G.O. (2019): Comparative depth estimation of iron-ore deposit using the Data-Coordinate Interpolation Technique for airborne and ground magnetic survey variation. *African Journal of Science, Technology, Innovation and Development (AJSTID).* 11(5), pp. 663–669, DOI:10.1080/20421338.2019.1572702.

[22] Reid, A.B., Ebbing, J., Webb, S.J. (2014): Avoidable Euler Errors – the use and abuse of Euler deconvolution applied to Potential fields. *European Association of Geoscientists & Engineers, Geophysical Prospecting,* 62(5).

[23] Omosanya, K.O., Akinbodewa, A.E., Mosuro, G.O. (2012): Integrated Mapping of Lineaments in Ago-Iwoye SE, SW Nigeria, *Intl. J. Sci. Technol.,* 1(2), pp. 68–79.

[24] Olowofela, J.A., Akinyemi, O.D., Badmus, B.S., Awoyemi, M.O., Olurin, O.T., Ganiyu, S.A. (2013): Depth estimation and source location of Magnetic anomalies from a Basement Complex Formation, using Local Wavenumber Method (LWM). *IOSR Journal of Applied Physics,* 4(2), pp. 33–38.

[25] Olurin, O.T., Olowofela, J.A., Akinyemi, O.D., Badmus, B.S., Idowu, O.A., Ganiyu, S.A. (2015): Enhancement and Basement Depth Estimation from Airborne Magnetic Data. *African Review of Physics,* 10(38), pp. 303–313.

[26] Wright, J.B., Hastings, D., Jones, W.B., Williams, H.R. (1985): *Geology and Mineral resources of West Africa*. George Allen and Unwin: London, 187 p.

Original Scientific Article

Received: February 19, 2021
Accepted: March 08, 2021
DOI: 10.2478/rmzmag-2020-0019

Site characterization for engineering purposes using geophysical and geotechnical techniques

Določevanje značilnosti območja za inženirske namene z uporabo geofizikalnih in geotehničnih metod

Aderemi A. Alabi*
Department of Physics, Federal University of Agriculture, Abeokuta, Ogun State, Nigeria
*derylab@yahoo.com

Abstract

Geophysical and geotechnical techniques were applied to determine the suitability of the subsurface structure of Akole community area, Abeokuta, Nigeria, for the construction of engineering structures (CES). Four vertical electrical soundings (VES) were carried out, and 10 samples from different points at 1 m depth were analysed to determine soil moisture content, specific gravity (SG), Atterberg limits and California bearing ratio (CBR). The geoelectric sections revealed a maximum of five layers with the typical sounding curves of AKH and HKH types. Sieve analysis and tests for compaction limit, Atterberg limits, SG, optimum moisture content and maximum dry density for compaction limit revealed that samples SP2, SP3, SP4, SP6, SP7, SP8, SP9 and SP10 are of low plasticity with SG values that fall within the permissible range, while SP1 and SP5 are of medium plasticity and their SG values fall below the range of standard specifications. CBR analysis showed that SP1 and SP5 have low load-bearing capacities. VES 1 and 2, linked with SP1 and SP5, are considered unstable and unsuitable to support the CES with shallow foundations; however, excavation of weak layers up to a depth of 5 m and reinforcement will enable the support.

Key words: electrical resistivity, engineering structure, grain size, Atterberg limits, compaction test

Povzetek

Določitev primernosti tal za gradnjo inženirskih objektov na območju skupnosti Akole v Nigeriji je bila izvedena s pomočjo uporabe geofizikalnih in geotehničnih metod. Izvedene so bile štiri navpične sondažne geo-električne meritve. Za določitev vlažnosti, specifične teže, konsistenčnih mej in kalifornijskega indeksa nosilnosti (CBR) je bilo preiskanih deset vzorcev tal iz različnih lokacij globine 1 m. Geo-električni prerezi so pokazali maksimalno pet različnih plasti s tipičnimi sondažnimi krivuljami tipa AKH in MKH. Na vzorcih tal z oznakami SP2, SP3, SP4, SP6, SP7, SP8, SP9 in SP10 so bile opravljene sejalna analiza, določitev meje zgoščevanja, določitev konsistenčnih mej, specifična teža, optimalna vlažnost in maksimalna suha gostota za mejo zgoščevanja. Vzorci imajo nizko stopnjo plastičnosti in specifično težo, ki spada v dovoljeno območje. Vzorca tal z oznakami SP1 in SP5 imata srednjo stopnjo plastičnosti in spadata pod območje standardnih zahtev. Preiskava s testom CBR je pokazala, da imata vzorca tal SP1 in SP5 nizko nosilnost na obtežbo. Preiskavi VES 1 in 2 sta prav tako pokazali, da sta vzorca SP1 in SP5 nestabilna ter neprimerna za temeljenje pri gradnji inženirskih objektov s plitvim temeljenjem, čeprav bi z odstranitvijo plasti globine do 5 m in armiranjem dosegli primerno nosilnost za temeljenje.

Ključne besede: električna upornost, inženirski objekti, velikost zrn, Atterbergerjeve meje, zgoščevalni preiskus

Introduction

Developing nations have suffered from recurring collapse of engineering structures over the years due to failure to carry out necessary investigations before the structures are erected [1–3]. Recently, the statistics of failures of building and engineering structures

throughout the nation has increased geometrically [4]. Factors responsible for failure of engineering structures are often attributed to substandard usage of building materials, old age of buildings, improper foundation design, non-compliance to specifications, inadequate supervision and nature of the sub-surface conditions of the ground on which the building is sited [5, 6]. The aftermath of structural failure of buildings is always huge, including loss of lives and valuable properties, as well as loss of financial investment.

Since the earth provides support for every engineering structure, it is important to conduct preconstruction investigation of the sub-surface of any proposed site. This is to ascertain the strength and the competence of the subsoil earth materials, as well as to carry out the timed post-construction monitoring of such structure to ensure its integrity [4, 7,]. Geophysical methods (particularly, the electrical resistivity technique) have been widely used for an extensive variety of engineering and environmental problems because of their reliability, efficiency and cost-effectiveness [4, 8]. The electrical resistivity technique has also proved to be a reliable tool for obtaining detailed information about the sub-surface structure, particularly for detecting irregularities in and the complexity of the geological sub-surface [9].

Geotechnical study is another investigative approach that can provide excellent insight into the engineering properties of sub-surface soil materials [5]. The geotechnical test uses the principle of soil and rock mechanics to investigate the sub-surface condition and to determine the relevant physical properties of the materials. Information, such as soil type, load-bearing capacity of materials, zone of weakness, resistance to penetration, compressibility and shrinkage limit, among others, is often necessary before designing a very good and strong foundation for a proposed engineering structure [10].

Site characterization for building construction purposes at the Federal University of Agriculture, Abeokuta, Nigeria, was conducted using geophysical and geotechnical methods [11]. The area considered in the study was found to be suitable for both shallow and deep foundations. However, there were some exceptions at a few points, wherein reinforcement was required to support shallow and deep foundations. Subsoil evaluation of the pre-foundation at the proposed site at the Polytechnic of Ibadan was conducted [12] using geophysical and geotechnical techniques. The study revealed that the clay content of the soil is low; the subsoil of the study area was therefore rated to be competent as foundation material to support the proposed structure.

Adequate understanding of soil properties is of paramount importance in the study of foundation integrity because it provides information on the material properties of the soils, including ability to support the load often exerted by the structure erected. The objective of this study is to use geophysical and geotechnical techniques to investigate the nature and engineering properties of the subsurface, its strength and capability (or otherwise) to bear the load of the engineering structure to be erected in Akole Community, Oke-Ata, Abeokuta, Southwestern Nigeria.

Materials and methods

Geomorphology and geology of the study area

The study area is located at Akole Community in Oke-Ata, Abeokuta North, Ogun State, Southwestern Nigeria, which lies between latitudes 7°8′16.9″ N and 7°8′24″ N and longitudes 3°17′9.2″ E and 3°17′13.4″ E. The ground in the study area lies at an elevation between 62 m and 78 m above sea level (Figure 1).

The climate is warm and tropical due to the rain-bearing ocean wind of the south-western monsoon and the northwest wind that arises from the Sahara desert. The rainy season of the study area starts around April and ends in October, with rainfall of nearly 1,238 mm per annum, while the dry season starts in November and ends in March. The area is located in a hummocky terrain with a well-pronounced undulating topography and prominent hills,

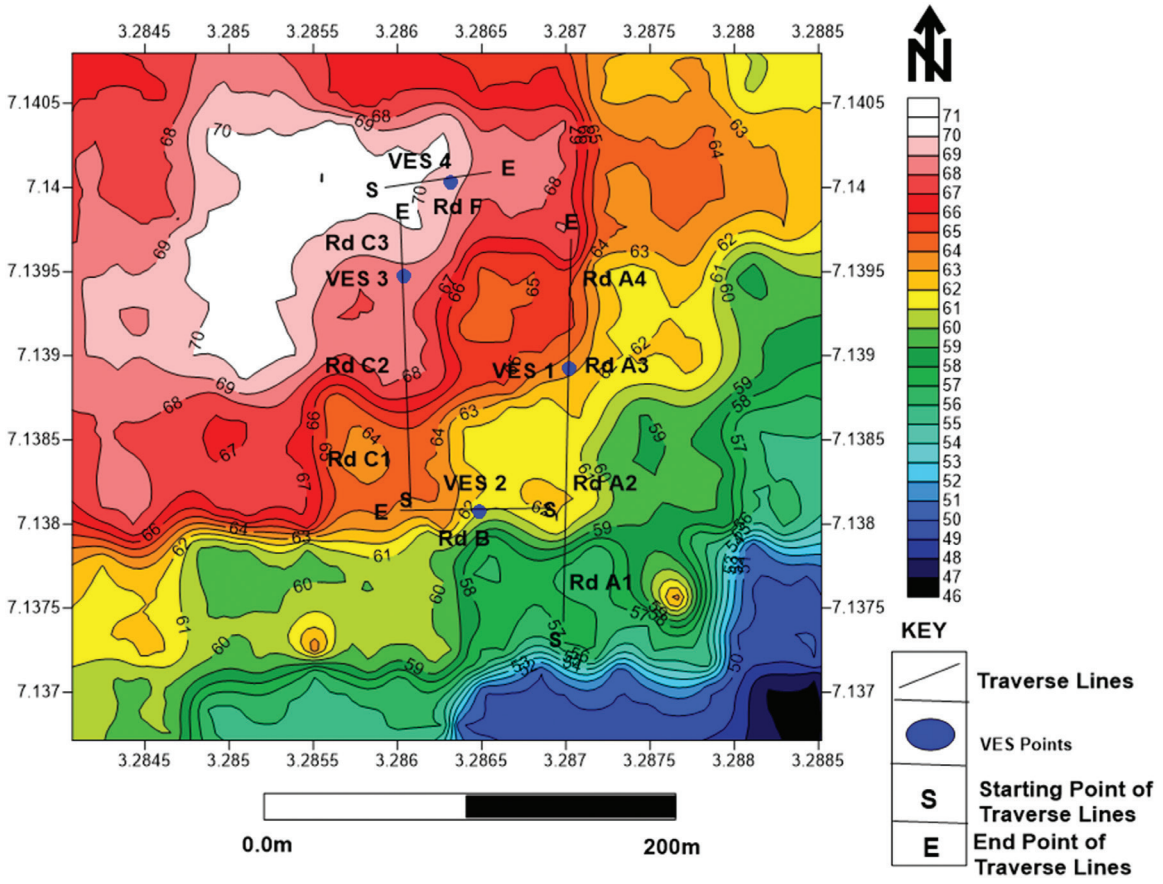

Figure 1: *Topographical map of the study area showing profile base image.*

characterized by a moderate slope varying in altitude. The study area falls within the Precambrian Basement rocks of Southwestern Nigeria, with six major lithologic units, namely quartzite, banded-gneiss, biotite-schist, quartz-biotite schist and pegmatite [13].

Fieldwork procedure for geophysical survey

The method used for the geophysical survey was the vertical electrical sounding (VES) using the Schlumberger electrode array. The Schlumberger array focusses on the vertical variation of sub-surface layers. The Schlumberger configuration of an electrode is quite sensitive to vertical sub-surface resistivity below the centre of the array and it is less sensitive to horizontal changes in the sub-surface [14]. Data from a total of four VESs were acquired in the study area, and each of the potential differences and currents measured at each point were recorded. The apparent resistivity (ρ_a) was computed from measurements of voltage (ΔV) and current (i) using Equation 1.

$$\rho_a = \frac{\pi\left[\left(s^2 - a^2\right)/4\right]}{a}\frac{\Delta V}{i} \quad (1)$$

where ρ_a is the apparent resistivity obtained, s is the distance between the potential electrodes, a is the distance between the current electrodes, ΔV is the potential difference measured and i is the current measured.

Using WinResist software, the apparent resistivity values obtained were plotted against the electrode spacing to acquire the VES curves.

Geotechnical method (laboratory tests for geotechnical survey)

The soil moisture content (SMC), which is the water between the pores of the soil, was

determined using the gravimetric method expressed by Equation 2 [15].

$$\mathrm{SMC}=\begin{pmatrix}(mass\ of\ Container+moistsoil)\\ -(mass\ of\ Container+drysoil)\\ \hline (mass\ of\ Container+drysiol)\\ -(mass\ of\ Container)\end{pmatrix} \quad (2)$$

The Atterberg limit test verifies the liquid (LL) and plastic (PL) limits of a fine-grained soil. The LL refers to the moisture content at which the soil begins to behave as a liquid material and begins to flow, while the PL is defined as the moisture content at which soil begins to behave as a plastic material. The LL and PL were determined using the Casagrande method, as described in American Society for Testing and Materials (ASTM) Standard D4318. The difference between the LL and the PL gives the plasticity index (PI). The compaction limit test describes the relationship between the moisture content and the dry density of a soil for a specified compactive effort (amount of energy that is applied to the soil). The compaction properties were determined using standard methods (ASTM D698 and ASTM D1557), the standard and modified efforts of 6,000 kN-m/m^3 and 27,000 kN-m/m^3, respectively, were chosen for the determination of the moisture–density relationship. The California bearing ratio (CBR) expresses the ratio of force per unit area required to penetrate a soil mass with standard circular piston at the rate of 1.25 mm/min to that required for the corresponding penetration of a standard material [16]. The CBR was determined following the procedure of ASTM D1883.

The specific gravity (SG) of the soil was determined using a water pycnometer-based standard test (ASTM D854-00) expressed by Equation 3.

$$SG=\left(\frac{(w_2-w_1)}{(w_2-w_1)-(w-w_4)}\right), \quad (3)$$

where w_1 = empty weight of pycnometer, w_2 = weight of pycnometer + oven-dried soil, w_3 = weight of pycnometer + oven-dried soil + water, and w_4 = weight of pycnometer + water.

The grain size analysis estimates the percentage of sand that was passed or retained by an individual sieve. A soil sample of 500 g was sieved to appropriate sieve sizes of 475, 236, 118, 600, 300, 150, 75 μm and weighed. The percentages of particles passing and particles retained, as well as the quantity passing, were calculated using Equations 4, 5 and 6, respectively.

$$P=\frac{Mr}{Tm}*100, \quad (4)$$

$$R=100-P, \quad (5)$$

$$Q_P=T_m-M_r, \quad (6)$$

where T_m = total mass of the soils, R = percentage retained, P = percentage passing, M_r = mass retained and Q_p = quantity passing.

Data processing and interpretation

Characteristics of the VES layers

VES 1

The geoelectric curve for VES 1 (Figure 2) depicts five different sub-surface layers, which are as follows: topsoil, with resistivity value of 180 Ω·m, thickness of 0.913 m and depth of 0.913 m; sandy clay, with resistivity value of 145 Ω·m, thickness of 1.24 m and depth of 2.15 m; laterite, with resistivity value of 332 Ω·m, thickness of 1.56 m and depth of 3.71 m; saturated sandy clay, with resistivity value of 107 Ω·m, thickness of 4.47 m and depth of 8.18 m; weathered basement, with resistivity value of 3,385 Ω·m and an inestimable thickness. Due to shrinkage and swelling of clayey soils, excavation must be done until an adequate-load-bearing layer is reached for shallow foundation construction within the VES Profile 1 region.

VES 2

The geoelectric curve for VES 2 (Figure 3) depicts four different sub-surface layers, which include the following: topsoil, with resistivity value of 248 Ω·m, thickness of 0.867 m and depth of 0.867 m; sandy clay, with resistivity value of 190 Ω·m, thickness of 4.03 m and

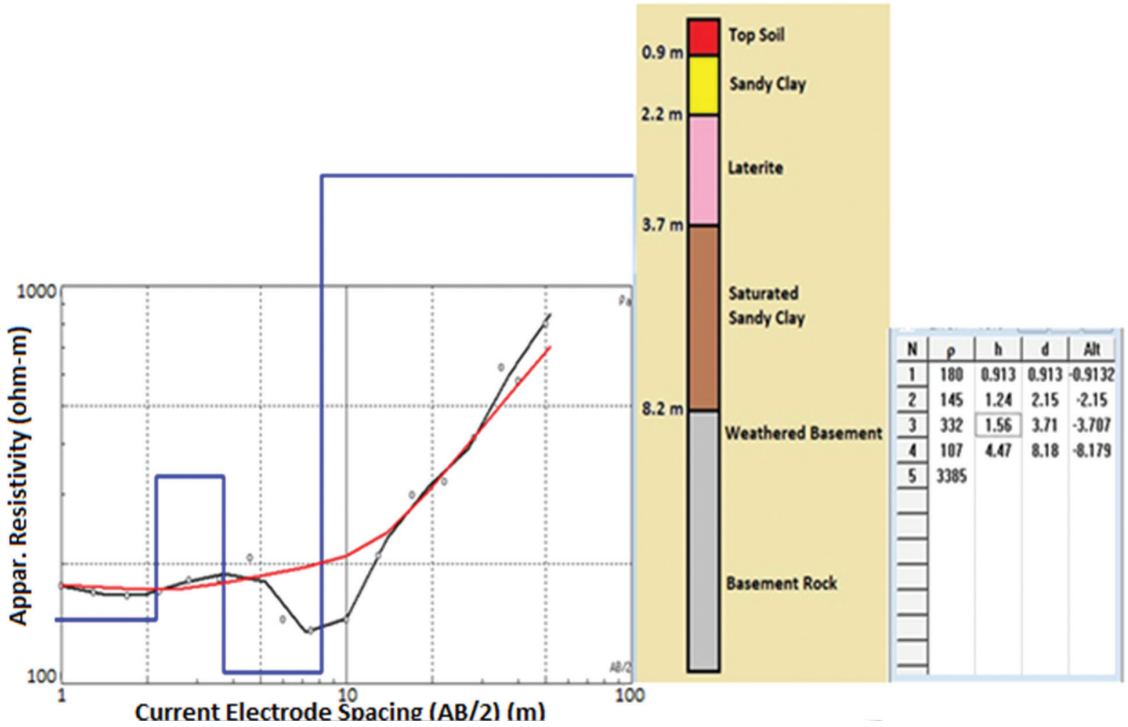

Figure 2: *Graph of apparent resistivity against electrode spacing for VES Profile 1. Notes: Blue line represents the phase values on the cross sections; the red line represents true resistivity; the black line in the graph represents apparent resistivity.*

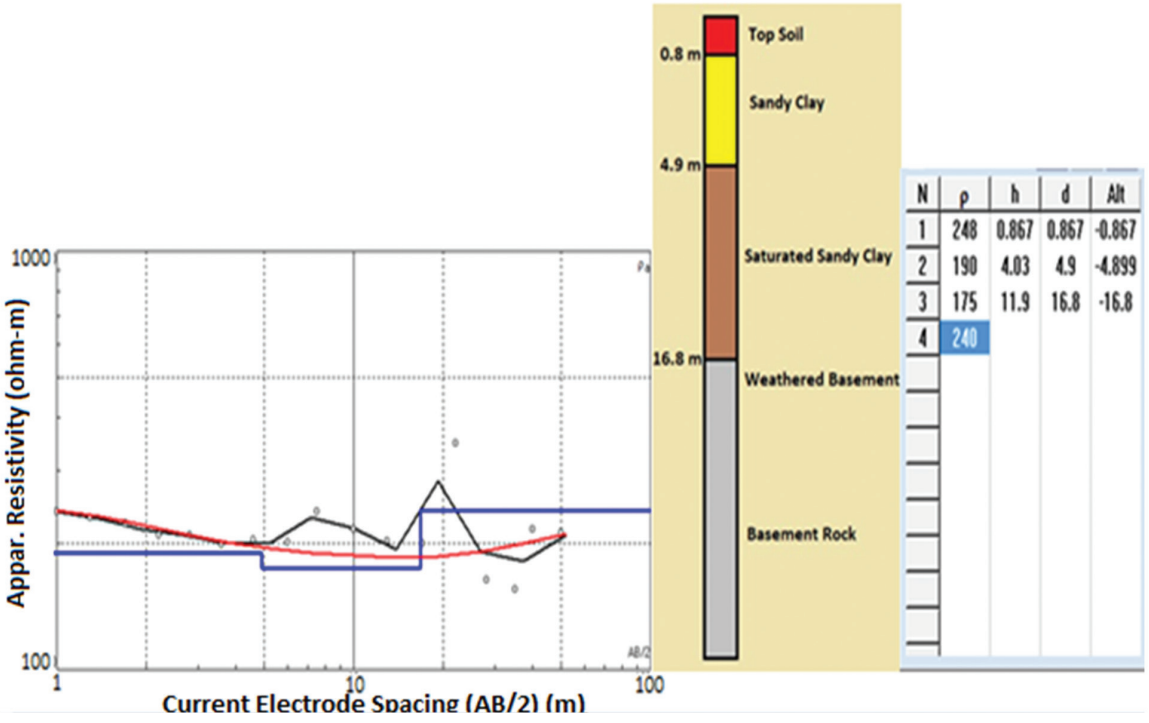

Figure 3: *Graph of apparent resistivity against electrode spacing for VES Profile 2. Notes: Blue line represents the phase values on the cross sections; the red line represents true resistivity; the black line in the graph represents apparent resistivity.*

depth of 4.9 m; saturated sandy clay, with resistivity value of 175 Ω·m, thickness of 11.9 m and depth of 16.8 m; weathered basement, with resistivity value of 240 Ω·m and an immeasurable thickness. The compactness of the soil increases as the depth below the earth's sub-surface increases; hence, it is strongly advised to increase the depth of the foundations constructed in VES Profile 2 to a depth not less than 3.1 m.

VES 3

Four different sub-surface layers were delineated for VES 3: the topsoil, with resistivity value of 267 Ω·m, thickness of 0.573 m and depth of 0.573 m; sandy clay, with resistivity value of 167 Ω·m, thickness of 0.833 m and depth of 1.41 m; indurated sandy clay, with resistivity value of 671 Ω·m, thickness of 9.92 m and depth of 11.3 m; weathered basement, with resistivity value of 4,041 Ω·m and an inestimable thickness (Figure 4). The soil constituents in the topsoil are fairly suitable for use in shallow foundations, while further reinforcement is essential for deep foundations.

VES 4

Four major sub-surface geoelectric layers were delineated from the interpretation results of VES 4; these include the following: the topsoil, with resistivity value of 290 Ω·m, thickness of 0.564 m and depth of 0.564 m; sandy clay, with resistivity value of 167 Ω·m, thickness of 0.752 m and depth of 1.32 m; indurated sandy clay, with resistivity value of 623 Ω·m, thickness of 7.81 m and depth of 9.13 m; weathered basement, with resistivity value of 4,355 Ω·m and an infinite thickness (Figure 5). The particles of soil constituting the topsoil are suitable for use in shallow foundations, and additional strengthening is necessary for deep foundations.

The VES profiles delineated a maximum of five geoelectric sub-surface layers. These are the top soil, sandy clay, laterite, saturated and indurated sandy clay, and basement rock with shallow sub-surface. The top soil – with resistivity values varying from 180 Ω·m to 290 Ω·m and thickness ranging from 0.56 m to 0.91 m – is composed of clayey sand and sand. The topsoil particles are relatively suitable for use in shallow foundations. The second layer is composed of sandy clay and clayey sand, with resistivity values ranging from 107 Ω·m to 332 Ω·m and thickness values between 0.76 m and 11.9 m. Saturated and indurated sandy clays have resistivity values varying from 240 Ω·m to 671 Ω·m and thickness varying between 7.81 m and 9.92 m, and the weathered/fresh basement has resistivity values ranging from 240 Ω·m to 4,355 Ω·m, with the depth to bedrock generally

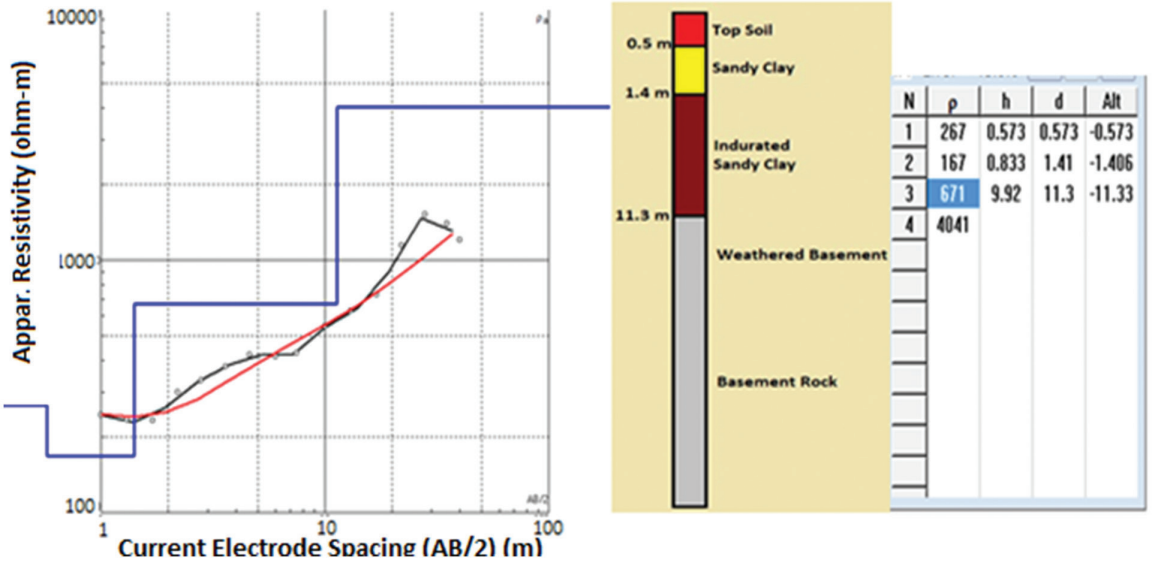

Figure 4: *Graph of apparent resistivity against electrode spacing for VES Profile 3. Notes: Blue line represents the phase values on the cross sections; the red line represents true resistivity; the black line in the graph represents apparent resistivity.*

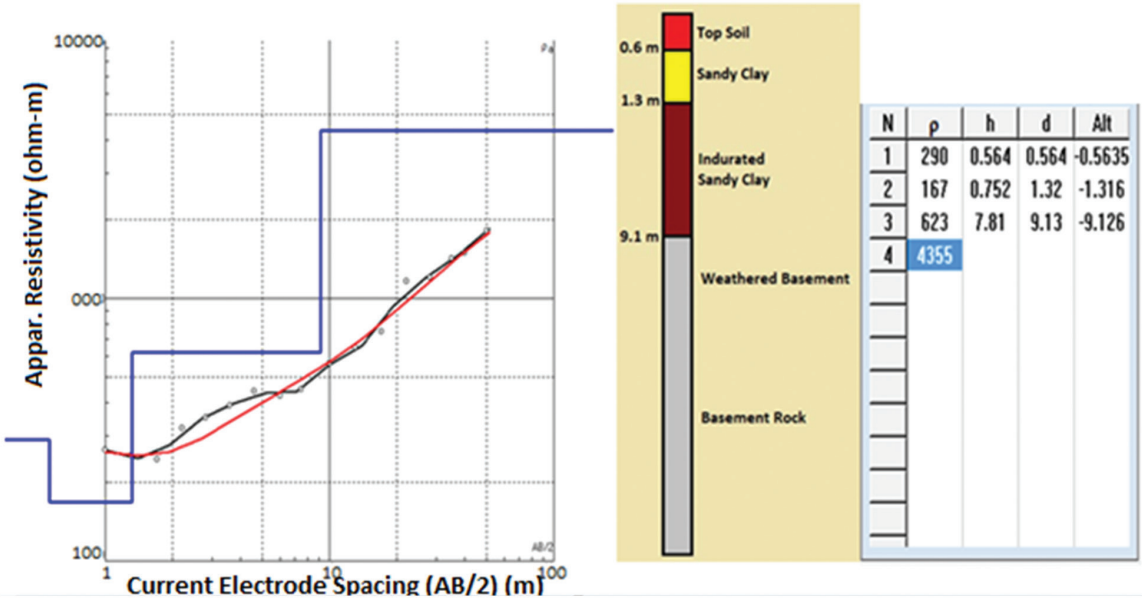

Figure 5: *Graph of apparent resistivity against electrode spacing for VES Profile 4. Notes: Blue line represents the phase values on the cross sections; the red line represents true resistivity; the black line in the graph represents apparent resistivity.*

Table 1. *Summary of the results of the VESs for the study area*

VES	Location	No. of layers	Resistivity (Ωm)	Thickness (m)	Depth (m)	Inferred lithology	Curve type
1	Latitude 7°08′ 17.2″ Longitude 3° 17′ 13.2″	1 2 3 4 5	180 145 332 107 3,385	0.91 1.24 1.56 4.47 –	0.91 2.15 3.71 8.18 –	Topsoil Sandy clay Laterite Saturated sandy clay Fresh basement	AKH
2	Latitude 7° 08′ 17.0″ Longitude 3° 17′ 12.9″	1 2 3 4	248 190 175 240	0.86 4.03 11.9 –	0.86 4.90 16.8 –	Topsoil Clayey sand Saturated sandy clay Weathered basement	HKH
3	Latitude 7° 08′ 17.2″ Longitude 3° 17′ 10.0″	1 2 3 4	267 167 671 4,041	0.57 0.83 9.92 –	0.57 1.41 11.3 –	Topsoil Sandy clay Indurated sandy clay Fresh basement	AKH
4	Latitude 7° 08′24.0″ Longitude 3° 17′ 10.3″	1 2 3 4	290 167 623 4,355	0.56 0.75 7.81 –	0.56 1.32 9.13 –	Topsoil Sandy clay Indurated sandy clay Fresh basement	AKH

VES, vertical electrical sounding.

being <20 m. The best layer that acts as hard rock terrain is the A-type. The A-combination types are characterized by high load-bearing capacity [17]. In the study area, A-combination types (AKH-3 and HKH-1) constitute 75% (Table 1) of the VES survey points, which suggest capacity for load bearing.

The geoelectric sections and representative horizontal electrical profiling curves of the study area revealed that the lithology of the area is made up of topsoil, sandy clay, laterite (covering a few portions), saturated/Indurated sandy clay and weathered/fresh basement rock (Figure 6).

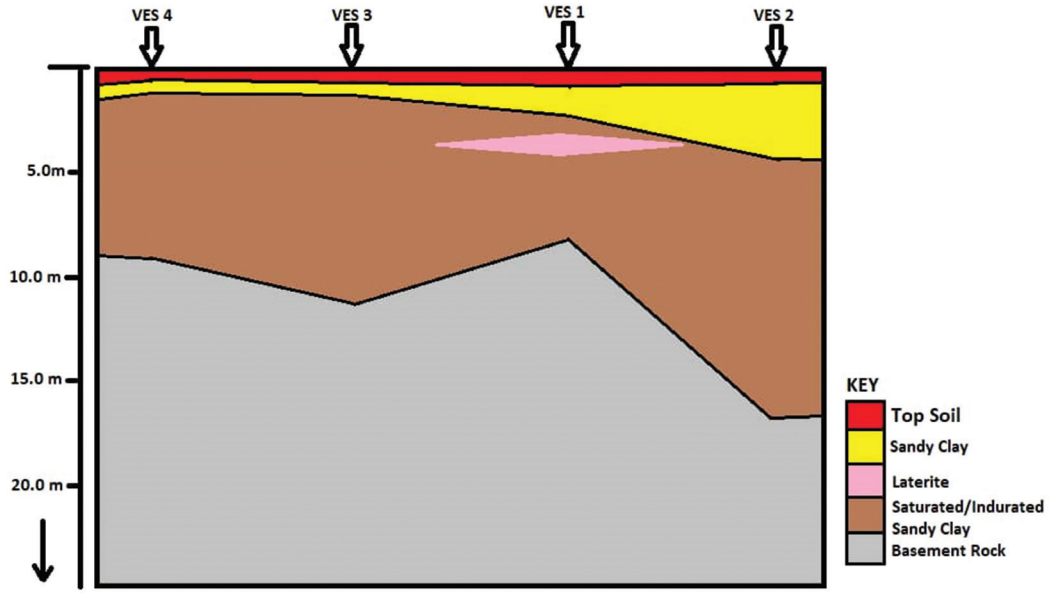

Figure 6: *Profiles of the geoelectric sections of the VES stations.*

Table 2. *Results of analyses of the Atterberg limits, SG, moisture content and compaction limit*

Sample points	SP1	SP2	SP3	SP4	SP5	SP6	SP7	SP8	SP9	SP10
LL	38.50	28.00	18.75	17.65	37.56	25.85	18.67	17.34	15.28	14.39
PL	23.97	18.25	13.5	14.09	24.21	17.96	13.81	12.37	12.63	11.98
PI	14.53	9.75	5.25	3.56	13.35	7.89	4.86	4.97	2.65	2.41
1st SG	2.35	2.55	2.64	2.38	2.40	2.67	2.58	2.71	2.57	2.75
2nd SG	2.45	2.57	2.80	2.80	2.45	2.67	2.55	2.38	2.71	2.50
Average SG	2.40	2.56	2.72	2.59	2.43	2.67	2.57	2.69	2.64	2.63
OMC (%)	38.67	14.90	15.20	16.52	47.56	13.94	16.24	11.87	12.57	10.21
MDD (kg/m^3)	1,445	2,506	2,100	1,720	1,250	2,850	1,790	3,011	2,910	3,500
Moisture content	23.97	17.25	13.50	14.09	24.21	16.03	13.81	12.34	12.63	11.98

LL, liquid limit; PL, plastic limit; PI, plasticity index; SG, specific gravity; OMC, optimum moisture content; MDD, maximum dry density; SP, sampling point.

Geotechnical results and discussion

Interpretation of Atterberg limit test

The PI of the soil samples (Table 2) revealed that soil samples SP2, SP3, SP4, SP6, SP7, SP8, SP9 and SP10 fall between PIs of 1% and 10%, which implies low plasticity, consisting of sand or silt with traces of clay, while soil samples SP1 and SP5 have PIs between 10% and 20%, depicting medium plasticity and composed of clayey loam soil. All the soil samples SP1–SP10 fall within the limits of the specifications, except SP1 and SP5, for which the LL and the PI exceeded the stipulated values of 35% and 12%, respectively, contrary to the Federal Ministry of Works and Housing (FMW&H) specification requirement in Clauses 6201 and 6252. The PI of soil samples SP1 and SP5 is above the standard limit and, therefore, they are considered to be highly plastic, which may pose a threat to the structure and consequently lead to structural failure.

Results of the SG test

Table 2 shows the SG values obtained for the different soil samples. All the samples fall between the ranges of specification, varying from 2.5 to

2.75, excluding samples SP1 and SP5, which fall below the limit recommended by FMW&H [18]. In a previous paper [19], it was noted that the SG of soil grains is a key attribute in the assessment of aggregate parameters for construction purposes. The higher the SG of the soil towards the upper limit of the soil standard, the better is the soil for construction purposes.

Soil moisture content

All the samples (Table 2) have moderate moisture content, except for samples SP1 and SP5, which have very high moisture content. Samples SP1 and SP5 are considered to be poor for engineering purpose because of their high content of moisture, and this implies that they have high ability to retain water without releasing it.

Results of the compaction limit test

The results for the compaction limit test for each sample shown in Table 2 illustrates that the MDD for the soil samples ranges from 1,250 kg/m^3 to 3,500 kg/m^3, and the OMC ranges from 10.21% to 47.56%. All the samples, except SP1 and SP5, fall within the specifications of the FMW&H (1997), which recommends the MDD to be >1,680 kg/m^3 and the OMC to be <18%. The density of the soil mass affects the strength of the soil, which implies that SP1 and SP5 have lower values compared to the standard values. The strength of a soil increases as its dry density increases; the potential for the soil to take on water at later times is decreased by higher densities.

Results of the CBR test

The overall CBR values for the soaked (CBR_s) and unsoaked (CBR_u) samples, as shown in Table 3, fall within the specified limits for all the soil samples analysed, except for SP1 and SP5. The FMW&H specification states that the minimum strength of the material should not be <80% for CBR (for unsoaked samples), while the minimum strength of the material should not be <10% after at least 48 h of soaking (for soaked samples). The CBR_s values ranged from 3.05% to 29.76%, while CBR_u ranged from 60.25% to 98.95%. The values for CBR_u and CBR_s are 60.25% and 5.62% for SP1 and

Table 3. *Results of the CBR test for the soil samples*

Sampling point	Location	CBR_u (%)	CBR_s (%)
SP1	Latitude 7° 08′ 15.8″ Longitude 3° 17′ 13.3″	60.25	5.62
SP2	Latitude 7° 08′ 17.2″ Longitude 3° 17′ 13.2″	89.34	14.00
SP3	Latitude 7° 08′ 18.8″ Longitude 3° 17′ 13.3″	91.00	18.00
SP4	Latitude 7° 08′ 20.5″ Longitude 3° 17′ 13.4″	97.00	21.00
SP5	Latitude 7° 08′ 17.0″ Longitude 3° 17′ 13.0″	70.45	3.95
SP6	Latitude 7° 08′ 16.9″ Longitude 3° 17′ 11.3″	84.37	12.89
SP7	Latitude 7° 08′ 17.2″ Longitude 3° 17′ 10.0″	90.56	20.86
SP8	Latitude 7° 08′ 18.8″ Longitude 3° 17′ 10.0″	97.96	27.95
SP9	Latitude 7° 08′ 20.5″ Longitude 3° 17′ 10.0″	98.95	29.76
SP10	Latitude 7° 08′ 24.0″ Longitude 3° 17′ 10.3″	98.00	28.00

Notes: CBR, California bearing ratio; CBR_s, CBR of soaked sample; CBR_u, CBR of unsoaked sample; SP, sampling point.

Table 4. *Summary of the results of sieve analysis*

Sample	Sieve number	4	8	16	30	50	100	200	PAN
	Diameter (μm)	475	236	118	600	300	150	75	
SP1	% Retained	14.43	12.70	12.99	13.99	9.05	13.08	11.26	12.50
	% Passing	85.57	72.87	59.88	45.89	36.84	23.76	12.50	0
SP2	% Retained	9.35	9.83	12.49	12.88	13.5	14.56	15.51	11.88
	% Passing	90.65	80.82	68.33	55.45	41.95	27.39	11.88	0
SP3	% Retained	9.72	10.06	12.27	12.43	12.79	14.62	15.60	12.51
	% Passing	90.28	80.22	67.95	55.52	42.73	28.11	12.51	0
SP4	% Retained	9.73	13.37	12.39	12.48	13.67	12.81	13.05	12.5
	% Passing	90.27	76.9	64.51	52.03	38.36	25.55	12.50	0
SP5	% Retained	10.04	10.23	12.35	12.53	12.67	14.63	15.04	12.51
	% Passing	89.96	79.73	67.38	54.85	42.18	27.55	12.51	0
SP6	% Retained	9.91	10.29	12.01	12.51	12.98	14.6	15.19	12.51
	% Passing	90.09	79.80	67.79	55.28	42.3	27.7	12.51	0
SP7	% Retained	9.93	10.43	12.56	12.7	13.32	15.56	13.00	12.50
	% Passing	90.07	79.64	67.08	54.38	41.06	25.5	12.5	0
SP8	% Retained	10.21	10.31	12.03	12.54	13;00	14.63	14.96	12.32
	% Passing	89.79	79.48	67.45	54.91	41.91	27.28	12.32	0
SP9	% Retained	9.84	10.37	12.41	12.24	13.02	14.56	15.03	12.53
	% Passing	90.16	79.79	67.38	55.14	42.12	27.56	12.53	0
SP10	% Retained	9.95	10.25	12.25	12.47	12.90	14.50	15.18	12.50
	% Passing	90.05	79.80	67.55	55.08	42.18	27.68	12.50	0

Note: SP, sampling point.

70.45% and 3.95% for SP5, respectively. This implies that the soil is clayey lateritic type of soil, which does not support heavy structures. In addition, moisture influx would be highly detrimental to the structures constructed at those locations.

Results of sieve analysis

All the soil samples SP1–SP10 (Table 4) fall within the limit of specifications for sieve analysis since the percentage by weight of 15.18% passing the No. 200 sieve does not exceed the stipulated value of 35%, as required by the FMWH (1997) in Clause 6201.

Conclusion

A series of geophysical and geotechnical investigations have been carried out to give proper insight into the nature of sub-surface dispositions and their delineation to ensure building foundation integrity in the study area. The inferred lithology from the VES results revealed a maximum of five geoelectric layers. The geotechnical method, which involved Atterberg limit tests, shows that all the soil samples have low PI and are composed of sand or silt with traces of clay, except samples SP1 and SP5 (soil samples extracted from VES 1 and VES 2), which have medium PI and are composed of clay soil. Soil samples SP1 and SP5 exceeded the stipulated value limit and therefore pose a threat of structural failure. All the soil samples, except SP1 and SP5, had average SG values within the range of standard specifications. The laboratory result for the CBR for soil samples SP1 and SP5 indicated that the soil is clayey lateritic, which is highly detrimental to structures due to influx of moisture. The sieve analysis result showed that the entire set of soil samples has a size range within the

limit of specifications and does not exceed the standard value. The result for compaction limit revealed that all the soil samples are within the specified standard, except SP1 and SP5. It is vital to note that shallow foundations for any engineering structure are considered unsuitable at the weak zones because of the presence of incompetent materials, which tend to pose a threat to the development of future civil engineering structures in any given area.

References

[1] Amadi, A.N., Eze, C.J., Igwe, C.O., Okunlola, I.A., Okoye, N.O. (2012): Architects and geologists view on the causes of building failures in Nigeria. *Modern Applied Science,* 6(6), pp. 31, DOI:10.5539/mas.v6n6p31.

[2] Ayininuola, G.M., Olalusi, O.O. (2004): Assessment of building failures in Nigeria: Lagos and Ibadan Case Study. *African Journal of Science and Technology*, 5(1), pp. 73–78, DOI:10.4314/ajst.v5i1.15321.

[3] Dimuna, K.O. (2010): Incessant incidents of building collapse in Nigeria. A challenge to stakeholders. *Global Journal of Researches in Engineering*, 10(4), pp. 75–84.

[4] Oyedele, K.F., Okoh, C. (2011): Subsoil investigation using integrated methods at Lagos, Nigeria. *Journal of Geology and Mining Research*, 3(7), pp. 169–179.

[5] Olayanju, G.M., Mogaji, K.A., Lim, H.S., Ojo, T.S. (2017): Foundation integrity assessment using integrated geophysical and geotechnical techniques: Case study in crystalline basement complex, Southwestern Nigeria. *Journal of Geophysics and Engineering*, 14(3), pp. 675–690, DOI:10.1088/1742-2140/aa64f7.

[6] Oluwafemi, O., Ogunribido, T.H. (2014): Integrated geophysical and geotechnical assessment of the permanent site of Adekunle Ajasin University, Akungba-Akoko, Southwestern, Nigeria. *Pelagia research library*, 5(2), pp. 199–209.

[7] Oladele, S., Oyedele, K.F., Dinyo, M.O. (2015): Pre-construction geoelectrical and geotechnical assessment of an engineering site at Alapere/Agboyi, Lagos, Nigeria. *Ife Journal of Science*, 17(3), pp. 543–552.

[8] Falae, P.O. (2014): Application of electrical resistivity in buildings foundation investigation in Ibese Southwestern Nigeria. *Asia Pacific Journal of Energy and Environment,* 1(2), pp. 95–107, DOI:10.15590/apjee/2014/v1i2/53748.

[9] Soupois, P.M., Georgakopoulos, P., Papadopoulos, N., Saltos, V., Andreadakis, A., Vallianatos, F., Sanis, A., Markris, J.P. (2007): Use of engineering geophysics to investigate a site for a building foundation. *Journal of Geophysics and Engineering*, 4(1), pp. 94–103, DOI:10.1088/1742-2132/4/1/011.

[10] Farinde, M.A., Oni, S.O. (2015): Geophysical and geotechnical characterization of newly constructed Abadina-Ajibode road, University of Ibadan, Ibadan. *Journal of Multidisciplinary Engineering Science and Technology (JMEST),* 2(1), pp. 363–378.

[11] Alabi, A.A., Adewale, A.O., Coker, J.O., Ogunkoya, O.A. (2017): Site characterization for construction purposes at FUNAAB using geophysical and geotechnical methods. *RMZ–Materials and Geoenvironment*, 64, pp. 1–14, DOI:10.2478/rmzmag-2018-0007.

[12] Adejumo, S.A., Oyerinde, A.O., Aleem, M.O. (2015): Integrated geophysical and geotechnical subsoil evaluation for pre-foundation study of proposed site of vocational skill and entrepreneurship center at The Polytechnic, Ibadan, SW, Nigeria. *International Journal of Scientific and Engineering Research,* 6(6), pp. 2229–5518.

[13] Akinse, A.G., Gbadebo, A.M. (2016): Geologic mapping of Abeokuta metropolis, southwestern Nigeria. *International Journal of Scientific and Engineering Research*, 7(8), pp. 2229–2518.

[14] Loke, M.H. (1999): Electrical imaging surveys for environmental and engineering studies; a practical guide to 2-D and 3-D surveys. *Self-Published Note Book*, pp. 15–57.

[15] Black, C.A. (1965): Methods of Soil Analysis. *Part 1, American Society of Agronomy*, No 9.

[16] Roy, T.K., Chattapadhyay, B.C., Roy, S.K. (2010): California bearing ratio evaluation and estimation: a study of comparison. *Indian Geotechnical Conference, IGC-2010, IIT, Mumbai*, pp. 19–22.

[17] Mookiah, M., Thiagarajan, S., Madhavi, G. (2015): Surface geo-electrical Sounding for the determination of aquifer characteristics in part of the Palar Sub-Basin, Tamilnadu, India. *International Conference on Science Technology Engineering and Management [ICON-STEM'15],* 8.

[18] Federal Ministry of Works and Housing (FMW&H). (1997): General specification for roads and bridges. *Vol II, Federal Highway Department, FMWH, Lagos, Nigeria,* 168 p.

[19] Gidigasu, M.D. (1976): *Laterite soil engineering* (*Pedogenesis and Engineering Principles)*. Elsevier Scientific Publishing Company: Amsterdam, 554 p.

Original Scientific Article

Received: February 17, 2021
Accepted: February 19, 2021
DOI: 10.2478/rmzmag-2020-0017

Geochemical Fingerprinting pf Oil-Impacted Soil and Water Samples In Some Selected Areas in the Niger Delta

Geokemični kazalniki z nafto nasičenih vzorcev zemljin in vode na nekaterih izbranih področjih delte reke Niger

Adeola V. Adeniyi*, Matthew E. Nton, Falode O. Adebanjo
Department of Geology, University of Ibadan, Ibadan, Nigeria
*Corresponding author: E-mail: adeolaadeniyi93@gmail.com

Abstract

With over 50 years of oil exploration and exploitation in the Niger Delta, there has been an increasing rate of environmental degradation due to hydrocarbon pollution. This study is aimed at tracing the sources of the oil spills and the distribution of pollutants in selected communities in the Niger Delta using geochemical techniques. A total of sixteen samples made up of ten crude oil-impacted soil samples taken at a depth of 30 cm and six water samples (two from boreholes, two from burrow pits and two from surface water – one from a river and the other from rain harvest as control) were collected. The identification and quantification of aliphatic hydrocarbons (AHs) and polycyclic aromatic hydrocarbons (PAHs) in the samples were performed with an Agilent 7890B gas chromatography flame ionisation detector (GC-FID). The AHs including pristane and phytane, together with seventeen priority PAHs, were identified. The values of AHs and PAHs in the water samples ranged from 0.13 mg/l to 5.78 mg/l and 0.09 mg/l to 1.109 mg/l, respectively, while that for the soil samples ranged from 22.52 mg/kg to 929.44 mg/kg and 10.544 mg/kg to 16.879 mg/kg, respectively.

Key words: PAH, aliphatic hydrocarbon, fingerprinting

Povzetek

Z več kot petdesetimi leti raziskovanja in pridobivanja nafte na območju delte reke Niger narašča stopnja degradacije okolja zaradi onesnaževanja z ogljikovodiki. Namen raziskave je slediti virom razlitij nafte in porazdelitev onesnaževal v izbranih skupnostih v delti reke Niger z uporabo geokemičnih pristopov. Skupno je bilo odvzetih 16 vzorcev, od tega 10 vzorcev z nafto nasičenih zemljin iz globine 30 cm ter 6 vzorcev vode, od tega dva iz vrtin, dva iz jame ter dva iz površinske vode (en vzorec iz reke in en iz deževnice). Z detektorjem plamenskega ioniziranja s plinskim kromatografom Agilent 7890B (GC-FID) je bila izvedena identifikacija in kvantifikacija alifatskih ogljikovodikov (AH) in policikličnih aromatskih ogljikovodikov (PAH). Identificirani so bili AH z vključujočim pristanom (pristane) in fitanom (phytane) skupaj s 17 PAH. Vrednosti AH in PAH v vzorcih vode se gibajo med 0.13 mg/l do 5.78 mg/l in 0.09 mg/l do 1.109 mg/l. Vrednosti AH in PAH v vzorcih zemljine se gibajo med 22.52 mg/kg do 929.44 mg/kg in 10.544 mg/kg do 16.879 mg/kg.

Ključne besede: PAH, alifatski ogljikovodik, kazalniki

Introduction

The Niger Delta is one of the major hydrocarbon provinces of the world, with an estimated reserve of about 23 billion barrels of oil and 183 trillion cubic feet of natural gas with ongoing exploration in the province for over 50 years [1]. Much of the oil industries located within this region have contributed immensely to the growth and development of the nation.

However, oil exploration activities have rendered the Niger Delta region one of the most severely degraded ecosystems in the world [2]. Crude oil spills are common in the

region with an estimated total of over 7,000 oil spill accidents reported over 50 years [3]. Studies have shown that the quantity of oil spilt over this period amounts to 9–13 million barrels, which is equivalent to 50 Exxon Valdez spills [4].

These spills occur through equipment failure, operational mishap, haulage, oil bunkering and/or vandalisation of pipelines leading to the destruction of aquatic and terrestrial flora and fauna of the Niger Delta region [5].

Geochemical or Oil fingerprinting is one of the ways of assessing and evaluating petroleum pollution. It involves the analysis of the released oil with gas chromatography (GC) and measurement of the hydrocarbon compound contents [6]. From the qualitative method (visual comparison of chromatograms) as well as quantitative determination of polycyclic aromatic hydrocarbons (PAHs) diagnostic ratio, *n*-alkane distribution and statistical analysis of data obtained are used for source identification and interpretation of chemical data from oil spills. An assessment and evaluation of hydrocarbon pollution are therefore essential to curb the growing rate of environmental degradation in the region as well as its social, economic and health impacts. This assessment includes; determination of sources, characterisation, distribution, and fate of organic pollutants such asPAHs and aliphatic hydrocarbons (AHs) in the Niger Delta. The objective is to evaluate the AH and PAHs which are said to be source-specific.

Location and geology of the study area

The study area lies within the Niger Delta region between latitudes 5°37′00″E–5°47′00″E and longitudes 5°53′00″N–6°02′30″N (Figure 1) and cuts across Sapele and Ethiope West Local government, Delta State, Nigeria. Stratigraphically, the Niger Delta consists of three formations, notably; Akata Formation, which is the oldest unit and constitutes under compacted shales, turbidites and silts. This is overlain by the paralic Agbada Formation, made up of alternating sequences of sandstone and shale which contains most of the hydrocarbon reservoirs in the basin while the youngest unit is the Benin Formation, which is made up of continental sands [7]. The area is

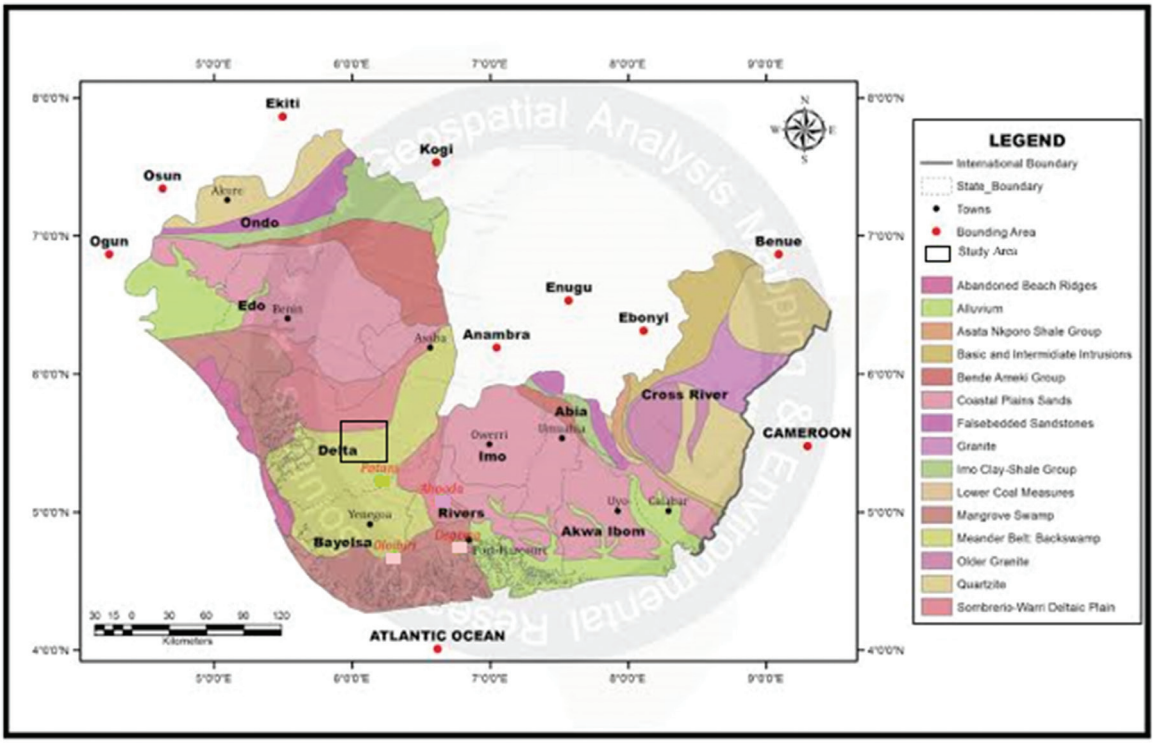

Figure 1: *Geological map of the Niger Delta region showing the study area (modified after Geological Map of Niger Delta [8]).*

characterised by an even topography. It is situated in the tropics and experiences a fluctuating climate characterised by rainy and dry seasons. The area is drained by minor rivers which are tributaries of the major River Ethiope with a dendritic pattern.

Materials and methods

Sampling and sample preparation

The field study involved the collection of soil and water samples from selected points as shown in Figure 2. A total of sixteen samples made up of ten crude oil-impacted soils taken at a depth of 30 cm and six water samples (two from boreholes, two from burrow pits plus and two from surface water – one from a river and the other from rain harvest as control) were collected. The water and soil samples were collected in clean, well-labelled glass jars and aluminium foils, respectively, and taken to the laboratory for analyses. Due to the relatively high volatility and instability of AHs and PAHs, the soils were not prepared using conventional soil preparation techniques such as grinding and sieving. However, the soil samples were dried by mixing the samples with 5 g of anhydrous sodium sulfate.

Analytical methods

Organic pollutants were separated from the soil and water samples using an ultrasonic extraction and a separatory funnel, respectively. The extracts were fractionated into the AH and PAH fractions by eluting with *n*-hexane and dichloromethane, respectively. The identification and quantification of AHs and PAHs were performed with an Agilent 7890B gas chromatography flame ionisation detector (GC-FID). The gas chromatographic column has a detection limit of 0.01 ppm. Separation occurs as the constituents of the vapour partition between the gas and liquid phases and oven temperature was programmed from 60°C

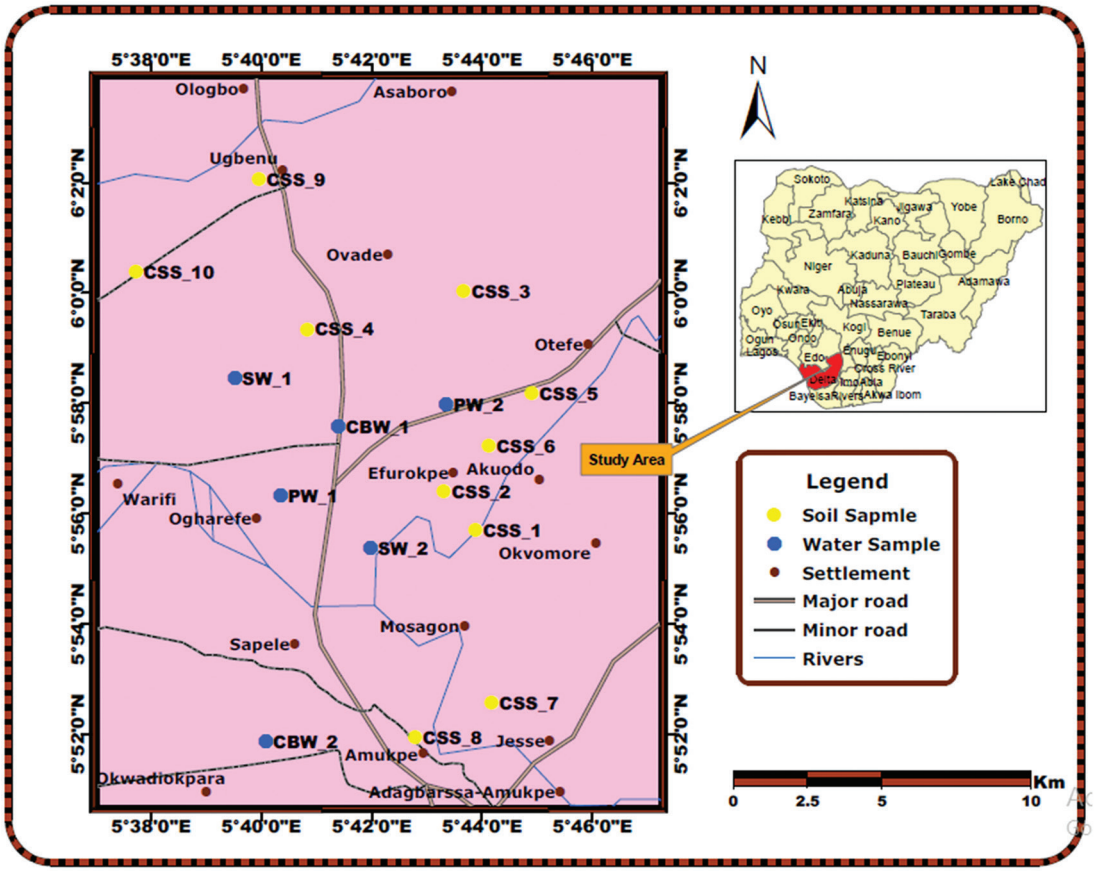

Figure 2: *Map of study area showing the sample points (insert: map of Nigeria showing the Niger Delta region).*

to 180°C. Identification of analytes was done by comparing the retention time of an individual compound to that of a reference standard.

Results and discussion

Concentration of AH and PAH

The results of the AH and PAHs in this study are shown in Table 1. The concentrations of the AHs and PAHs found in the studied samples are low when compared with values from other areas in the Niger Delta (Table 2). However, in this study, the concentrations are higher than the regulatory limits given by the United Nations Environment Programme (UNEP) [9].

Occurrence, distribution and sources of PAHs

The distribution of seventeen priority PAHs in the water and soil samples in the study area is presented in Table 3. The main PAH pollutants in the studied areas were found to be Chrysene, Acenaphthene, Methylnaphthalene, Naphthalene, Anthracene, Benzo(g,h,i) perylene, Fluorene, Indeno(1,2,3-cd)perylene and Phenanthrene. It is important to note that the sum of the PAHs in the contaminated soil samples is 10.54–16.89 times higher than the standard level (1 mg/kg) of heavy [10]. The level of PAH pollution in the control sample (Sw-1) is very low as compared with those from the other samples studied. The spatial distribution of PAHs in this study is shown in Figure 3 and indicates a predominance of three-ring PAHs which suggests recent deposition according to Jiao et al. [11]. The abundance of three-ring PAHs in the study area is in agreement with studies of some oil-polluted sites in the Niger Delta [12]. The four-ring PAHs are also abundant and they indicate the persistence of high molecular weight (HMW) PAHs in the environment. According to Li et al. [13], petrogenic sources are those PAHs derived from petroleum spills while pyrogenic sources are generated by incomplete combustion of fossil fuel such as coal, crude oil and natural gas plus biomass. Diagnostic ratios such as Phenanthrene/Anthracene, Fluorene/Pyrene, Benz(a)pyrene/Chrysene, Naphthalene/Acenaphthene, Anthracene/(Phenanthrene + Anthracene), Fluoranthene/(Fluoranthene +

Table 1: *Results of concentration of the AHs and PAHs present in the soil and water samples*

Sample name	Sample medium	AHs	PAHs
Css_1	Soil	37.59 mg/kg	16.88 mg/kg
Css_2	Soil	25.70 mg/kg	11.66 mg/kg
Css_3	Soil	34.43 mg/kg	14.72 mg/kg
Css_4	Soil	22.52 mg/kg	14.77 mg/kg
Css_5	Soil	929.44 mg/kg	14.54 mg/kg
Css_6	Soil	79.55 mg/kg	15.91 mg/kg
Css_7	Soil	36.85 mg/kg	13.11 mg/kg
Css_8	Soil	34.86 mg/kg	10.54 mg/kg
Css_9	Soil	44.73 mg/kg	12.15 mg/kg
Css_10	Soil	41.93 mg/kg	15.81 mg/kg
Cbw_1	Water	0.22 mg/l	0.09 mg/l
Cbw_2	Water	0.13 mg/l	0.29 mg/l
Pw_1	Water	5.78 mg/l	0.86 mg/l
Pw_2	Water	5.14 mg/l	1.11 mg/l
Sw_1	Water (control)	0.61 mg/l	0.17 mg/l
Sw_2	Water	2.08 mg/l	0.86 mg/l

AH, aliphatic hydrocarbon; PAHs, polycyclic aromatic hydrocarbons.

Table 2: *Comparison of AH and PAH present in the studied samples with those found in some other areas in the Niger Delta and some regulatory standards*

Sample medium	Reference	AHs (mg/l)	PAHs (mg/l)
Contaminated soil	**Present study**	22.52–929.44	10.54–16.88
	Olawoyin et al. [14]	7,878.8–76,510.9	31.4–132.0
	Adedosu et al. [12]	575.96–1,202.47	7.40–78.30
	Udoetok and Osuji Leo [24]	77.64–3,946.58	8.16–3,756.81
	United Nations Environment Programme (UNEP) [9]	10	No limit
	Department of Petroleum Resources (DPR) [15]	No limit	1.00
	United States Environmental Protection Agency (USEPA) [10]	No limit	1.00
Borehole	**Present study**	0.13–0.22	0.09–0.29
	Olawoyin et al. [14]	No limit	119.90–450.58
	Ibezue et al. [29]	0.03–0.422	0.002–0.007
	WHO	0.0002	0.0002
	Department of Petroleum Resources (DPR) [15]	No limit	0.1
Surface water	**Present study**	0.61–2.08	0.17–0.86
	Inyang et al. [30]	2.5–183.0	No limit
	European Union Environmental Protection Agency (EUEPA) [25]	0.3	No limit
	Department of Petroleum Resources (DPR) [15]	No limit	0.0001
	WHO	No limit	0.05
Contaminated water	**Present study**	5.14–5.78	0.86–1.11
	Inyang et al. [30]	2.5–183.0	No limit
	European Union Environmental Protection Agency (EUEPA) [25]	0.3	No limit
	WHO	No limit	0.05

AH, aliphatic hydrocarbon; PAH, polycyclic aromatic hydrocarbon.

Pyrene), Benzo(a)anthracene/(Benzo(q)anthracene+ Chrysene), Indeno(1,2,3-cd)perylene/(Indeno (1,2,3-cd)perylene + Benzo(g,h,i)perylene) and low molecular weight (LMW) hydrocarbon/HMW hydrocarbon have been utilised in deducing the source of pollution [18, 20, 23, 26, 28]. From the source diagnostic indices as presented in Table 4, most PAHs in the study area are from petrogenic sources with a minor contribution from pyrogenic sources.

Normal alkanes and isoprenoids distribution and sources

Although some components of the PAHs and AHs in the study area have been degraded, the majority of the other components still persist in the environment which may affect groundwater, rivers and soils. This may be injurious to both human and animal health. Some sources of the PAH and AH studied are pyrolytic, i.e. from combustion/bush fire occasioned by explosion of oil tankers, oil installations, leakages from oil pipes and pipelines explosion during oil bunkering or pipeline vandalism. All these have bearing on agriculture, water supply settlement and the biodiversity within the study area.

Cancer risk assessment

PAHs are known to be injurious to health. The eight PAHs typically considered as possible carcinogens are Benzo(a)anthracene, Chrysene, Benzo(b)fluoranthene, Benzo(k)fluoranthene,

Table 3: *Occurrence and spatial distribution of PAHs in the soil and water samples*

PAHs	Water samples (mg/l)						Soil samples (mg/kg)									
	Cbw_1	Cbw_2	Pw_1	Pw_2	Sw_1	Sw_2	Css_1	Css_2	Css_3	Css_4	Css_5	Css_6	Css_7	Css_8	Css_9	Css_10
Nap	BDL	0.04	0.098	0.043	BDL	0.046	0.814	0.819	0.809	0.758	1.228	1.004	0.913	0.807	0.746	0.788
Mnap	BDL	BDL	0.066	0.176	BDL	0.064	1.814	1.007	1.356	1.106	3.249	1.548	1.264	1.093	1.235	1.350
Acep	BDL	BDL	0.056	0.037	BDL	0.066	3.352	1.148	1.666	0.683	1.459	2.311	1.672	1.340	1.740	1.830
Ace	BDL	0.07	0.081	0.087	BDL	0.073	1.404	1.437	1.420	1.558	3.020	1.536	1.401	1.410	1.376	1.433
Fl	BDL	BDL	0.036	0.173	BDL	0.042	0.768	BDL	0.697	1.216	1.085	0.959	0.706	0.697	0.769	0.771
Phe	BDL	0.06	0.061	0.048	BDL	0.057	0.985	1.041	1.032	1.027	0.174	1.509	0.961	0.803	0.801	0.958
Ant	BDL	0.01	0.010	0.133	0.166	0.017	0.364	0.274	0.375	0.744	0.111	1.632	0.336	0.222	0.233	0.265
Flu	BDL	0.05	0.046	0.040	BDL	0.057	0.924	0.906	1.156	0.841	0.088	0.301	1.027	0.759	0.747	0.927
Pyr	BDL	BDL	BDL	BDL	BDL	BDL	BDL	BDL	BDL	BDL	0.146	0.250	BDL	BDL	BDL	BDL
BaA	BDL	BDL	0.133	0.050	BDL	0.015	0.299	BDL	0.313	0.707	0.259	0.134	0.292	0.124	0.104	0.269
Chr	0.02	0.05	0.205	0.137	BDL	0.033	1.217	0.296	0.758	1.265	0.108	0.483	0.620	0.241	0.491	0.082
BbF	0.02	0.01	0.010	0.042	BDL	0.105	1.592	0.728	0.506	2.668	0.085	0.447	0.501	0.108	1.149	0.066
BkF	0.02	0.01	0.018	0.010	BDL	0.018	0.860	0.320	0.199	0.434	0.269	0.169	0.393	0.157	0.242	0.248
BaP	0.02	BDL	BDL	0.025	BDL	0.015	0.252	0.215	0.883	0.228	0.091	0.366	0.167	0.413	0.203	0.283
DahA	BDL	BDL	0.026	0.012	BDL	0.014	0.202	0.211	0.290	0.194	0.065	0.151	0.359	0.516	0.263	0.295
InP	0.01	BDL	BDL	0.038	BDL	0.114	0.912	1.895	0.407	0.665	0.562	0.396	0.598	0.659	0.182	3.374
BghiP	BDL	BDL	BDL	0.060	BDL	0.126	1.119	1.362	2.852	0.673	2.545	2.722	1.899	1.193	1.869	2.870
Total	0.09	0.3	0.856	1.109	0.166	0.863	16.879	11.657	14.720	14.768	14.543	15.917	13.108	10.544	12.151	15.807
Mean	0.005	0.02	0.050	0.065	0.010	0.051	0.993	0.688	0.866	0.869	0.855	0.936	0.771	0.620	0.715	0.930

Ace, Acenaphthene; Acep, Acenaphthylene; Ant, Anthracene; BaA, Benzo(a)anthracene; BaP, Benzo(a)pyrene; BbF Benzo(b)fluoranthene; BDL, Below Detection Limit; BghiP, Benzo (g, h, i) perylene; BkF, Benzo(k)fluoranthene; Chr, Chrysene; DahA, Dibenzo (a, h) anthrace; Fl, Fluorene; Flu, Fluoranthene; InP, Indeno (1, 2, 3-cd) perylene; Mnap, 2-Methylnaphthalene; Nap, Naphthalene; Phe, Phenanthrene; Pyr, Pyrene.

Benzo(a)pyrene, Dibenzo(a,h)anthracene, Indeno(1,2,3-cd)pyrene and Benzo(g,h,i) perylene. In particular, Benzo(a)pyrene has been identified as being highly carcinogenic. The World Health Organization (1993) revealed that Benzo(a)pyrene concentration of 0.7 µg/l corresponds to an excess lifetime cancer risk of 10–5. The BaP-equivalent (BaPE) is used as a way to access carcinogenic risk due to the contamination by PAHs. The BaPE not only includes the risk due to BaP but also calculates all of the carcinogenic PAHs, where each of the PAH is weighed according to its carcinogenicity in relation to the carcinogenicity of BaP, which is measured by 1. This index can be calculated with this equation [17]; BaPE = BaP + (BaA*0.06) + (BkF*0.07) + (BbF*0.07) + (DahA*0.06) + (InP* 0.08). BaPE ranged from 0 mg/l to 0.042 mg/l and 0.22 mg/kg to 1.16 mg/kg in the water and soil samples, respectively. The highest value of BaPE in the samples is in Css_3, hence indicating

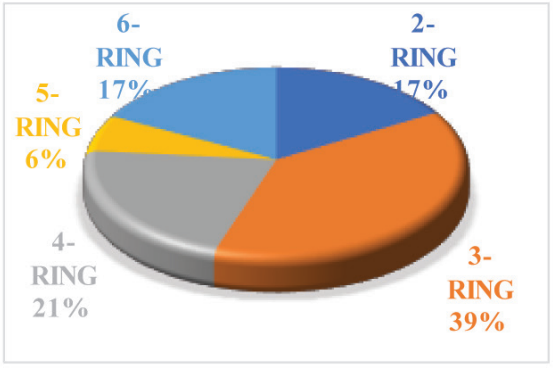

Figure 3: *The spatial distribution of the PAH rings in the water and soil samples. PAH, polycyclic aromatic hydrocarbons.*

Table 4: *PAH diagnostic ratios of the studied soil and water samples in comparison with that of standard references (after Tobiszewski and Namieśnik [21])*

PAH diagnostic ratio	Value range	Source	Reference	Value ranges from studied samples	Inferred source
ΣLMW/ΣHMW	<1 >1	Pyrogenic Petrogenic	Zhang et al. [26]	0–2.45	Petrogenic/pyrogenic
Fl(Fl + Pyr)	<0.5	Petroleum Emissions	Ravindra et al. [20]	0–0.4	Petroleum emissions
	>0.5	Diesel Emissions			
Ant(Phe + Ant)	<0.1 >0.1	Petrogenic Pyrogenic	Pies et al. [18]	0–0.21	Petrogenic/pyrogenic
Flu(Flu + Pyr)	<0.4 0.4–0.5 >0.5	Petrogenic Fossil fuel Combustion Grass, wood, coal combustion	De La Torre-Roche et al. [27]	0–0.4	Petrogenic/mixed source of fossil fuel and combustion
BaA/ (BaA + Chr)	0.2–0.35	Coal combustion	Akyüz and Çabuk [23]	0–0.31	Coal combustion/ petrogenic
	>0.35	Vehicular emission			
	<0.2	Petrogenic	Yunker et al. [28]		
	>0.35	Combustion			
InP/ (InP + BghiP)	<0.2	Petrogenic	Yunker et al. [28]	0–0.23	Petrogenic/petroleum combustion
	0.2–0.5	Petroleum Combustion			
	>0.5	Grass, Wood, Coal Combustion			

ΣLMW/ΣHMW, the sum of low molecular weight hydrocarbon/the sum of high molecular weight hydrocarbon.

Table 5: *The concentrations of AHs in the soil and water samples*

AHs	Water samples (mg/l)						Soil samples (mg/kg)									
	Cbw_1	Cbw_2	Pw_1	Pw_2	Sw_1	Sw_2	Css_1	Css_2	Css_3	Css_4	Css_5	Css_6	Css_7	Css_8	Css_9	Css_10
C8	BDL	BDL	BDL	0.11	BDL	0.51	12.76	1.13	0.59	0.30	2.38	BDL	1.32	1.44	1.77	9.42
C9	BDL	BDL	0.02	0.01	BDL	BDL	BDL	BDL	BDL	BDL	BDL	BDL	BDL	BDL	BDL	BDL
C10	BDL	BDL	0.81	0.17	BDL	0.01	BDL	BDL	BDL	BDL	0.94	BDL	BDL	BDL	0.29	0.59
C11	BDL	BDL	0.08	0.04	BDL	0.04	1.63	BDL	BDL	BDL	11.06	BDL	BDL	BDL	BDL	0.53
C12	BDL	BDL	0.18	0.11	BDL	BDL	BDL	BDL	BDL	BDL	6.35	BDL	BDL	0.06	BDL	0.04
C13	BDL	BDL	0.23	0.18	BDL	0.14	2.43	0.36	0.46	BDL	11.24	BDL	BDL	0.18	1.28	3.06
C14	BDL	0.02	0.33	0.23	0.03	0.01	0.53	0.77	0.66	0.42	47.91	0.09	BDL	0.17	0.57	0.56
C15	BDL	BDL	0.31	0.23	BDL	BDL	BDL	BDL	BDL	0.06	48.04	0.88	0.13	0.29	BDL	BDL
C16	BDL	0.04	0.33	0.25	0.02	0.01	0.85	0.19	0.12	0.69	29.37	3.90	0.31	0.39	0.95	0.89
C17	BDL	BDL	0.31	0.25	BDL	BDL	BDL	BDL	BDL	BDL	9.39	6.82	BDL	BDL	BDL	BDL
C18	BDL	0.03	0.28	0.23	0.01	0.04	0.45	0.10	0.73	0.60	17.20	7.94	0.13	BDL	0.93	0.64
C19	BDL	0.01	0.21	0.20	0.02	BDL	BDL	0.27	0.22	0.13	16.14	7.08	BDL	0.19	0.14	BDL
C20	BDL	0.02	0.22	0.28	0.03	0.05	0.39	1.18	0.65	0.78	24.05	7.78	1.24	1.36	1.65	0.74
C21	BDL	BDL	0.20	0.19	BDL	BDL	BDL	BDL	BDL	0.12	15.49	6.19	0.04	BDL	BDL	BDL
C22	BDL	BDL	0.26	0.22	0.02	0.02	1.37	0.57	0.28	BDL	15.23	5.27	1.49	1.71	0.45	0.17
C23	0.01	BDL	0.26	0.17	BDL	BDL	0.13	BDL	BDL	0.24	11.69	4.35	BDL	0.42	BDL	BDL
C24	0.01	0.02	0.36	0.23	0.03	BDL	BDL	BDL	0.60	1.62	19.32	4.16	0.38	0.34	BDL	0.05
C25	0.02	BDL	0.30	0.17	BDL	BDL	0.40	BDL	BDL	0.19	13.90	3.17	BDL	BDL	BDL	BDL
C26	0.02	BDL	0.12	0.16	BDL	0.04	0.73	0.66	1.01	0.74	12.47	2.75	1.40	1.14	1.15	0.96
C27	0.02	BDL	0.14	0.14	BDL	BDL	0.59	BDL	BDL	0.31	10.58	2.44	BDL	0.19	BDL	BDL
C28	0.01	BDL	0.11	0.12	BDL	0.03	0.86	0.30	0.71	0.54	18.87	1.93	0.96	1.18	0.80	0.68
C29	BDL	BDL	0.08	0.10	BDL	BDL	0.24	BDL	BDL	BDL	30.88	1.19	BDL	BDL	BDL	BDL
C30	BDL	BDL	0.08	0.05	BDL	BDL	BDL	BDL	BDL	BDL	29.12	0.29	BDL	BDL	BDL	BDL
C31	BDL	BDL	0.08	0.08	BDL	BDL	1.06	BDL	BDL	BDL	15.14	1.11	0.63	0.32	BDL	BDL

(*Continued*)

Table 5: Continued

AHs	Water samples (mg/l)						Soil samples (mg/kg)									
	Cbw_1	**Cbw_2**	**Pw_1**	**Pw_2**	**Sw_1**	**Sw_2**	**Css_1**	**Css_2**	**Css_3**	**Css_4**	**Css_5**	**Css_6**	**Css_7**	**Css_8**	**Css_9**	**Css_10**
C32	BDL	BDL	BDL	BDL	BDL	0.11	BDL	2.47	4.62	0.72	4.53	BDL	BDL	0.44	5.40	3.79
C33	BDL	BDL	BDL	0.31	BDL	0.40	5.05	8.38	12.62	2.20	13.12	BDL	3.23	4.24	13.73	10.84
C34	BDL	BDL	BDL	BDL	BDL	BDL	BDL	BDL	BDL	BDL	15.04	3.88	3.66	BDL	BDL	BDL
C35	BDL	BDL	BDL	BDL	0.07	BDL	BDL	BDL	11.16	BDL	6.12	BDL	BDL	BDL	BDL	BDL
C36	0.13	BDL	BDL	0.75	0.03	0.02	8.12	7.66	BDL	6.97	11.78	BDL	9.81	7.43	12.83	11.78
C37	BDL	BDL	0.15	BDL	0.26	0.65	BDL	BDL	BDL	BDL	5.90	BDL	9.99	11.26	BDL	BDL
C38	BDL	BDL	BDL	BDL	BDL	BDL	BDL	BDL	BDL	BDL	2.27	BDL	BDL	BDL	BDL	BDL
C39	BDL	BDL	BDL	BDL	BDL	BDL	BDL	BDL	BDL	BDL	BDL	BDL	BDL	BDL	BDL	BDL
C40	BDL	BDL	BDL	BDL	BDL	BDL	BDL	BDL	BDL	BDL	BDL	BDL	BDL	BDL	BDL	BDL
PRISTANE	BDL	BDL	0.27	0.16	BDL	BDL	BDL	BDL	BDL	5.32	392.91	6.70	BDL	BDL	BDL	BDL
PHYTANE	BDL	BDL	0.04	0.02	0.08	BDL	BDL	1.67	BDL	0.56	61.00	1.64	2.12	2.10	BDL	BDL
Pr/nC17	0	0	0.90	0.63	0	0	0	0	0	0	41.84	0.98	0	0	0	0
Total	0.22	0.13	5.78	5.14	0.61	2.08	37.59	25.69	34.43	22.52	929.44	79.55	36.85	34.86	44.73	41.94

AH, aliphatic hydrocarbon.

Table 6: *The AH diagnostic ratios (after Sojinu et al. [22])*

Sample	CPI	OEP
Cbw_1	0.29	1.81
Cbw_2	0.06	0
Pw_1	0.76	0.82
Pw_2	0.71	0.79
Sw_1	2.14	0
Sw_2	1.47	0
Css_1	0.44	0.21
Css_2	0.60	0
Css_3	2.46	0
Css_4	0.24	0.27
Css_5	0.85	0.72
Css_6	0.87	0.94
Css_7	0.68	0.006
Css_8	1.09	0.31
Css_9	0.57	0
Css_10	0.48	0
Mean	0.86	0.37

AH, aliphatic hydrocarbon.

that PAHs at this sample point have high carcinogenic effects.

Conclusion

The prevalence of petrogenic-derived PAHs was confirmed in the studied samples. AHs in both media originated from both petrogenic and biogenic. The AHs are products from both terrestrial and marine inputs. The pollution level of the study area is high as compared with USEPA, DPR and WHO standards which poses health hazards. However, the values are lower compared with other areas in the Niger Delta. The PAH and AH diagnostic ratios have proven to be useful in tracking pollution emission sources and have helped in assessing the level of degradation of oils in impacted soils and water.

Acknowledgements

The authors gratefully acknowledge the support of the African Union for the scholarship given to the first author to carry out this research, Pan Ocean Oil Corporation for assisting with sample collections and Jawura Environmental Laboratory, Ikeja Lagos for the geochemical analyses.

References

[1] Sonibare, O., Alimi, H., Jarvie, D., Ehinola, O.A. (2008): Origin and occurrence of crude oil in the Niger Delta, Nigeria. *Journal of Petroleum Science and Engineering*, 61, pp. 99–107.

[2] Kadafa, A.A. (2012): Environment impacts of oil exploration and exploitation in the Niger delta. *Global Journal of Science Frontier Research Environment and Earth Sciences*, 12(3), pp. 19–25.

[3] United Nations Development Programme (UNDP) (2006): *Niger Delta Human Development Report, Abuja.*

[4] Federal Ministry of Environment Abuja, Nigerian Conservation Foundation Lagos, WWF UK and CEESP-IUCN Commission on Environmental, Economic, and Social Policy (2006): Niger Delta Resource Damage Assessment and Restoration Project, 350 p.

[5] Zabbey, N. (2008): Persistent oil spillage at Bodo creek; unprecedented impacts on ecosystem stability, biodiversity and food security of Ogoni communities. A Report Issued by The Environment and Conservation Program, Centre for Environment, Human Rights and Development (CEHRD), Eleme, Rivers State, Nigeria, 130 p.

[6] Osuji, L.C., Idung, I.D., Ojinnaka, C.M. (2006): Hydrocarbon speciation by fingerprinting technique and diagnostic vanadium/nickel ratio of Mgbede-20 oil-impacted site in the Niger Delta Basin of Nigeria. *Journal of Environmental Forensic*, 7, pp. 259–265.

[7] Short, K.C., Stauble, A.J. (1967): Outline of geology of Niger Delta. *American Association of Petroleum Geologists Bulletin*, 51, pp. 761–779.

[8] Geological Map of Niger Delta [online]: GAMERS – Geospatial Analysis Mapping and Environmental Research Solutions [cited 01/09/2019]. Available on: *https://www.gamers.com.ng.*

[9] United Nations Environment Programme (UNEP). (2011): *UNEP Environmental Assessment of Ogoniland; Site Specific Fact Sheets*; *UN Environment:* Nairobi, Kenya, pp. 1–11.

[10] United States Environmental Protection Agency (USEPA) (1996): Test methods: polycyclic aromatic hydrocarbons – method 8270B, Environmental Monitoring and Support Laboratory, Cincinnati, OH.

[11] Jiao, H., Wang, Q., Zhao, N., Jin, B., Zhuang, X., Bai, Z. (2017): Distributions and sources of polycyclic aromatic hydrocarbons (PAHs) in soils around a chemical plant in Shanxi, China. *International Journal of Environmental Research and Public Health,* 14(10), pp. 1198–1201

[12] Adedosu, T.A., Adedosu, H.O, Sojinu, O.S., Olajire, A.A. (2013): N-Alkanes and polycyclic aromatic hydrocarbons (PAHs) profile of soils from some polluted sites in Niger Delta, Nigeria. *Environmental Earth Sciences Journal,* 68, pp. 2139–2144.

[13] Li, G.C., Xia, X.H, Yang, Z.F, Wang, R., Voulvoulis, N. (2006*):* Distribution and sources of polycyclic aromatic hydrocarbons in the middle and lower reaches of the Yellow River, China. *Environmental Pollution,* 144, pp. 985–993.

[14] Olawoyin, R.S., Oyewole, C.W., McGlothlin, B., Heidrich, S.O., Abegunde, A.N., Okareh, O.T. (2014): Characteristic fingerprints of polycyclic aromatic hydrocarbons and total petroleum hydrocarbons pollution in petrochemical areas. *International Journal of Environmental Pollution and Solutions,* 2(1), pp. 1–19.

[15] Department of Petroleum Resources (DPR) Environmental Guidelines and Standard for the Petroleum Industry in Nigeria (2018).

[16] Udeh O.V., Osuji, L.C., Achugasim, O. (2018): Aliphatic hydrocarbon fingerprints of some crude oil polluted soils from Niger Delta, Nigeria. *Chemical Engineering and Science,* 5(1), pp. 1–5.

[17] Liu, Y., Ling, C., Qing-hui, H., Wei-ying, L., Yin-jian, T., Jian-fu, Z. (2009): Source apportionment of polycyclic aromatic hydrocarbons (PAHs) in surface sediments of the Huangpu River, Shanghai, China, *Science of the Total Environment*, 407, pp. 2931–2938.

[18] Pies, C., Hoffmann, B., Petrowsky, J., Yang, Y. Ternes, T.A., Hofmann, T. (2008): Characterization and source identification of polycyclic aromatic hydrocarbons (PAHs) in river bank soils*. Chemosphere Journal,* 72, pp. 1594–1601.

[19] Sakari, M., Ting, L.S., Houng, L.Y., Lim, S.K., Tahir, R., Adnan, F.A.F., Yi, A.L.J., Soon, Z.Y., Hsia, B.S., Shah, M.D. (2012): Urban effluent discharge into rivers: A forensic chemistry approach to evaluate the environmental deterioration. *World Applied Science Journal,* 20, pp. 1227–1235.

[20] Ravindra, K., Sokhi, R., Van Grieken, R. (2008): Atmospheric polycyclic aromatic hydrocarbons: Source attribution, emission factors and regulation. *Atmospheric Environment,* 42(13), pp. 2895–2921.

[21] Tobiszewski, M., Namieśnik, J. (2012): PAH diagnostic ratios for the identification of pollution emission sources. *Environmental Pollution*, 162, pp. 110–119.

[22] Sojinu, O.S., Sonibare, O.O., Zeng, E.Y. (2012): Concentrations of Polycyclic aromatic hydrocarbons in soils of a mangrove forest affected by forest fire. *Toxicological and Environmental Chemistry Journal,* 93, pp. 450–461.

[23] Akyüz M., Çabuk H., (2010): Gas particle partitioning and seasonal variation of polycyclic aromatic hydrocarbons in the atmosphere of Zonguldak, Turkey. *Science of the Total Environment*, 408, pp. 5550–5558.

[24] Udoetok, I.A., Osuji Leo C. (2009): Gas chromatographic fingerprinting of Crude oil from Idu-Ekpeye oil spillage site in Niger Delta, Nigeria. *Environmental Monitoring Assessment,* 141, pp. 359–364.

[25] European Union Environmental Protection Agency (2009): Framework for the use of rapid measurement techniques (RMT) in the risk management of sediment and water Contamination, UK.

[26] Zhang, W., Zhang, S.C., Wan, C., Yue, D.P., Ye, Y.B., Wang, X.J. (2008): Source diagnostics of polycyclic aromatic hydrocarbons in urban road runoff, dust, rain and canopy through fall. *Environmental Pollution,* 153, pp. 594–601.

[27] De La Torre-Roche, R.J., Lee, W.Y., Campos-Díaz, S.I., (2009): Soil borne polycyclic aromatic hydrocarbons in El Paso, Texas: Analysis of a potential problem in the United States/Mexico border region. *Journal of Hazardous Materials,* 163, pp. 946–958.

[28] Yunker, M.B., Macdonald, R.W., Vingarzan, R., Mitchell, R.H., Goyette, D., Sylvestre, S. (2002): PAHs in the Fraser River basin: A critical appraisal of PAH ratios as indicators of PAH source and composition. *Organic Geochemistry*, 33, pp. 489–515.

[29] Ibezue, V.C., Odesa, E.G., Ndukwe, J.O., Nwabineli, E.O. (2018): Hydrocarbon concentration levels in groundwater in Jesse and Environ, Ethiope West L.G.A. Delta State, Nigeria. *International Journal of Computer Applications Technology and Research,* 7(7), pp. 241–254.

[30] Inyang, S.E., Aliyu, A.B., Oyewale, A.O. (2018): Total petroleum hydrocarbon content in surface water and sediment of Qua-Iboe River, Ibeno, Akwa-Ibom State, Nigeria. *Journal of Applied Science and Environmental Management,* 22(12), pp. 1953–1959.